Technical University of Crete

School of Chemical and Environmental Engineering

Kriging enhanced analysis of groundwater conditions for the island of Crete with Self-Organizing Maps in Tympaki,Crete.

Post-graduate Thesis of
Spyropoulos Fotios

Committee:

Professor Karatzas George (Supervisor)

Professor Nikolaidis Nikolaos

Professor Varouchakis Emmanouil

Chania,2023

Περίληψη

Ο στόχος αυτής της εργασίας είναι η διερεύνηση της συνδυασμένης εφαρμογής απλού Kriging και αλγόριθμου Αυτοοργανώμενων Χαρτών στην υδρογεωλογία. Το απλό Kriging χρησιμοποιήθηκε για την πρόβλεψη του υδραυλικού ύψους στην περιοχή μελέτης. Η χρήση των Αυτοοργανώμενων Χαρτών έχει σαν σκοπό την ομαδοποίηση των παρατηρήσεων εντός της περιοχής μελέτης, πάνω στις οποίες εφαρμόζεται το Kriging. Η περιοχή μελέτης που εξετάστηκε η μεθοδολογία είναι ο υδροφόρος του Τυμπακίου στην Κρήτη. Ο υδροφόρος του Τυμπακίου είναι γενικά πορώδης ομοιογενής με μερικές διαφοροποιήσεις στις υδραυλικές του ιδιότητες. Η σύζευξη των αλγορίθμων αξιολογείτε βάσει των ακόλουθων κριτηρίων επικύρωσης Mean Absolute Error, Maximum Absolute Error, Root Mean Square Error και Correlation Coefficient. Κάθε ομάδα παρατηρήσεων ονομάζεται συστάδα (cluster) και ένα ολόκληρο σύνολο συστάδων ονομάζεται τοπολογία. Διερευνήθηκαν διαφορετικές διαμορφώσεις συστάδων για την επιλογή της τοπολογίας με την καλύτερη απόδοση. Προκειμένου να αξιολογηθεί η βελτίωση της πρόβλεψης χρησιμοποιώντας τον αλγόριθμο Αυτο-Οργανώμενων Χαρτών, πραγματοποιήθηκε η πρόβλεψη απλού Kriging με τα ακόλουθα αποτελέσματα: Mean Absolute Error 6.9 m, Maximum Absolute Error 56.5 m, Root Mean Square Error 11.7 m and Correlation Coefficient 92%. Η τοπολογία με τις καλύτερες επιδόσεις αποτελούνταν από 6 ομάδες παρατηρήσεων, οι οποίες διαφοροποιήθηκαν με βάση τη θέση και τις υδραυλικές ιδιότητες τους. Η τοπολογία με τις καλύτερες επιδόσεις παρήγαγε τα ακόλουθα εύρη κριτηρίων επικύρωσης: Mean Absolute Error 0.39-2 m, Maximum Absolute Error 1.7-33 m, Root Mean Square Error 0.7-8.7 m and Correlation Coefficient 81-93%, με μια ακραία τιμή -14% που αποδίδεται σε γραμμική και όχι στοχαστική πρόβλεψη. Επιπλέον, η ομαδοποίηση παρείχε πληροφορίες σχετικά με τις ιδιότητες των ετερογενειών της μελέτης περίπτωσης. Η προτεινόμενη μεθοδολογία απέδωσε βελτιωμένα αποτελέσματα, ακόμη και στις πρώτες διαμορφώσεις ενώ η γενική μορφή της μεθοδολογίας, την καθιστά εφαρμόσιμη για άλλες περιοχές μελέτης με μικρές τροποποιήσεις.

Abstract

The main objective of this work is to investigate the pairing of Self-Organizing Maps with Ordinary Kriging techniques as applied to hydrogeology. Ordinary Kriging predicts the values of hydraulic head in a case study. The use of Self-Organizing Maps aims to create groups of observations in the case study, to which Ordinary Kriging is applied. The implementation of the proposed methodology was carried out on the case study of the aquifer of Tympaki, Crete. The Tympaki aquifer is a generally homogenous porous aquifer with local differences in hydraulic properties. The pairing is evaluated using the following validation criteria: mean absolute error, maximum absolute error, root mean square error and correlation coefficient. Each group of observations is called a cluster and a whole set of clusters is called a topology. Different configurations of clusters were investigated to select the best topology. In order to assess the improvement of prediction using the Self-Organizing Map algorithm the Ordinary Kriging prediction was performed with the following results: Mean Absolute Error 6.9 m, Maximum Absolute Error 56.5 m, Root Mean Square Error 11.7 m and Correlation Coefficient 92%. The best performing topology consisted of 6 observation groups divided by location and hydraulic properties by the Self-Organizing Map algorithm. The best topology resulted in the following ranges of validation criteria: Mean absolute error 0.39-2 m, maximum absolute error 1.7-33 m, root mean square error 0.7-8.7 m and correlation coefficient 81-93% with an outlier of -14% due to linear and non-stochastic prediction. In addition, the grouping provided insight on the properties of the heterogeneities of the case study. The proposed methodology yielded improved results, even in the initial configurations and it applicable to other case studies with very few modifications due to its generic structure.

Ευχαριστίες

Θα ήθελα να ευχαριστήσω τον Καθηγητή Γεώργιο Καρατζά τόσο για την επιστημονική συνεισφορά του σε αυτή την εργασία όσο και για την εξαιρετική συνεργασία που είχαμε όσο ήμουν μέρος του ερευνητικού εργαστηρίου του. Έπειτα θα ήθελα να ευχαριστώ τον Επίκουρο Καθηγητή Εμμανουήλ Βαρουχάκη, που μου έδωσε την ιδέα για την παρούσα εργασία και σημαντική βοήθεια καθ' όλη την εκπόνηση της. Ακόμα θα ήθελα να ευχαριστήσω τον Καθηγητή Νικόλαο Νικολαΐδη που δέχτηκε να είναι μέλος της τριμελούς επιτροπής μου. Τέλος θα ήθελα να ευχαριστήσω τον Αντρέα Παυλίδη και τον Αντώνη Λυρώνη, για την βοήθειά τους με τον κώδικα του μοντέλου.

Context

Table of Figures

1   Introduction

1.1   Scope of Thesis

This thesis was conducted in the framework of the requirements of the postgraduate master studies "Sustainable Engineering and Climate Change" with specialization in sustainable water and wastewater management. The scope of this thesis is to explore the pairing of standard geostatistical method with artificial intelligence, in hydrogeological applications. The goal was to reduce the geostatistical error by applying a given method in subgroups of observations, rather than the entire dataset. The geostatistical method used was Ordinary Kriging, which was selected after an extensive literature review. Self-Organizing Maps were used as the artificial intelligence algorithm since they have been applied several times in the field of environmental engineering. The proposed method was applied to the hydrogeological basin of Tympaki, Crete. After the application of the proposed methodology multiple maps are yielded predicting the hydraulic head value in subsections of a case study. By performing Kriging in subsections of the study area elected by the Self-Organizing Map, the performance metrics of Kriging are improved thus the error of prediction is reduced. An added benefit of this methodology is that, compared to other models, such as finite element models, the data required exclude the temporal aspect of the phenomenon. As a consequence, the prediction yielded describe a mean state of the groundwater in a case study. For case studies with dispersed and not consistent recordings of hydraulic head values the proposed methodology facilitates accurate predictions that could be the basis for groundwater resources management plans and best practices in the agricultural sector.

1.2   Theoretical Background

1.2.1   Basic Concepts of Ordinary Kriging

Kriging has been synonymous with geostatistical interpolation since its inception in the 1950's by mining engineer D.G. Krige. Its main original and most important application concerns reserve estimates, but over the decades it has found use in other fields such as hydrogeology. The standard version of kriging is called Kriging and is the predictive model used in this work.

$$Z(s) = \mu + \varepsilon'(s) \qquad\qquad 1$$

s: the spatial location of a variable
$Z(s)$: the probabilistic value of a variable
μ: the global mean
$\varepsilon'(s)$: the spatially correlated stochastic part of variable

As it can be seen, the model consists of a probabilistic process that correlates the values of a variable with its spatial distribution in a 2D, 3D or even 4D plane. From this Kriging can be viewed as a refined inverse distance interpolation given the following prediction equation.

$$\hat{z}_{OK}(s_0) = \sum_{i=1}^{n} w_i(s_0) \cdot z(s_i) = \lambda_0^T \cdot z \qquad\qquad 2$$

λ_0: the vector of Kriging weight w_i
z: the vector of n observations

From the above expression arises the question of the values that each weight should have. Semivariance ($\gamma(h)$) is introduced into the methodology as a means of estimating the weights to reflect their spatial autocorrelation structure.

$$\gamma(h) = \frac{1}{2} E\left[\left(z(s_i) - z(s_i + h)\right)^2\right] \qquad\qquad 3$$

$z(s_i)$: the value of a variable at a sample point
$z(s_i + h)$: the value of a neighbor at the distance $s_i + h$

With n observations there are, $n \cdot (n-1)/2$ pairs for which the semivariance can be calculated. Plotting all semivariences versus their distance yields a variogram cloud. For a standard distance, the semivariences are averaged, these averages are called lags, and when plotted against the mentioned distances the experimental variogram is obtained. The typical image of a variogram is an increasing curve at small distance, that stabilizing at a plateau at greater distance. The mathematical interpretation of this image states that the values of a variable become more similar at short distance, up to a certain point. This is known as the spatial auto-correlation effect, which can describe the stochastic components of a system that can otherwise be described by a deterministic function(Hengl et al., 2007; Zimmerman and Stein, 2010).

After an experimental variogram is calculated, it is fitted to a variogram model. Typical models are linear, spherical, exponential, circular, etc. Fitting is usually done by an iterative, reweighted least squares estimation. The weights are deterministic in nature being estimated by the number of pairs in a lag squared divided by the distance N^2/h. This means that higher weight values can be expected in small, crowded areas of the record. The variable can be defined as stationary if multiple variograms are similar to each other. If a sampled variogram is stationary, the target variable can be called covariance stationary. In the Kriging method the main assumption is that the variable is stationary. The three empirical parameters define the properties of a variogram the nugget, sill and range. The nugget indicates the measurement error and in ideal conditions should be zero, the sill indicates the sampled variance, and range parameter is 10% defined by the spatial extent of the data. The range parameter must be distinguished from the practical range or the range of spatial dependence (i.e., the distance at which the semivariance is close to 95% of the sill). The sill parameter (C_1) is different from the sill variation ($C_1 + C_0$), which includes the nugget. There can also be variograms that show no spatial correlation and are defined only by the nugget parameter. Finally, the unbound variograms indicate that the lags projected cannot produce a sill, which in turn means that either more data are need in order to create more lags or that all lags correlated strongly with each other. Either way the results produced from those variograms are similar to those of an inverse distance interpolation. All the topics discussed in this sections are graphically represented in the figure below (Hengl et al., 2007; Zimmerman and Stein, 2010).
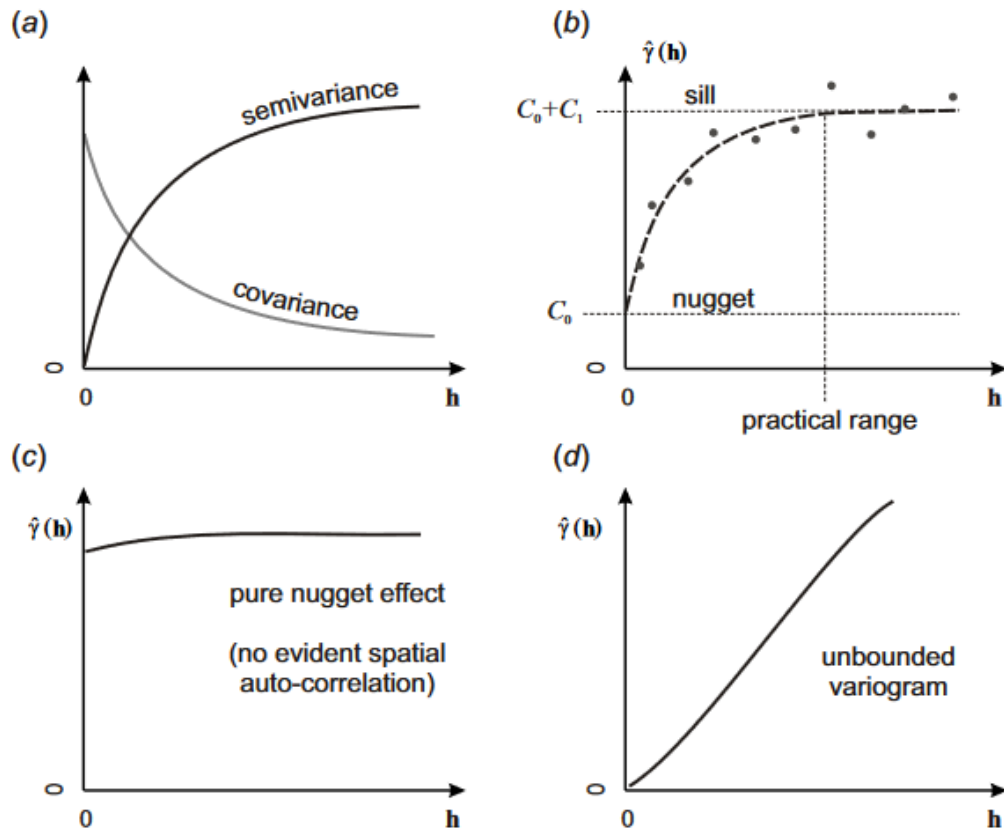
Figure 1.1: Basic variogram consepts (Hengl et al., 2007)

After estimating the variogram, it is possible to create semivariances at all locations and determine the corresponding Kriging weights. The Ordinary Kriging (OK) weights are solved as follows:

$$\lambda_0 = C^{-1} \cdot c_0 \; ;$$
$$C(|h| = 0) = C_0 + C_1 \qquad\qquad 4$$

C: the covariance matrix derived from $n \times n$ observations
c_0: the vector of covariances at new locations
λ_0: the vector of Kriging weight

The relation between covariance and semivariance is as shown below:

$$C(h) = C_0 + C_1 - \gamma(h) \qquad\qquad 5$$

$C(h)$: the covariance function
$\gamma(h)$: the semivarience function

Another assumption of Ordinary Kriging is that the data do not follow a trend (Zimmerman and Stein, 2010). In groundwater there is almost a trend indicating either a general increase or decrease in hydraulic head temporally or spatially, or a seasonal pattern (Σπυρόπουλος, 2021; Στεργιου, 2021). These trends can be described deterministically as a polynomial or harmonic equation resulting from the analysis of the recorded data. For a spatial analysis, as performed in this work, only spatial trends can be determined. The first order polynomial trend surface model is as follows:

$$\mu(s; \beta) = \beta_0 + \beta_1 s_1 + \beta_2 s_2 \qquad\qquad 6$$

s: the coordinates of the surface model
μ: the mean value at s_1 and s_2 coordinates
β: the unrestricted parameters

1.2.1.1 Semivariogram Models

A list of the most used theoretical semivariograms is presented below, including the spherical, Gaussian, exponential, power law and linear functions.

$$\text{Exponential: } \gamma_z(\boldsymbol{r}) = \sigma_z^2 \left[1 - \exp\left(-\frac{|\boldsymbol{r}|}{\xi}\right)\right] \qquad 7$$

$$\text{Spherical: } \gamma_z(\boldsymbol{r}) = \sigma_z^2 \left[\frac{1.5|\boldsymbol{r}|}{\xi} - 0.5\left(\frac{|\boldsymbol{r}|}{\xi}\right)^3\right] \theta(\xi - |\boldsymbol{r}|)$$
$$\text{if } \xi - |\boldsymbol{r}| < 0, \theta = 0, \text{else if } \xi - |\boldsymbol{r}| > 0, \theta = 1 \qquad 8$$

$$\text{Gaussian: } \gamma_z(\boldsymbol{r}) = \sigma_z^2 \left[1 - \exp\left(-\frac{r^2}{\xi^2}\right)\right] \qquad 9$$

$$\text{Power-law: } \gamma_z(\boldsymbol{r}) = c|\boldsymbol{r}|^{2H}, 0 < H < 1$$
$$c \text{ is the coefficient and H the Hurst exponent.} \qquad 10$$

σ_z^2: the variance
$|\boldsymbol{r}|$: the Euclidean norm of the lag vector $\boldsymbol{r}$
ξ: the characteristic length.(Goovaerts et al., 2005)

1.2.2 Basic Concepts of Self-Organizing Maps

Self-Organizing Maps or Kohonen maps were developed by Teuvo Kohonen as an alternative architecture to more traditional artificial network architectures. The main application related to this work is the spatial partitioning and organization of responses into topologically related subsets (Kohonen, 1990). Self-organizing maps have a large capacity for abstract classification, which can find application in hydrogeology due to the high level of abstraction in such physical problems (Nourani et al., 2016). The basis for the development of this type of networks is competitive learning. In this process, an observed set ($x(i)$) and a randomly (or semi-randomly) generated simulated set ($m(i)$) are iteratively compared, with the end result of the process being the best fitting simulated set that has the least distance from the observed set. A species proposed for the optimal placement of a $m(i)$ minimizes the expected r[th] power of the reconstruction error (Kohonen, 1990):

$$E = \int ||x - m_c||^r p(x)dx \qquad 11$$

E: the expected r[th] power of the reconstruction error
x: the vectorial input of observations
m_c: the reference vector
$p(x)$: the approximation to a continuous probability density function of x
dx: the volumetric distance
c: the index indicating the best fitting vector

1.2.3 Description of the Study Area

The study area includes the municipality of Tympaki, which is part of the Prefecture of Heraklion in Crete, Greece. The boundaries of the case study aligned with the boarders of the municipality, which has a permanent population of about 10.000 residents. The neighboring basin of Messara is one of the most agricultural areas of Crete. In order to meet irrigation needs, the Faneromenis Dam was built in 2005 in the eastern part of the case study. To the west of the case study lies the Libyan Sea, to the east the foot of Mt. Dikti,s to the north the mountain range of Psiloritis and to the south the much smaller mountain range of Asterousia. Finally, the case study is crossed by the rivers Koutsoylitis and Mageras.

In the study area the agricultural sector is quite developed and the intensity of production requires large amounts of irrigation water. Due to the geographical position of the area, the cultivation of olives, grains, fruits and vegetables, and citrus fruits is favorable. The cultivated area is about 4800 acres, most of which is dry cultivation of olive trees, which do not require irrigation water, since the needs are met by precipitation. The growing season of the crops begins around February and usually ends in the fall. It can be assumed that there is a high demand for water during the summer season. This demand is to a considerable extent by pumping groundwater (Stathatou, 2011).
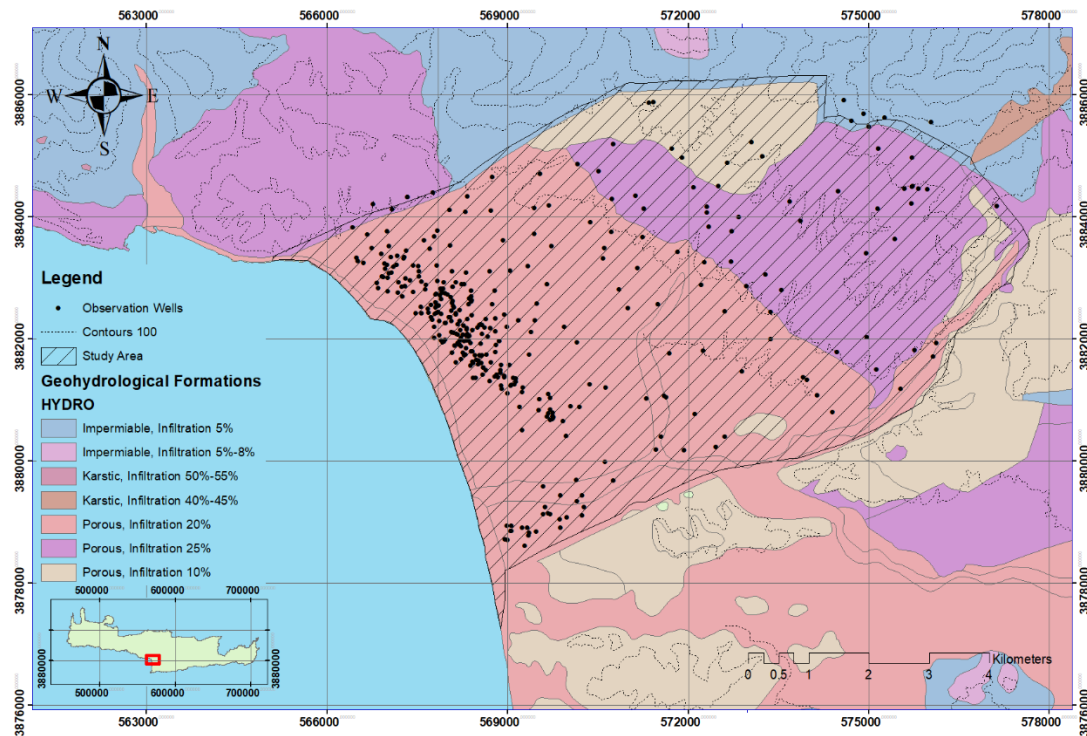
Figure 1.2: General map of the case study

Figure 1.1 above contains all case study information directly relevant to this work. The black dots represent all observation points (348 observations) used in this work. The hydraulic head value for each well is the mean hydraulic head value derived from two measurements, one during the wet season and one during the dry season of the hydrological year. Within the study area there are three distinct hydrogeological formations that comprise the hydrological basin. All formations within the study area are porous with varying percentages of infiltration. In general, most of the observation points are located near the coastal front of the study area where there is a plain with agricultural activities. The remaining observation points are scattered throughout the study area. They can be divided into smaller groups based on their location, which is influenced by local hydrogeological characteristics. In the southern part, there are subgroups influenced by the river discharge. In the northern part, the subgroups are influenced by the different hydrogeological formations, with all three different groups present. Additionally, the steep changes in altitude affect the hydraulic head values since all aquifers are unconfined. Finally, the subgroups can be differentiated by the location of the observation points in the study area. The exact definition of these subgroups is done with the algorithm of Self-Organizing map.

1.2.3.1 Geological Characteristics

The geology of Crete is characterized by the leptoid development of several tectonic sections resulting from processes that reached their peak the Tertiary period with the dipping of the African plate under the Eurasian plate. The lower geologic section consists of an indigenous system that includes plates of semi-transformed limestone slabs, underlying limestones, dolomites and shale intrusions. This is followed by a section of Neogenic and Quaternary deposits and sediments (Κριτσωτάκης, 2009).
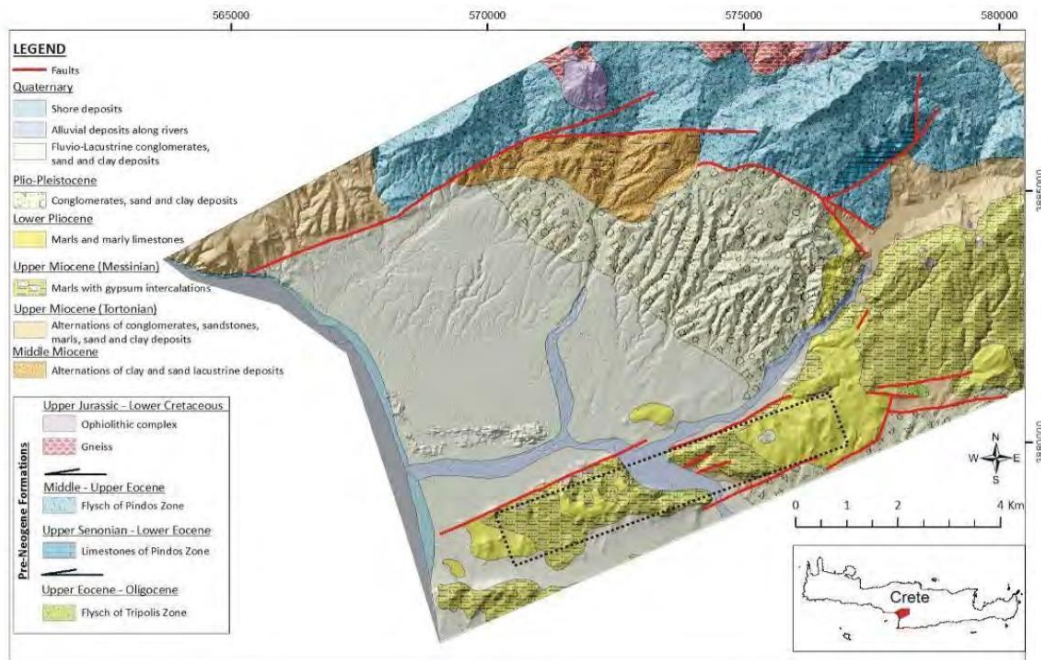
Figure 1.3: Geologic Map of Tympaki, the dotted lines show Phestos ridge (Panagopoulos et al., 2017)

The wider area of the Messara Plain is characterized by very heterogeneous alluvial formations with alternating horizontal and vertical silty and sandy cobblestones. However, in the case study the alluvial formations are spatially limited along the flow of Geropotamos River. In the lowlands of the area, a Pleistocene formation with fluctuating water permeability predominates. The sea level was at a lower level than today after the deposition of the Pleistocene formations, so new trenches were formed by the erosion of the Geropotamos watercourse. The maximum depth of these trenches was found to be 75 m below the present sea level in the Moires area and the maximum depth found in the wider area is 80 m in the Platy area (adjacent basin west of Tympaki). The depth of the ditch is of the order of 100 m from the ground surface, decreasing upstream and at the Phaistos ridge it is 60 m from the ground surface (Κριτσωτάκης, 2009). Below this system are several ditches that may cause variations, in recorded water depth in nearby wells. The case study contains 10 trenches most of which are located above some inland pumping wells, as shown below, which could locally affect hydraulic head locally (Panagopoulos et al., 2017). TO the east is Quaternary layer of plistogenic deposits mainly composed of marl with some proportions of sand and cobble stones, characterized by high water conductivity. To the north is a layer of myogenic deposits consisting of marl with low water conductivity. Outside the boundaries of the case study, to the northeast there is an impermeable flysch that belongs to the geological formation of the Pindos Mountains. In the

northeast of the case study there are myogenic deposits of cobblestone while outside the southern part there are myogenic deposits of marl.
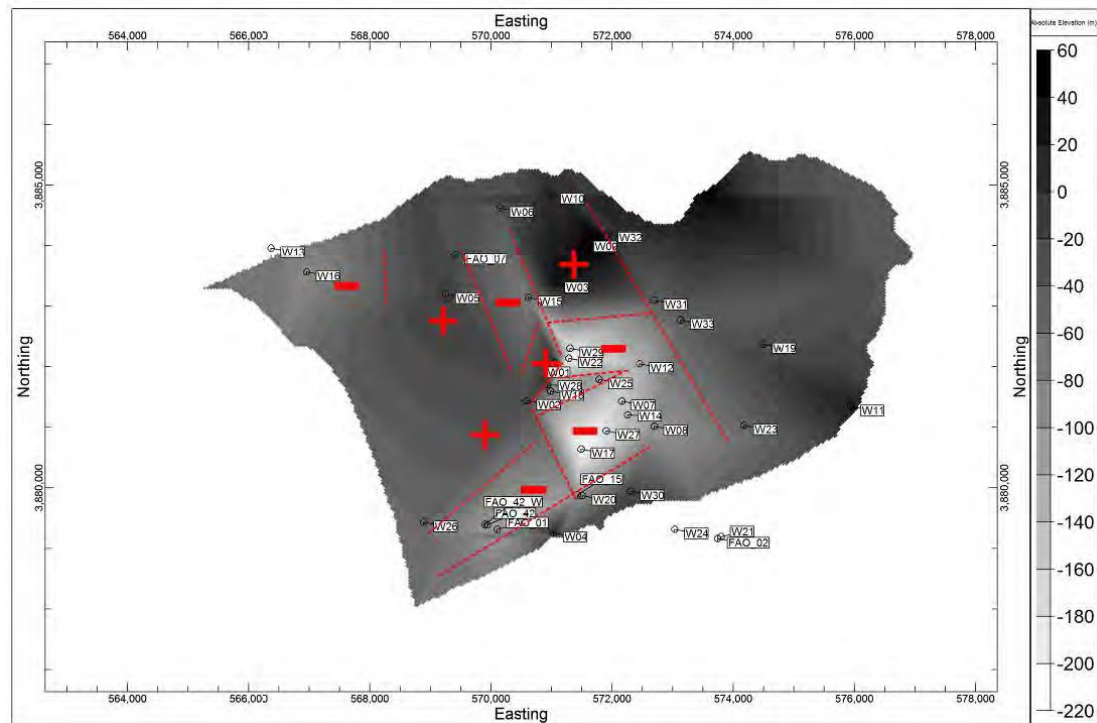
Figure 1.4: Map of the upper layer of neogenic deposits and trenches in Tympaki basin. (The legend indicates absolute altitude in meters) (Panagopoulos et al., 2017)

1.2.3.2   Hydrogeological Characteristics

In the wider area of Messara a change in the consumption of water resources was observed during the hydrological years 1973 to 2005, due to human intervention. The water demand in the south of the area is largely met by pumping groundwater along the watercourse that crosses the alluvial aquifer in the western part of Messara plain. To the southwest of the area is the Moira aquifer, which is fed by the Geropotamos and whose lower reaches feed the Pleistocene aquifer within the study area through the Phaistos Strait. The Messara alluvial basin is not hydrologically connected to the Tympaki basin in any other way. In addition, the formations outside the study area the north and south further isolate the study area hydrogeologically (Κριτσωτάκης, 2009).

The hydraulic profile height is well known from previous case study work. The higher values of hydraulic head are measured in the northern part, near the permeable formation which recharges the aquifers (Σπυρόπουλος, 2021; Στεργιου, 2021). Specifically, the case study can be broadly divided into 2 major formations consisting of alluvial material. At the seafront side the alluvial aquifer consists of broad material that has higher values of water conductivity. In addition to the minor changes in ground elevation, the hydraulic head appears to decrease slowly from west to east. The other formation consists of fine-grained material, with low values of hydraulic conductivity. As a result of this, the hydraulic head profile is steep the contours are closer to each other, as shown below (Dokou et al., 2017).
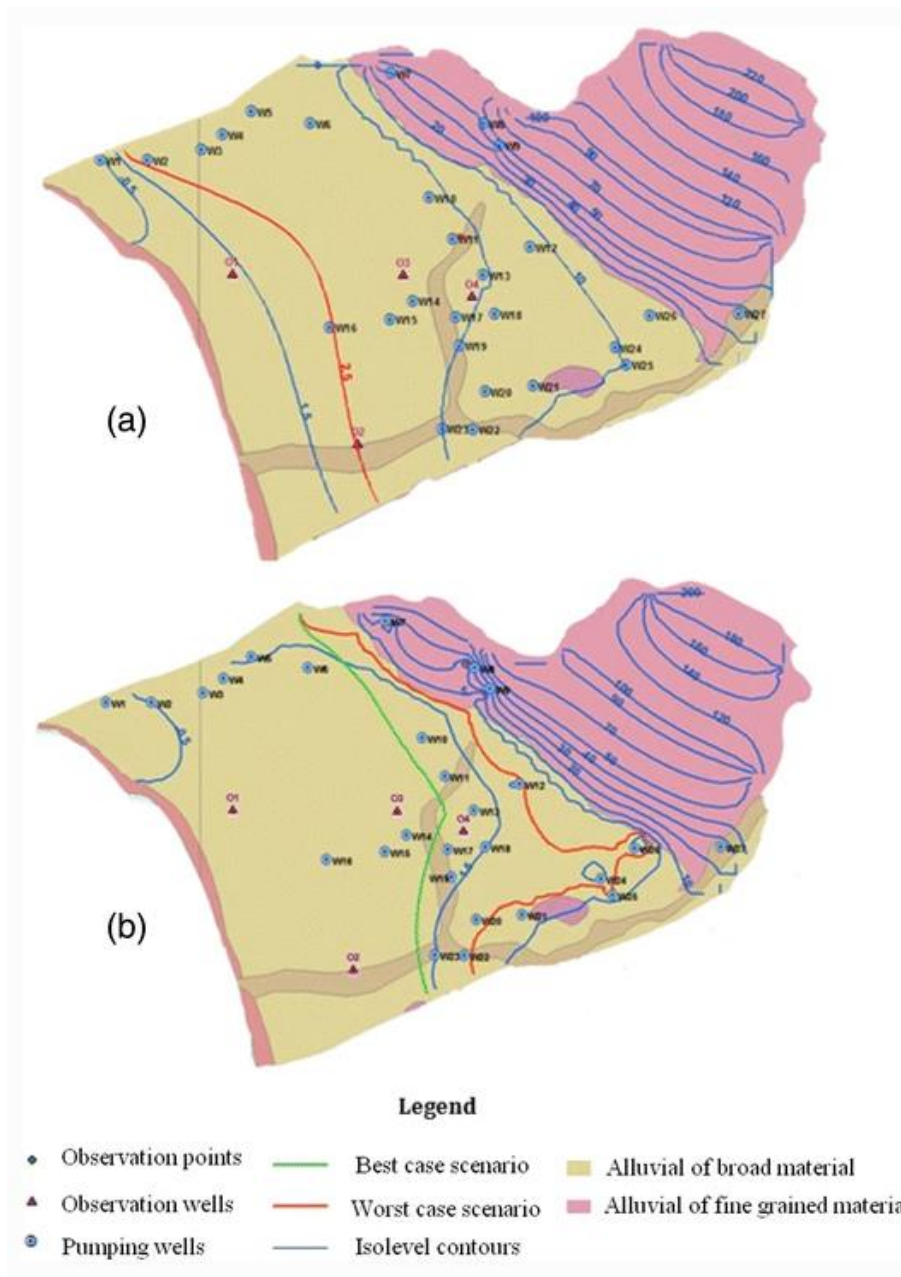
Figure 1.5: Hydraulic head contours the wet and dry period for the Tympaki aquifer (Dokou et al., 2017)

On the coastal front, salinization phenomena were observed due to agricultural activities in the area that mainly includes the Pleistocenic aquifer (Kourgialas et al., 2016). In another study the salinization front in the northern part was found to have penetrated further into the aquifer (2-3 km from the seafront) than the larger body of the intrusion zone (1 km from the seafront) (Vafidis et al., 2016). In the southern part, on the other hand, the saltwater intrusion zone appears to converge toward the seafront at the lower boundaries of the study area. This can be attributed to the semi-constant recharge of the aquifer by the Geropotamos River (Lollino et al., 2015)
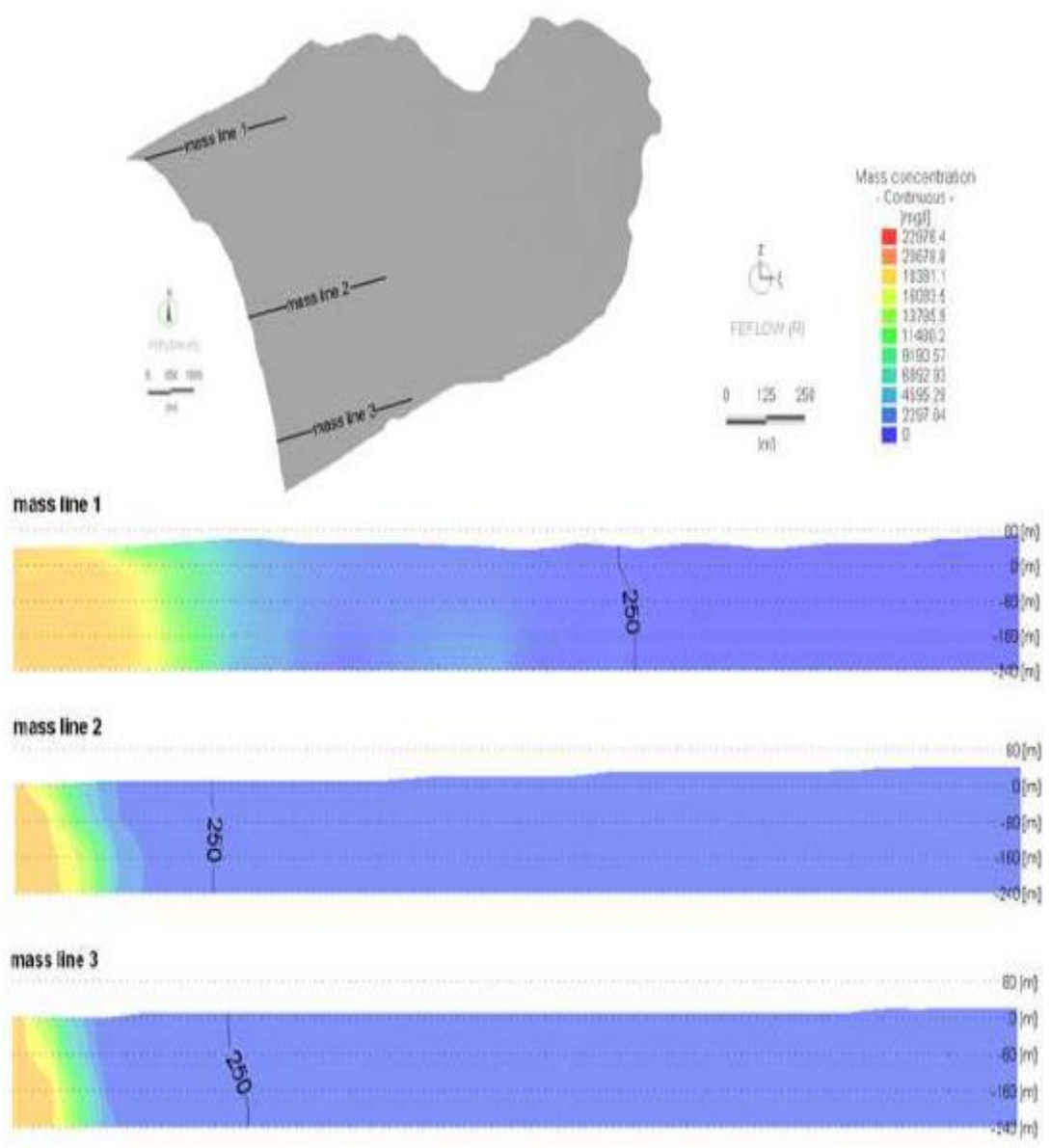
Figure 1.6: Salination intrusion zone in the coastal front of Tympaki, with three representative slices of the aquifer (Kourgialas et al., 2016)
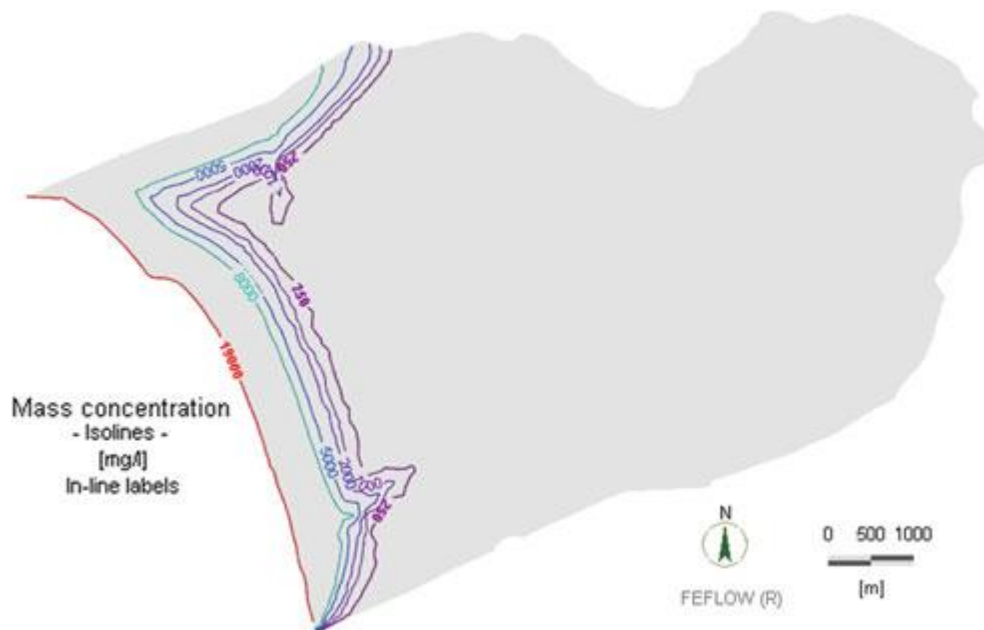
Figure 1.7: Map of mass concentration of chlorides (contours represent concentration mg/L) (Lollino et al., 2015)

In the case study, a fluctuation of precipitation is observed on an annual basis, with high values in winter and low to none in summer. There are also fluctuations in precipitation due to the topology of the study area. The northern part of the case study has the highest values. High values are also recorded in the southern part compared to precipitation in the valley, but lower than in the northern part. Both regions with high values can be explained by the distinctive morphology of Psiloritis Mountain and Phaistos Ridge (Paparrizos et al., 2016).
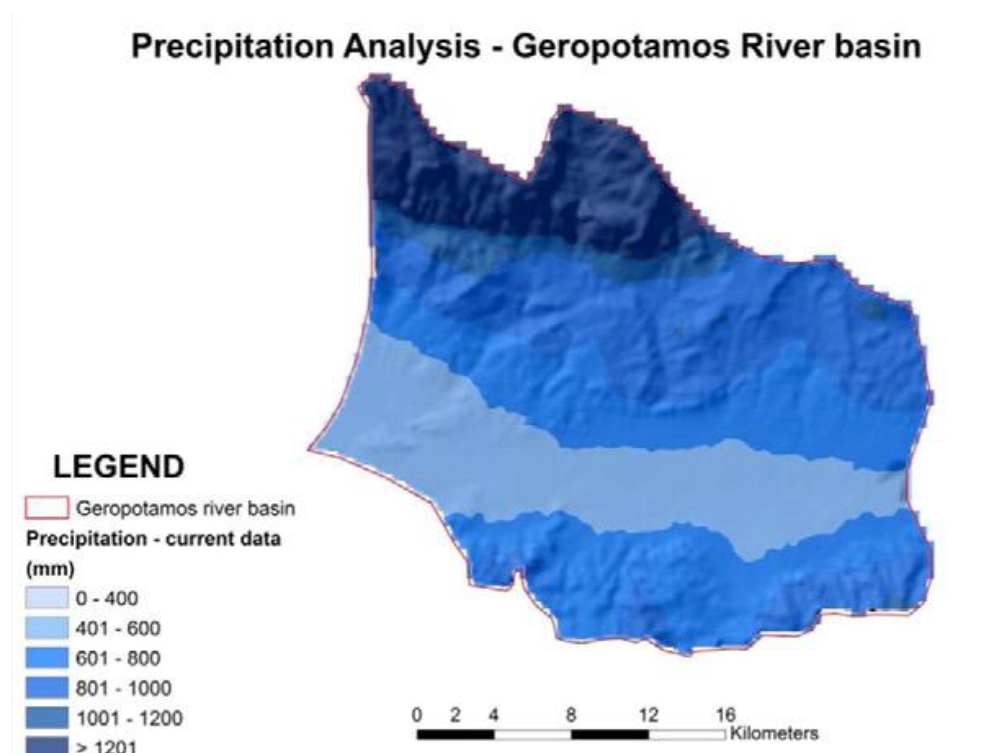
Figure 1.8: Yearly cumilative rainfall for the Geropotamos basin (greater area of Tympaki region) for the years 1981-2000 (Paparrizos et al., 2016)

1.3   Literature Review

Self-organizing maps (SOMs) have shown promising results in clustering observations using multi factor parameters. Such clustering has applications in numerous environmental disciplines. For example classifying areas covered by a particular vegetation using SOMs (Filippi and Jensen, 2006) or discriminating fish communities based on spatial distributions, land cover, environmental gradients and water quality (Kwon et al., 2012). From the cases presented above, it can be inferred that SOMs are capable of successfully classifying seemingly complex environmental datasets. With respect to hydrogeology, SOMs have found numerous applications in predicting groundwater quantity and quality. In the hydrogeochemical evolution of an aquifer, chemical concentration is strongly correlated with spatial distribution and SOMs can produce maps with different ranges of possible concentrations (Yu et al., 2018). SOMs can have inputs of spatial coordinates and concentrations, but can also include other factors such as water flow, geologic and hydrogeologic background and environmental stresses (Li et al., 2020; Zhu et al., 2020). Even more specific attributes can be added as inputs ,such as well depth or corresponding groundwater level and aquifer type (confined or unconfined) (Nakagawa et al., 2020).

Hydrogeologic applications of SOMs may include as inputs both quantitative data from field measurements and qualitative data that help characterize and define the system in question. For classification, quantitative inputs, such as ion concentration can be related to water salinity. By creating three classes foe water salinity (freshwater, moderate salinity and high salinity) the coastal aquifer case study was divided into different sections, allowing for better water use practices with relatively few observations (35 in total) (Belkhiri et al., 2018). In coastal aquifers, salinity concentration varies throughout the hydrologic year, and SOMs provide accurate concertation clustering for both wet and dry periods with no overlap between clusters (Amiri and Nakagawa, 2021). The lack of overlap on a spatial and temporal basis can result in clusters with well-defined characteristics and properties, even though they are being part of a larger connected system, such as an aquifer. Compared to other forms of clustering SOMs appear to outperform the more common k-means clustering and have similar results to fuzzy c-means (Lee et al., 2019). High-precision clustering has been used to pre-classify data inputs to other hydrologic and hydrogeologic models. In SWAT (Soil and Water Assessment Tool), SOMs can be used in defining Hydrologic Response Units (HRUs), by providing finely classified data for soil properties (Rivas-Tabares et al., 2020). In the DRASTIC models (**D**epth to water, net **R**echarge, **A**quifer media, **S**oil media, **T**opography, **I**mpact of vadose zone, and hydraulic **C**onductivity), SOMs clustering followed by Kriging extrapolation increased overall accuracy. Kriging extrapolation was used as means to validate clustering through the variograms generated, which ultimately defined the affection zone of each cluster(Rezaei et al., 2017). SOMs can also be used as surrogate models for hydraulic conductivity predictions that can be extrapolated to the entire case study by applying Kriging (Jiang et al., 2021). In addition, preclassification using SOMs can improve groundwater level predictions, when coupled with backpropagation network models for multiple sites in a case study. It is also important to note that the required inputs are spatial coordinates and groundwater level parameters that are easy to obtain (Chen et al., 2011). Methods that combine AI with Kriging can be applied to simulations of groundwater level and quality, not only in porous media but also in karstic springs(Canion et al., 2019).

SOMs can also explain the spatiotemporal relationship between surface and groundwater, by classifying data of groundwater flow, surface water flow and rainfall,

the generated maps describe the relationships among the above parameters (Chen et al., 2018). In a combination of SOMs and Kriging for groundwater level prediction, clustering was performed using the groundwater level observations from the well, then Kriging was performed for each cluster, and finally the best-fitting cluster was selected (Chang et al., 2016). The main difference between the aforementioned work and the present project is that Kriging is performed for the entire case study area even though the well data are clustered, while Kriging is performed separately for each cluster in this work. AI is well suited for nonlinear problems such as groundwater simulations, but in cases of contaminant concentrations with clear trends Kriging or deterministic approaches are more appropriate (Chowdhury et al., 2010). In groundwater contamination simulations, a multiple layer backpropagation network was used to classify danger zones and was compared to a single Kriging variogram (Kavusi et al., 2020). Artificial Neural Networks have also been used to compensate for the uncertainty of the semivariogram in Kriging methods (Senoro et al., 2021).

Kriging can be a robust method for predicting and monitoring groundwater levels or quality, from OK which is the most common technique to Co-Kriging which is the multivariable equivalent of OK (Belkhiri et al., 2020). Spatiotemporal analysis with Kriging is achieved by performing several different Kriging analysis at different timeframes, the results of this technique create multiple maps that can show the evolution of a phenomenon and as before multiple Kriging techniques when used together can provide more accurate results (Rostami et al., 2020). While OK has many applications for spatiotemporal analysis, it is also appropriate in regions with declining trends in groundwater levels (Hasan et al., 2021). In addition, OK can be used to monitor groundwater quality. In a case study, it was coupled with sequential Gaussian simulation for smoothing purposes, an issue that OK faces (Aryafar et al., 2020). In terms of quality, Indicator Kriging was applied, where a threshold for detection is set, resulting in reliable neighbors (Kechiched et al., 2020). In another work, Ordinary and Indicator Kriging were used to simulate arsenic contamination, with OK performing better than IK despite sample heterogeneity (Liang et al., 2018). However, IK is not applicable in modeling groundwater levels because there is no detection threshold and even negative values contain important information about the heterogeneity of the system under study. Finally, Empirical Bayesian Kriging is a technique that replicates and partitions observed data and can compensate for uncertainty in semivariogram, making it an ideal technique for modeling small data sets; sometimes it outperforms OK (Bouhout et al., 2022; Senoro et al., 2021).

In summary, AI is a promising tool for improving Kriging methods. In particular SOMs have shown promising results in several different methods, although most of their applications are a stage of classification after performing Kriging. Moreover, pre-classification of datasets enhances the performance of Kriging methods, but this rarely happens when SOMs are used. In this work, pre-classification with SOMs aims to form classes whose distinguishing features are spatial coordinates and groundwater level. The intention behind this, is to create of possible neighborhoods where observations are more correlated compared to the correlation between all observation points throughout the case study area. Finally, regarding the Kriging techniques studied, OK seems to be the most commonly used in the literature. Although it is the simplest, it has reliably shown robust results commensurate with other more complex techniques. Considering this and the fact that the proposed methodology combines the two tools in a previously unexplored way, OK is considered the most appropriate technique for the purposes of this work.

2   Methodology
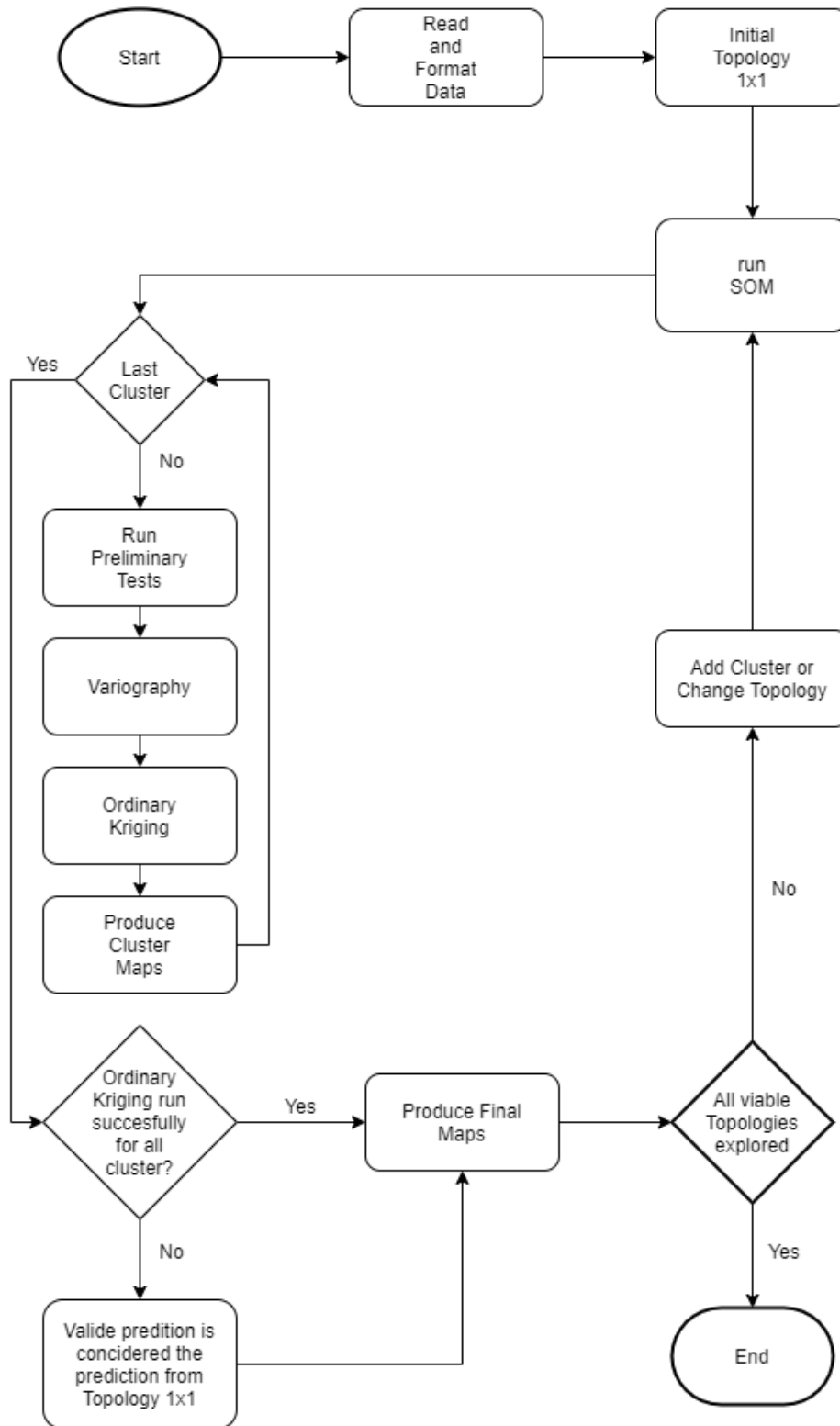
Figure 2.1: Flowchart of the Proposed Methodology

In this work the main data set consists of 341 observations containing X-Y coordinates and hydraulic head value. The objective of this work is to define sub-datasets that will improve the Ordinary Kriging results. The proposed methodology proceeds as follows: Performing OK on the entire dataset, investigating different pre-classification arrangements (topologies) and evaluating the performance of OK for each topology. This rudimentary analysis of the methodology is explained in more detail below.

The first step of the algorithm is to read and format the required data. The data are organized in a table format to facilitate calculations in MATLAB. They are formatted into coordinates and hydraulic head values, which are generally the inputs to both SOM and OK.

The initial topology is set to 1x1 which is the baseline for evaluating all the different topologies.

The SOM algorithm forms the pre-classification part of the methodology. The inputs of the SOM model are the X-Y coordinates and the value of the hydraulic head. The outputs are the same values but classified in clusters. This selection ensures that the classification is based on the location of the observations in the field and the various hydraulic properties or conditions that are correlated to the hydraulic head value. In this use of SOM each observation is assigned to a single cluster, and OK is applied to each cluster separately. There is a possibility of overlapping predictions from OK, but only for small areas at the boundaries of each cluster (Amiri and Nakagawa, 2021). It is worth noting that a cluster that underperforms compared to the original topology has no effect on a cluster that performs acceptably or better than the original topology. Each different combination of clusters constitutes a topology, e.g., the first topology for which Kriging is performed is 1x1, i.e., a single cluster, i.e., the entire dataset; therefore, SOM is not required for this topology. Adding another cluster results in two more possible topologies,1x2 and 2x1 since it is possible that the classification results in a cluster with different observations in each cluster. Both of them are investigated. In the 2x2 topology, this problem does not exist. In 2x3 and 3x2 the process is the same as above, and again they are examined last. In more granulated topologies it is not guaranteed that each cluster will contain a viable amount of observations for OK to be performed. In summary the SOM algorithm either classifies correlated observations among themselves or exclude uncorrelated observations and overall refines the inputs from OK.

The preliminary studies refer to the hydraulic head values. The statistical parameters determined are minimum value, maximum value, median value, mean value, standard deviation, skewness and kurtosis. These tests are important to determine if a subset of data follows the normal distribution, which is one of the main assumptions of Kriging (Hengl et al., 2007). In this work, it is validated by plotting and comparing the empirical and gaussian cumulative probability density functions. Voronoi polygons are created as an indicator of the possible Kriging prediction.

Variography in Ordinary Kriging requires detrended data sets. In all clusters, the only trend in the hydraulic head value was a linear decrease in correlation with altitude, i.e., from inland to coastal front. Trend prediction is evaluated by the Correlation Coefficient and Mean Absolute Error between the linear trend model and the data. By removing the trend from the data set the hydraulic head values are converted to variations in hydraulic head. Empirical isotropic variograms were created for all clusters and then compared to 4 different theoretical variogram models. These

were an exponential, a spherical, a gaussian and a power law, of which the power law was generally considered the most appropriate. If a cluster could not produce a variogram that matched one of the theoretical models and the relationship between all clusters was not completely linear, the variogram from the 1x1 topology was used to determine the input parameters for Kriging.

The Kriging technique was used in this work is Ordinary Kriging. OK requires as input the X-Y coordinates, the derived values of the hydraulic head (fluctuations), the range obtained from the variography, the theoretical model estimated from the variography and the radius of the neighborhoods. Validation of the estimates is performed by measuring the Mean Error, Mean Absolute Error, Root Mean Squared Error and Correlation Coefficient between the estimated and derived values. Finally, two maps are produced for each cluster containing the estimates at the validation points and the standard deviation at the validation point.

The predictions are a result of an iterative process requiring multiple tests, in order to secure that the assumptions taken by Kriging are satisfied. The results of those test are presented in the Kriging Results chapter and are repeated for each topology. In this section, the graphs yielded from each topology are briefly presented. The first graph is the spatial distribution of observations in each cluster produced by the SOM algorithm. The second graph contains a histogram with the all the hydraulic head values in the cluster and the empirical cumulative probability curve. The third graph utilizes the empirical cumulative probability curve to fit it to a gaussian theoretical curve, this step is one the most important step in the process, since for the performance of Kriging; the empirical and gaussian theoretical cumulative probability curves should be approximate to each other. The following set of graphs describe the process of detrending the subsets of data, starting from the fourth graph which is the Voronoi polygons for each cluster. This graph is not required but is an added test to confirm that the fifth graph which is the linear trend of hydraulic head values in each cluster is correct. After the detrending, variography is performed as described above, in each cluster. The sixth graph contains the variograms, in which the observations are fitted to one of the theoretical models mentioned in the semivariogram models' section. This step requires trial and error to some extent, since there is no reliable technique to predetermine the best fitting model, in the results section the best fitting models are presented. The seventh graph depicts the frequency of the values of cross validation errors from the Kriging estimation. The eighth graph contains the Ordinary Kriging (OK) estimation of hydraulic head values within the domain of each cluster. Finally, the ninth graph contains the OK standard error deviation which is an additional visual metric for the assessment of uncertainty of the prediction.

2.1 Validation Criteria
2.1.1 Error

$$Error = Y_i^{obs} - Y_i^{sim} \qquad\qquad 12$$

2.1.2 Mean Absolute Error (MEA)

$$MEA = \sum_{i=1}^{n} \frac{|Y_i^{obs} - Y_i^{sim}|}{n} \qquad\qquad 13$$

2.1.3 Root Mean Squared Error (RMSE)

$$RMSE = \sqrt{\sum_{i=1}^{n} \frac{(Y_i^{obs} - Y_i^{sim})^2}{n}} \qquad\qquad 14$$

2.1.4 Correlation Coefficient (CC)

$$CC = \frac{n\sum_{i=1}^{n} Y_i^{obs} \cdot Y_i^{sim} - \sum_{i=1}^{n} Y_i^{obs} \cdot \sum_{i=1}^{n} Y_i^{sim}}{\sqrt{\left[n\sum_{i=1}^{n} Y_i^{obs\;2} - \left(\sum_{i=1}^{n} Y_i^{obs}\right)^2\right] \cdot \left[n\sum_{i=1}^{n} Y_i^{sim\;2} - \left(\sum_{i=1}^{n} Y_i^{sim}\right)^2\right]}} \qquad 15$$

Y_i^{obs}: the observed value
Y_i^{sim}: the simulated value

3 Results
## 3.1 Self-Organizing Map Results
3.1.1 Topology 1x2
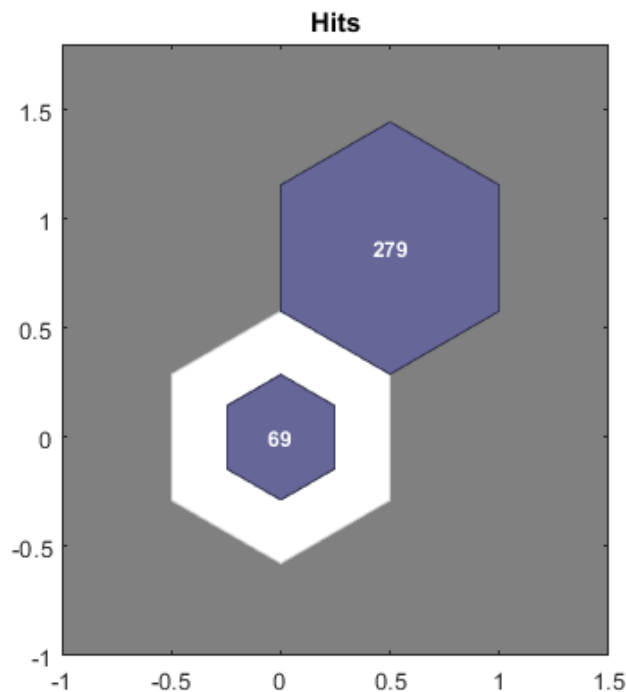


Figure 3.1: Distribution of observations in clusters 1-2
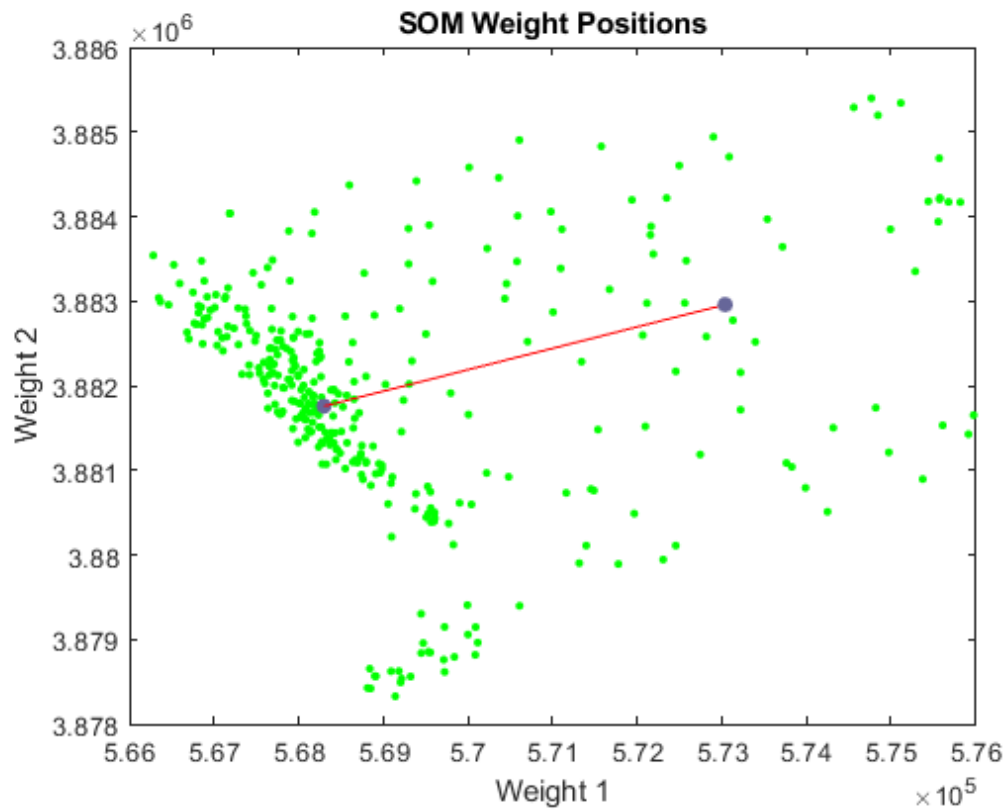
Figure 3.2: Spatial distributions of observations and their related cluster

3.1.2 Topology 2x1
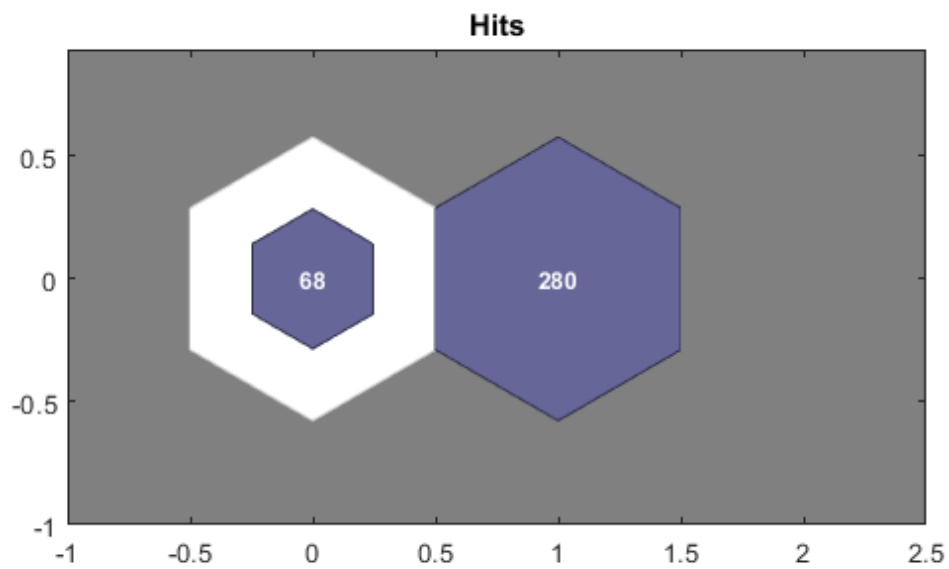
*Figure 3.3: Distribution of obsevrations in clusters 1-2*
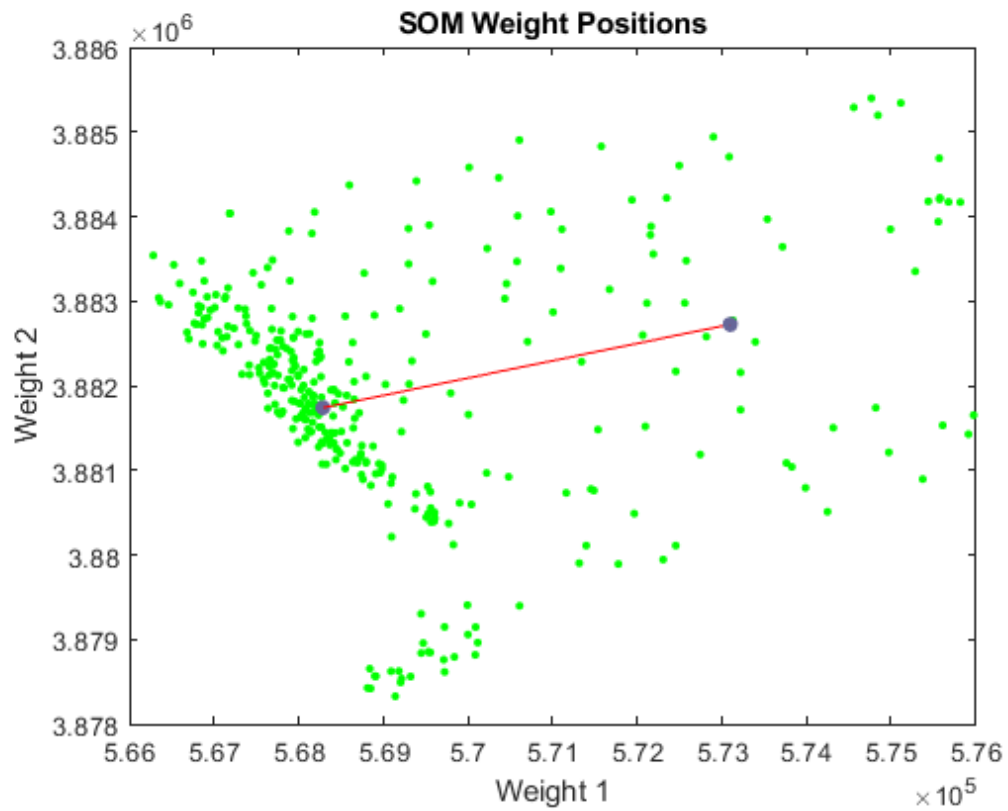
Figure 3.4:Spatial distributions of observations and their related cluster

3.1.3 Topology 2x2
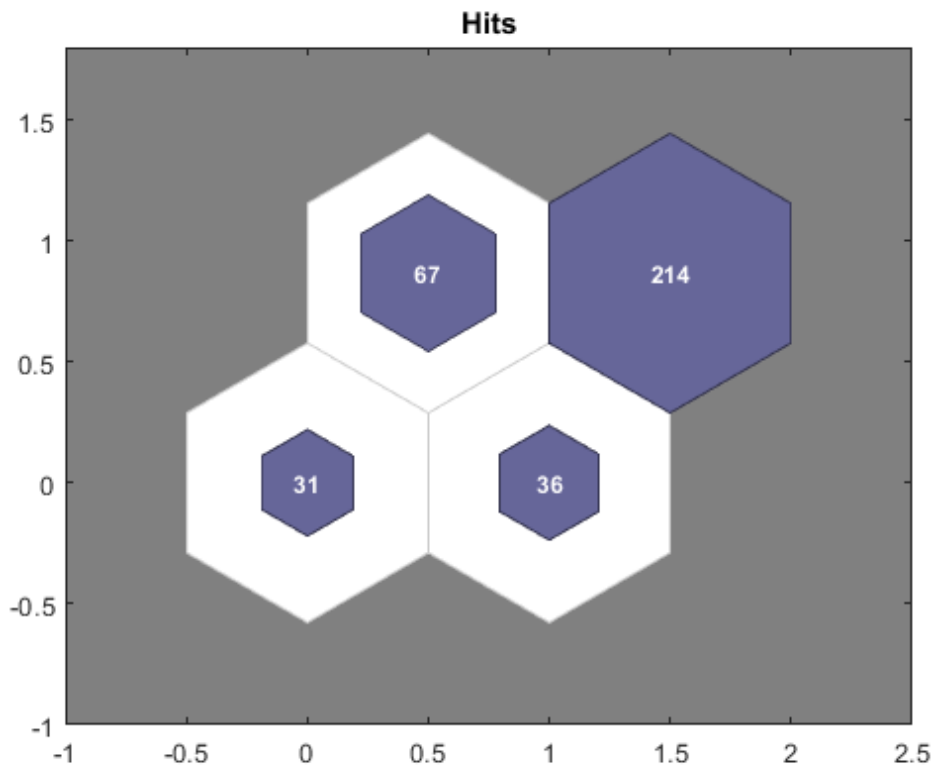
*Figure 3.5: Distribution of obsevrations in clusters 1-2, 3-4 (bottom to top)*
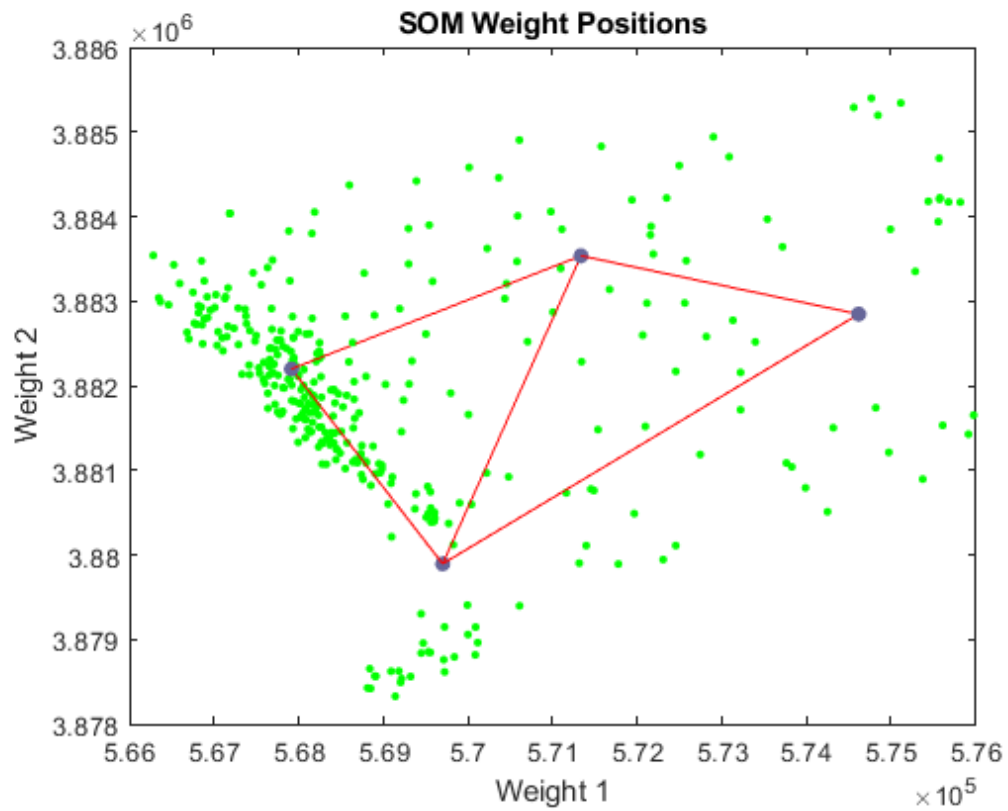
Figure 3.6: Spatial distributions of observations and their related cluster

3.1.4 Topology 2x3
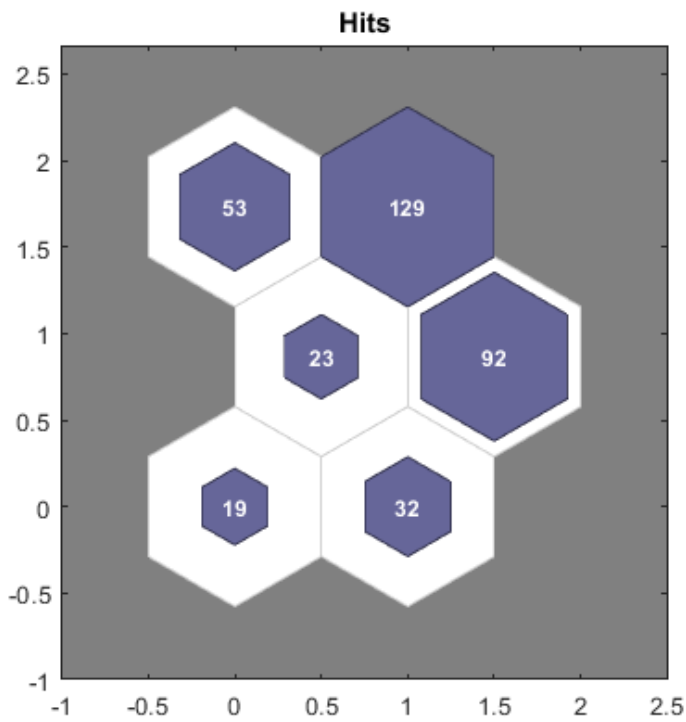
Figure 3.7: Distribution of obsevrations in clusters 1-2, 3-4, 5-6 (bottom to top)

Figure 3.8: Spatial distributions of observations and their related cluster

3.1.5 Topology 3x2
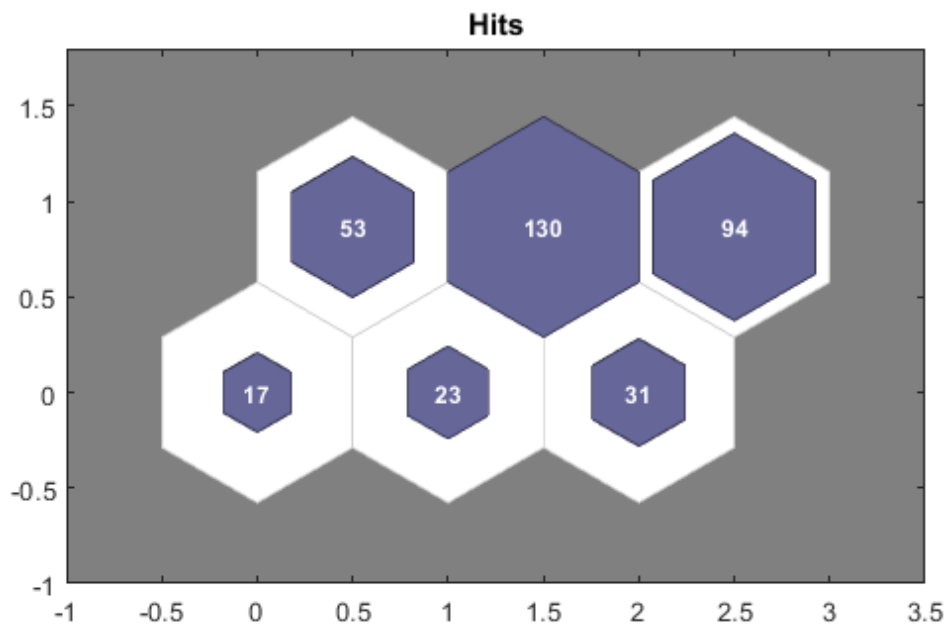
Figure 3.9: Distribution of obsevrations in clusters 1-2-3,4-5-6 (bottom to top)

Figure 3.10: Spatial distributions of observations and their related cluster

3.2 Kriging Results

3.2.1 Topology 1x1
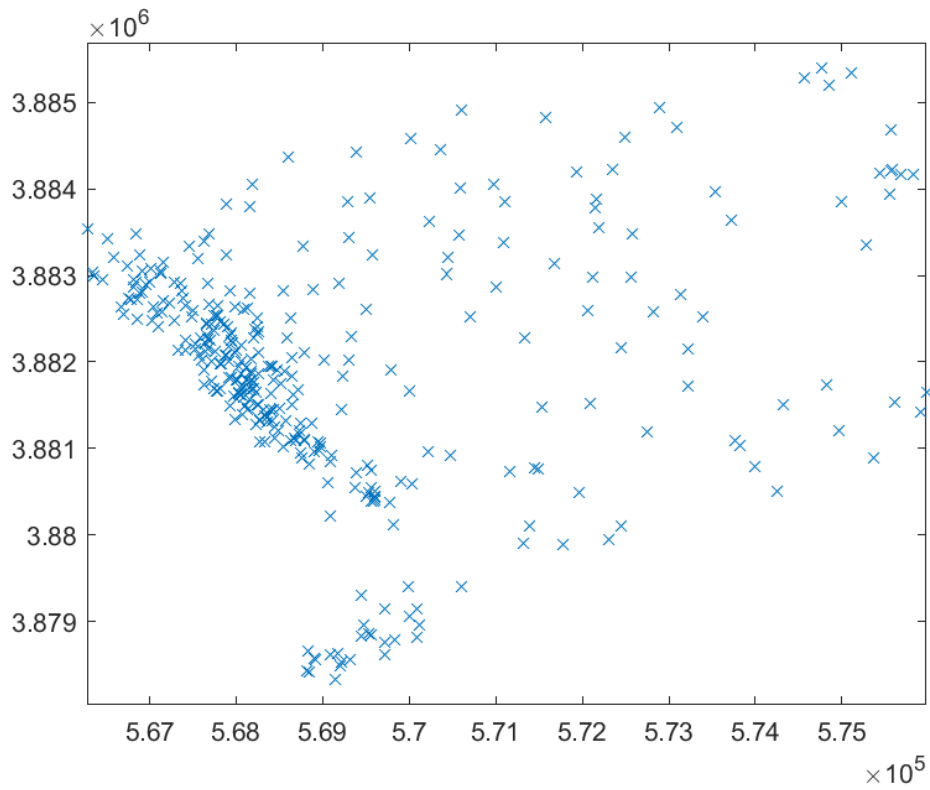
*Figure 3.11: Spatial distribution of observation points in the whole case study*
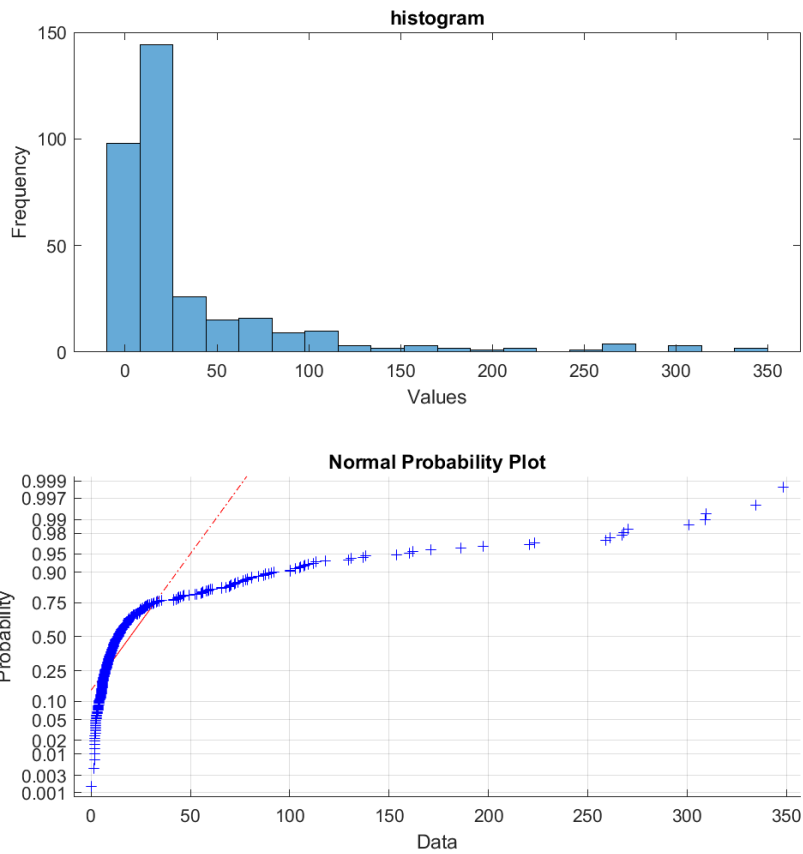
Figure 3.12: Histogram and probability curve for all hydraulic head values
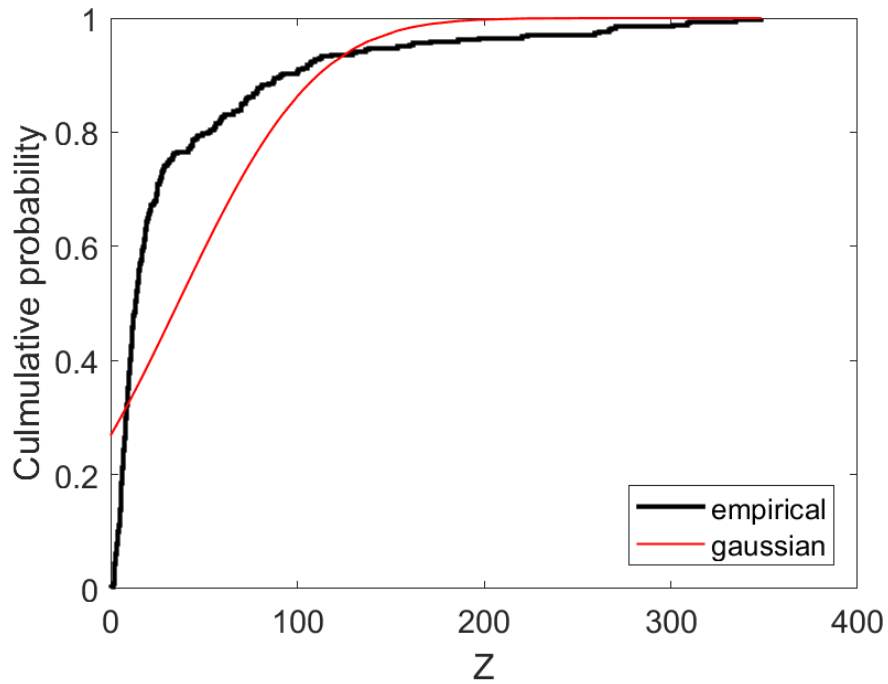
Figure 3.13: Cumulative Probability curve empirical and theoretical gaussian over all hydraulic head values
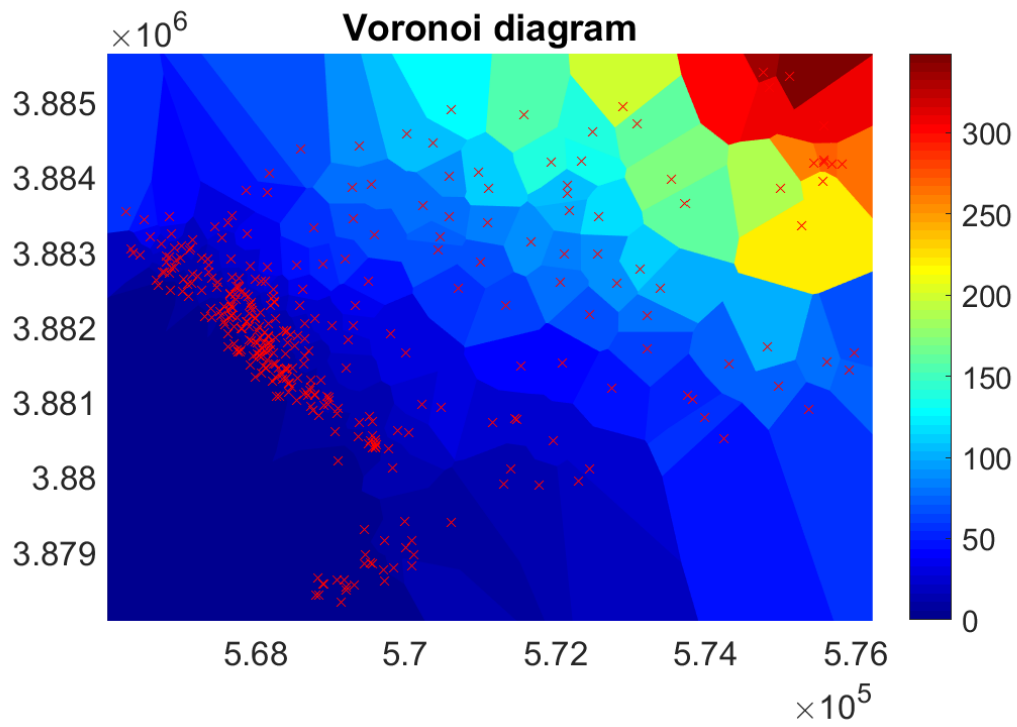
Figure 3.14: Voronoi polygons for hydraulic head observation points in the whole case study
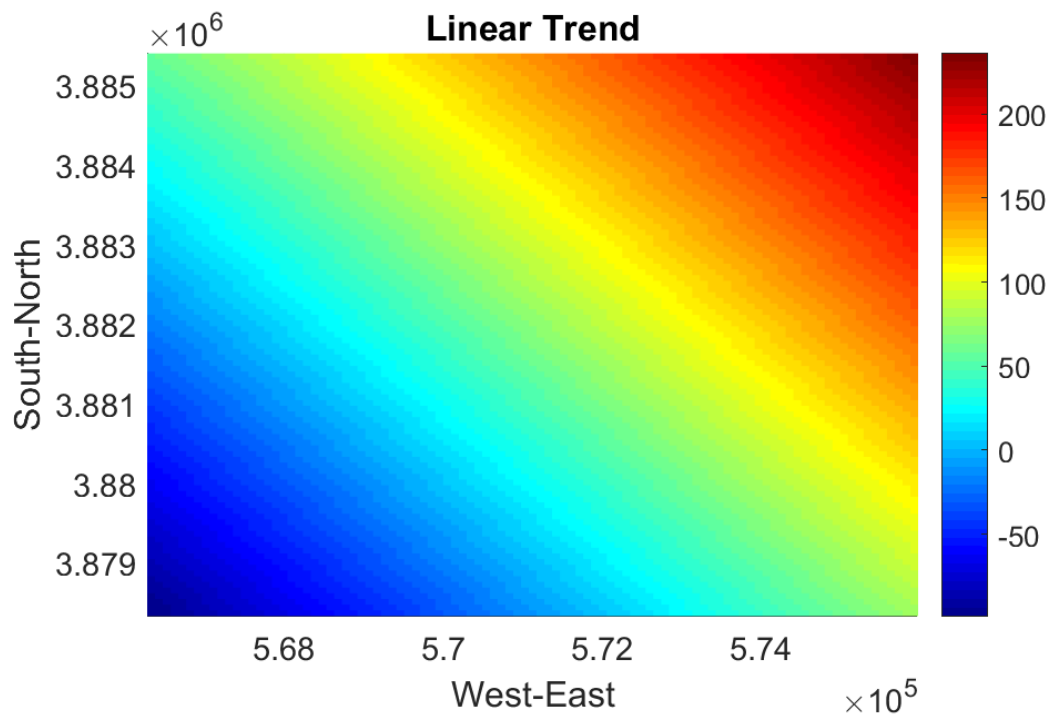
Figure 3.15: Linear trend over the case study
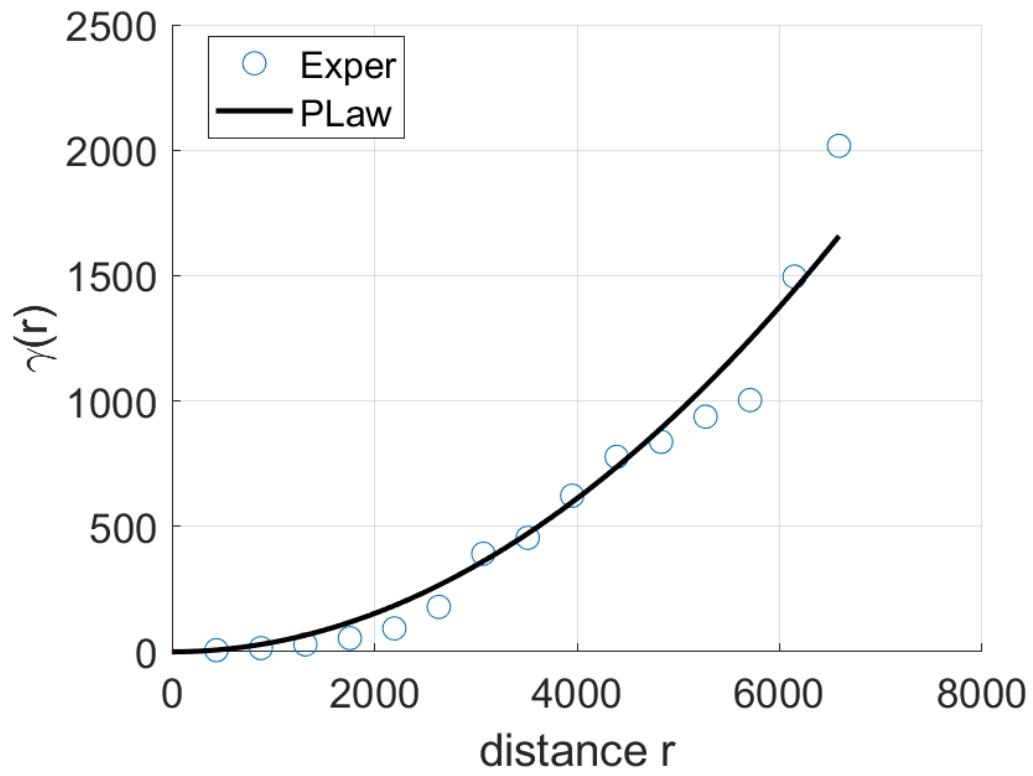
Figure 3.16: Global Variogram
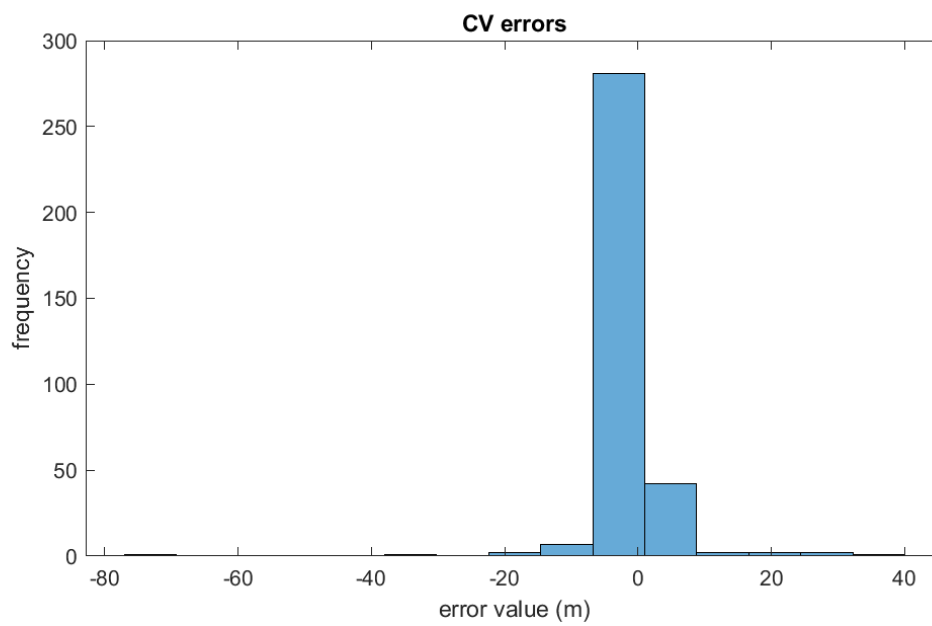
Figure 3.17: Cross Validation errors for all estimations of topology 1x1
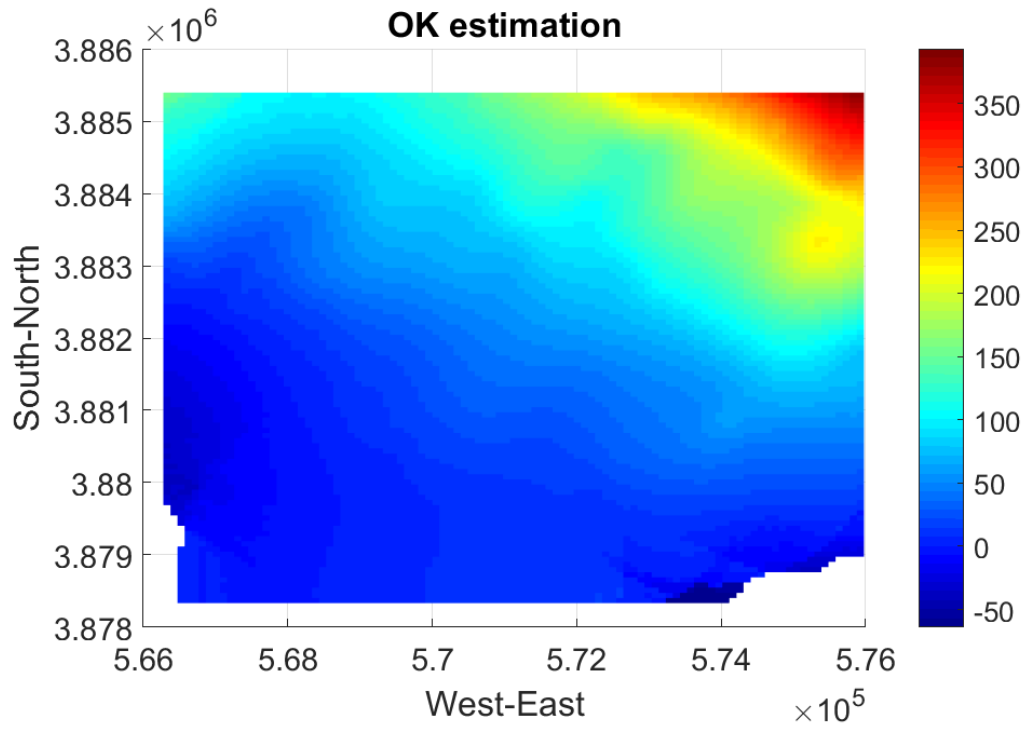
Figure 3.18: Ordinary Kriging estimation for the whole case study
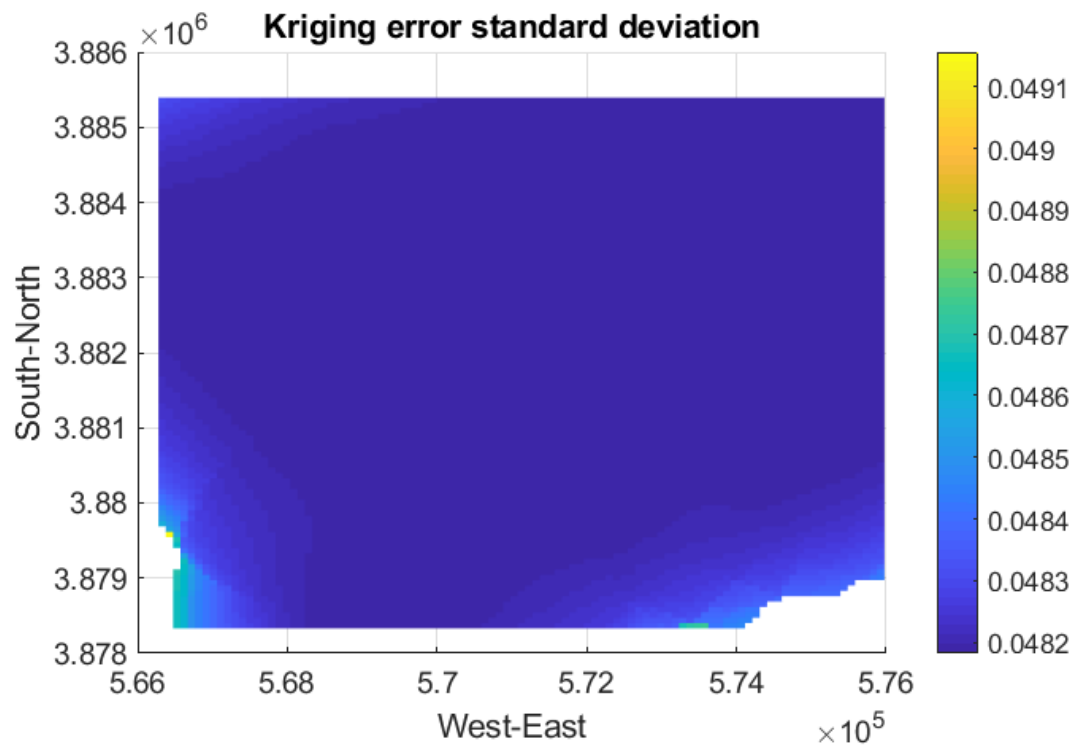
Figure 3.19: Kriging error standard deviation the whole case study

3.2.2 Topology 1x2
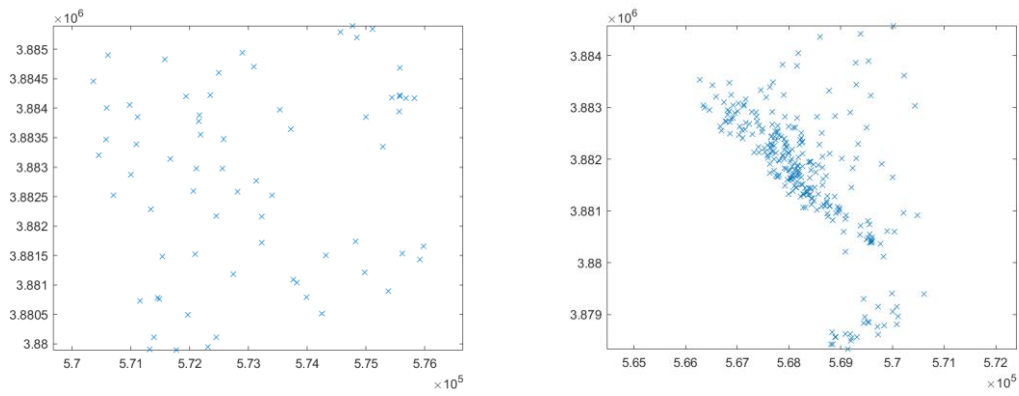
Figure 3.20: Spatial distribution of observation points for clusters 1-2
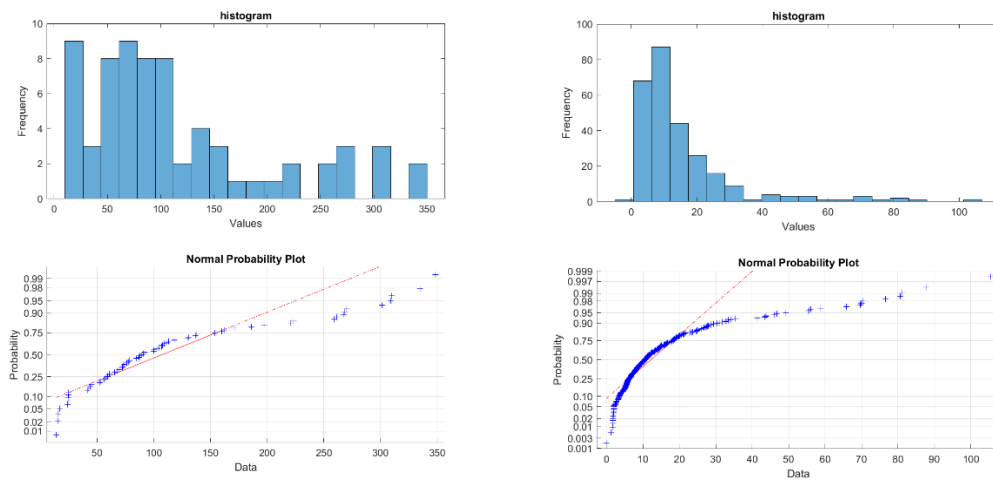
Figure 3.21: Histogram and probability curve for clusters 1-2
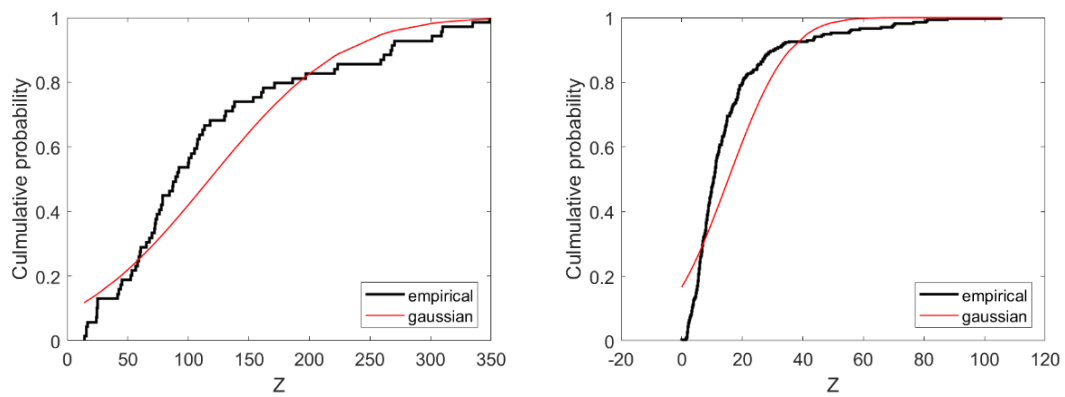

Figure 3.22: Cumulative Probability curve empirical and theoretical gaussian for clusters 1-2
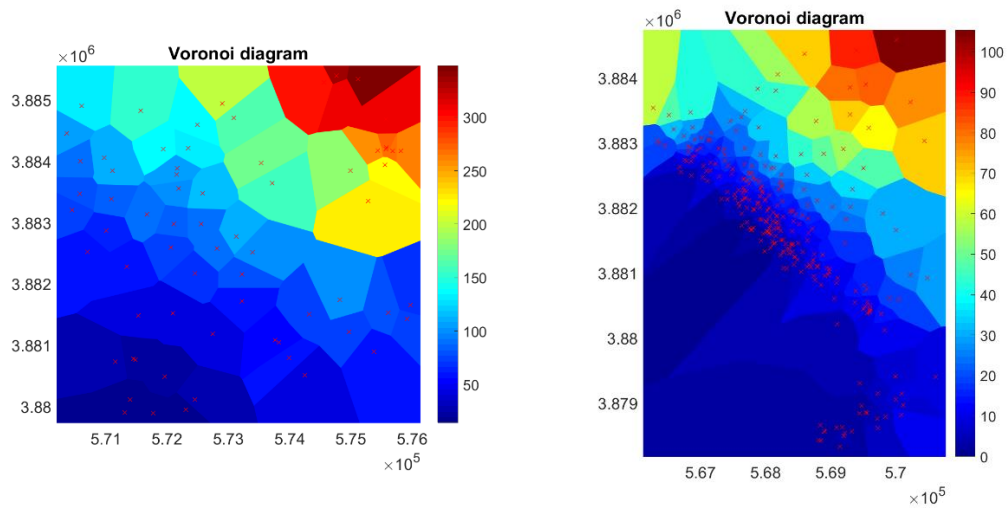
Figure 3.23: Voronoi polygons for hydraulic head observation points for clusters 1-2
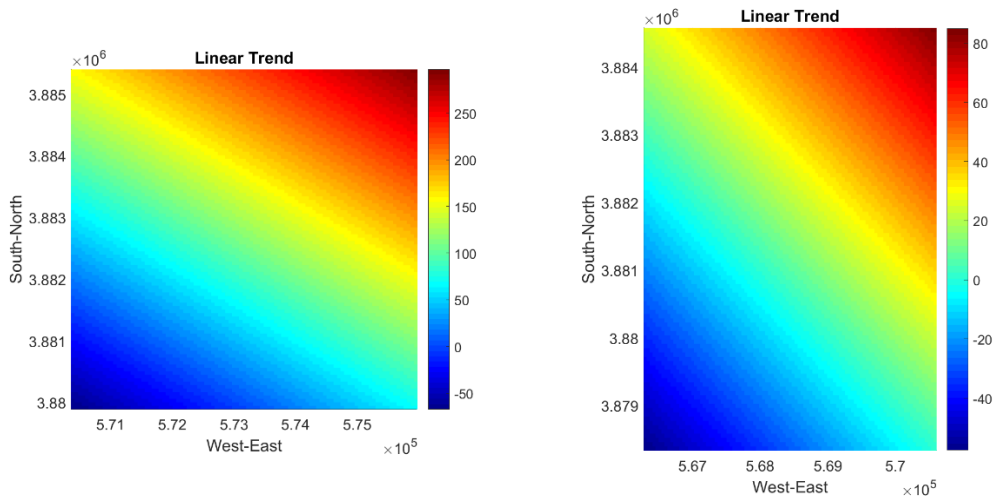
Figure 3.24: Linear trend for clusters 1-2
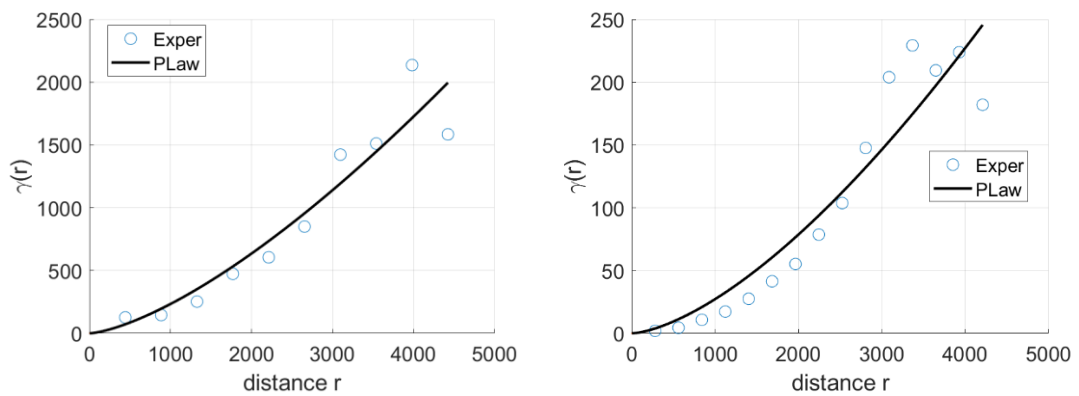
Figure 3.25: Variograms for clusters 1-2
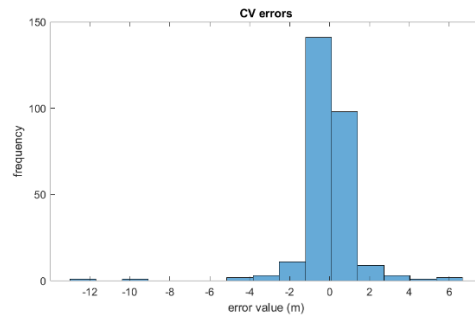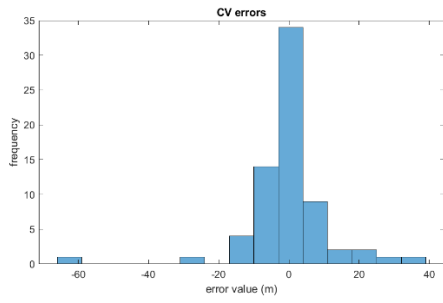
Figure 3.26: Cross Validation errors for estimations of clusters 1-2
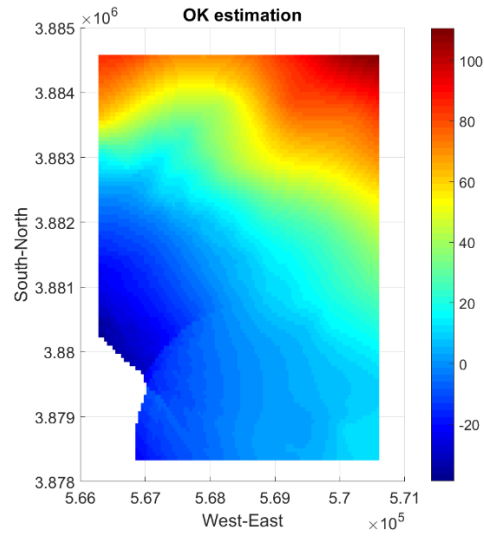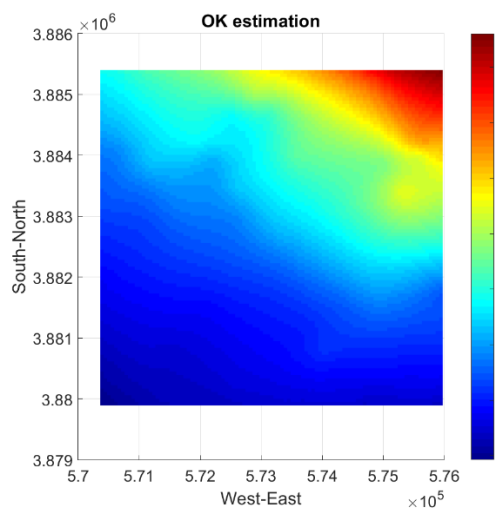
Figure 3.27: Ordinary Kriging estimation for clusters 1-2
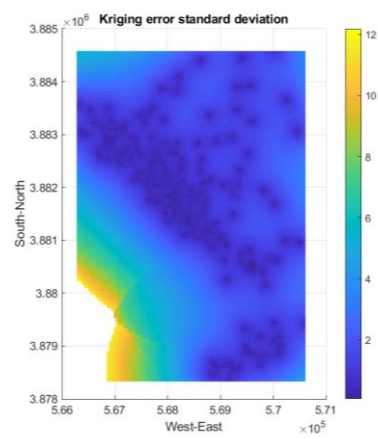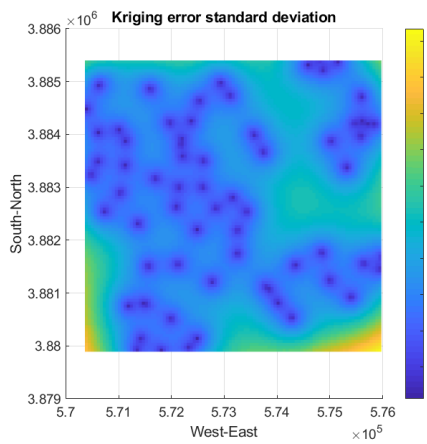
Figure 3.28: Kriging error standard deviation for clusters 1-2

3.2.3 Topology 2x1
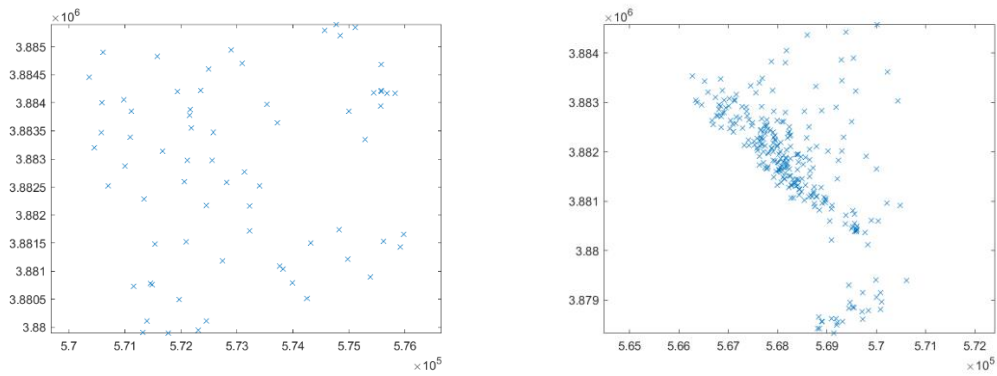
Figure 3.29:Spatial distribution of observation points for clusters 1-2
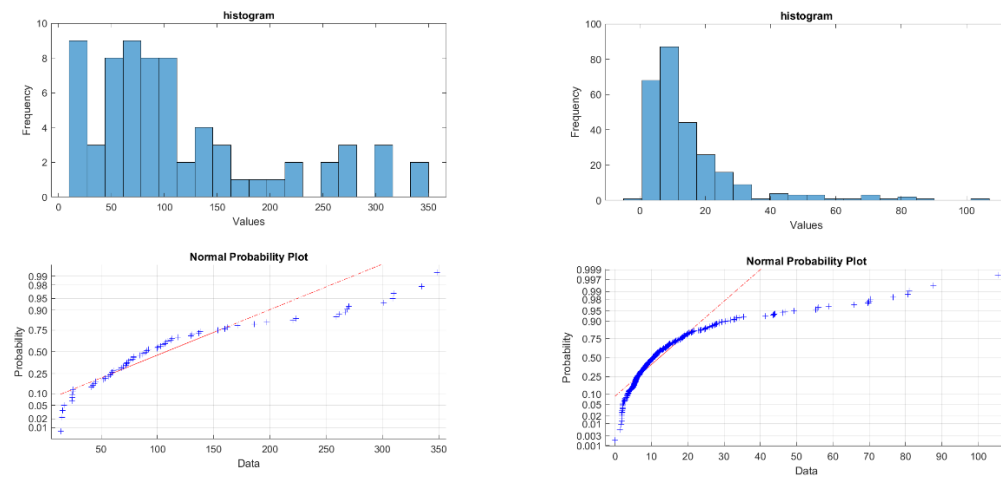
Figure 3.30: Histogram and probability curve for clusters 1-2
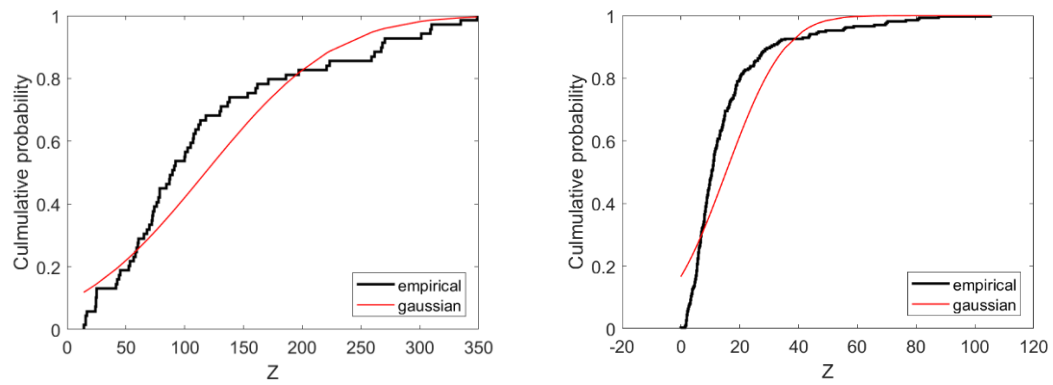
Figure 3.31: Cumulative Probability curve empirical and theoretical gaussian for clusters 1-2
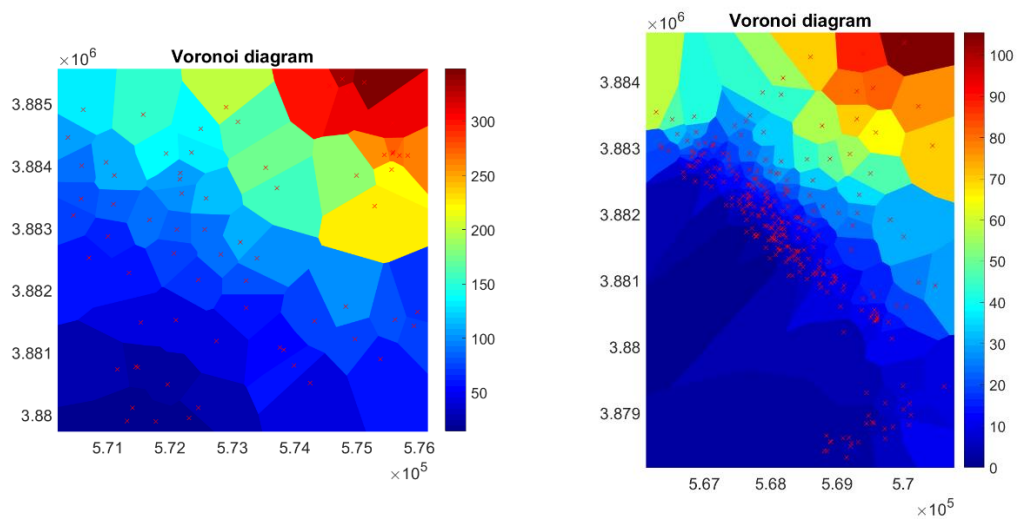
Figure 3.32: Voronoi polygons for hydraulic head observation points for clusters 1-2
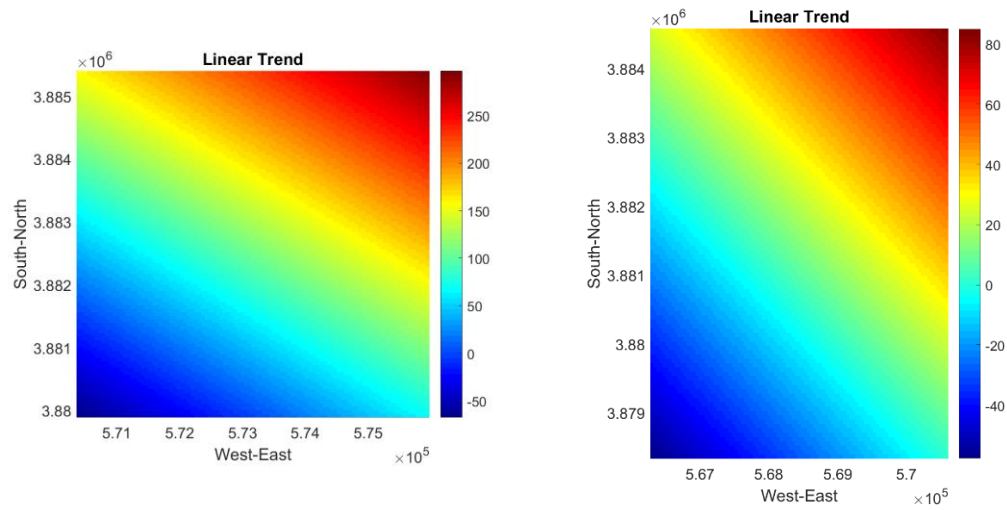
Figure 3.33: Linear trend for clusters 1-2
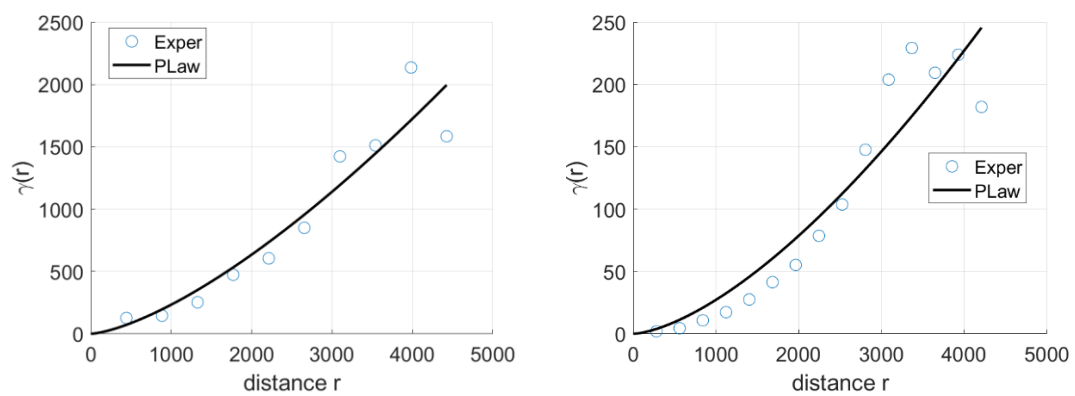
Figure 3.34: Variograms for clusters 1-2
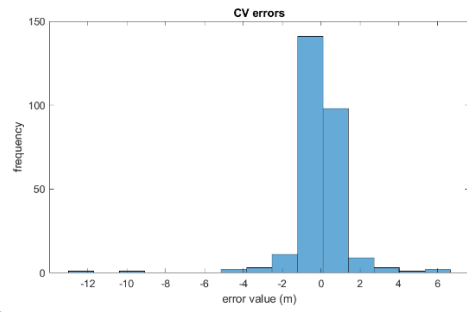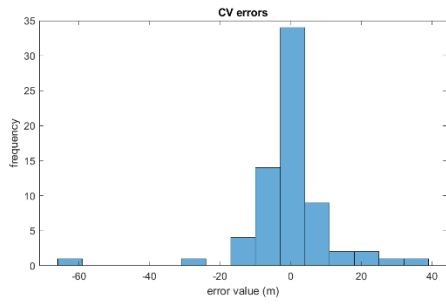
Figure 3.35: Cross Validation error for estimations of clusters 1-2
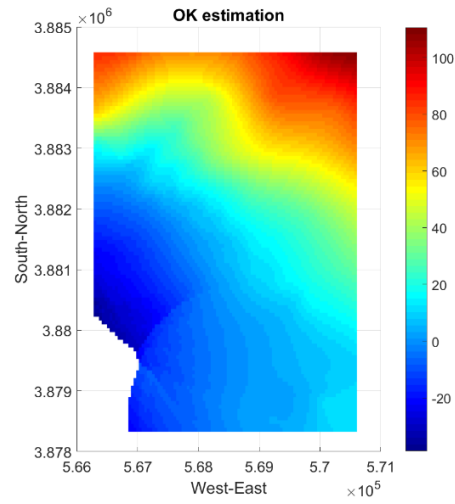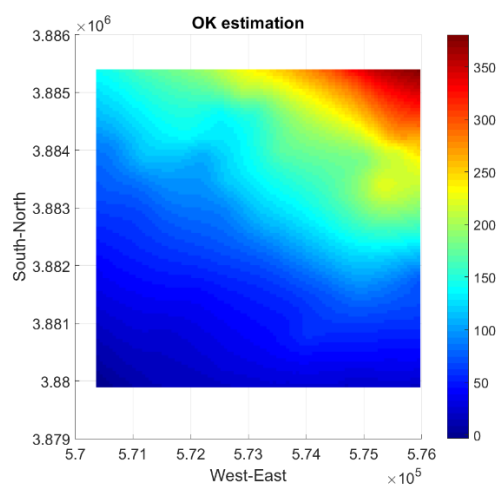
Figure 3.36: Ordinary Kriging estimation for clusters 1-2
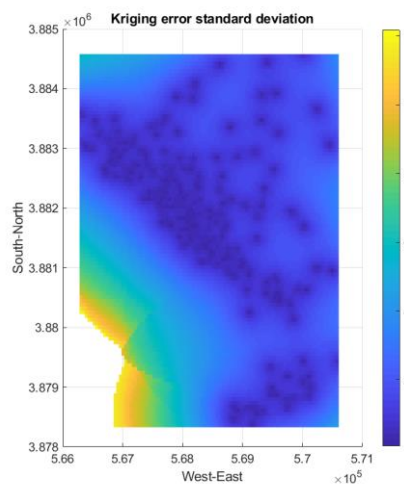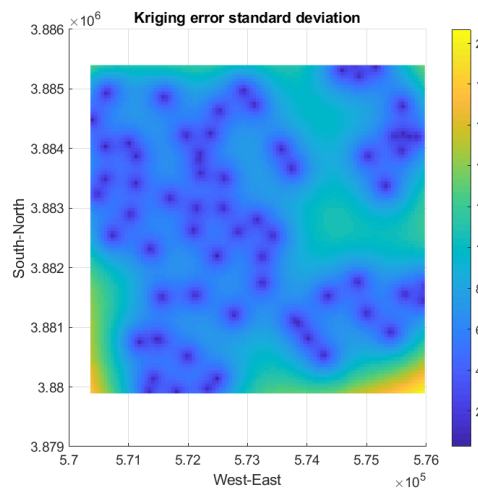
*Figure 3.37: Kriging error standard deviation for clusters 1-2*

3.2.4 Topology 2x2
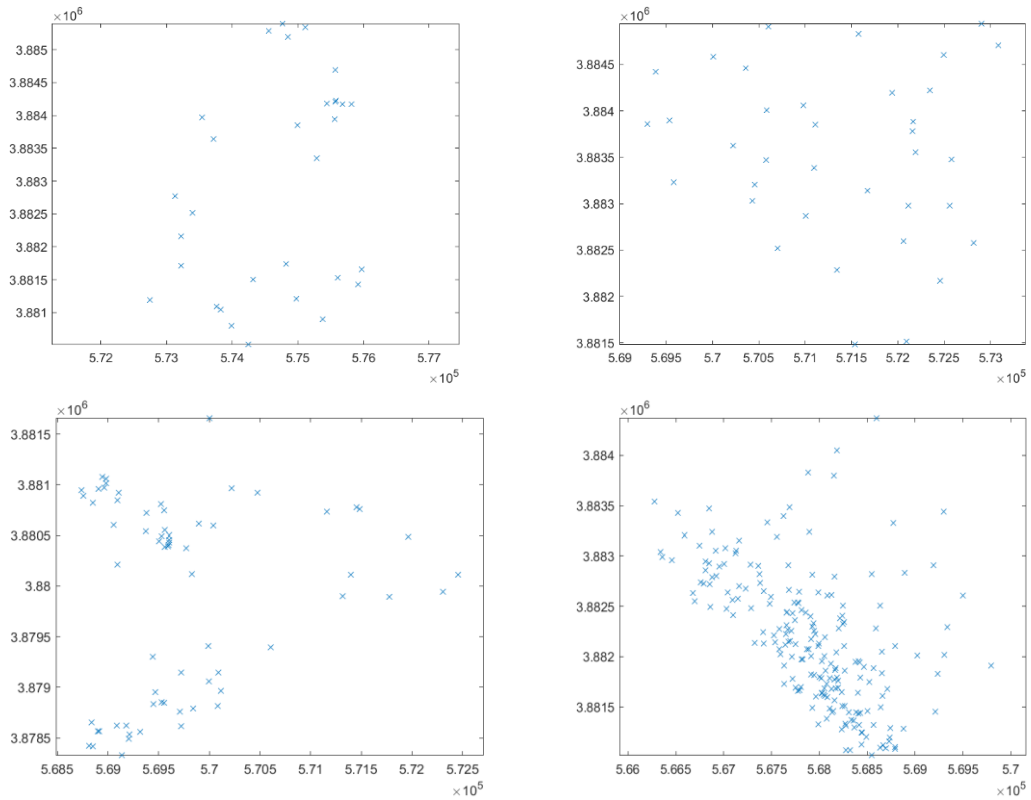
Figure 3.38: Spatial distribution of observation points for cluster 1-2, 3-4
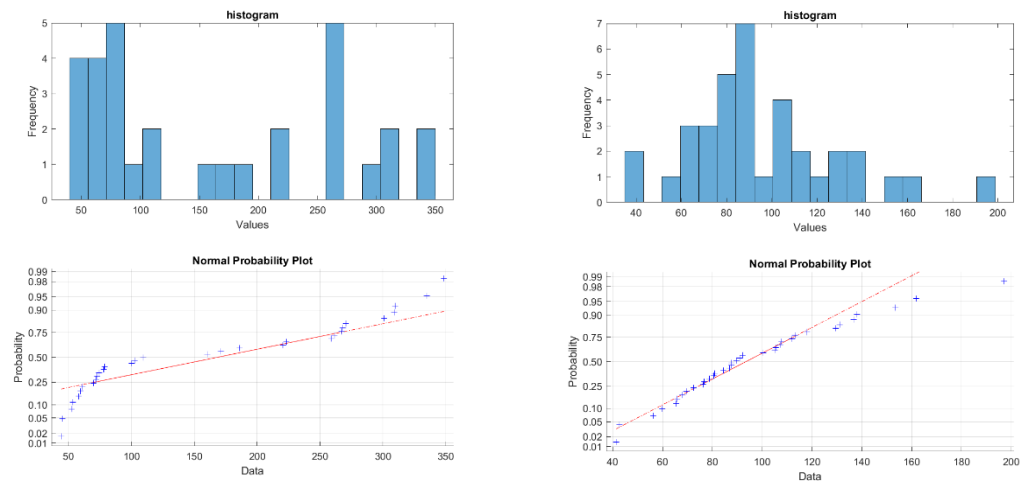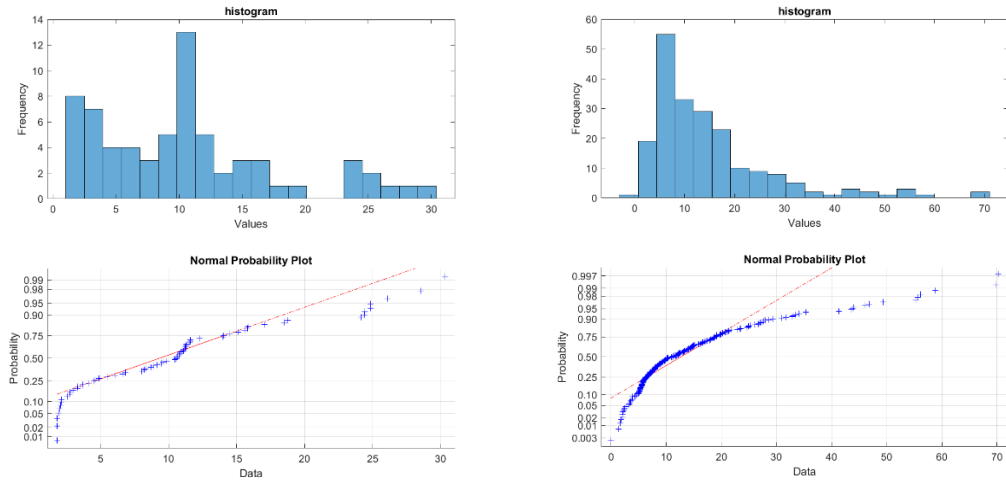
Figure 3.39: Histogram and probability curve for clusters 1-2, 3-4
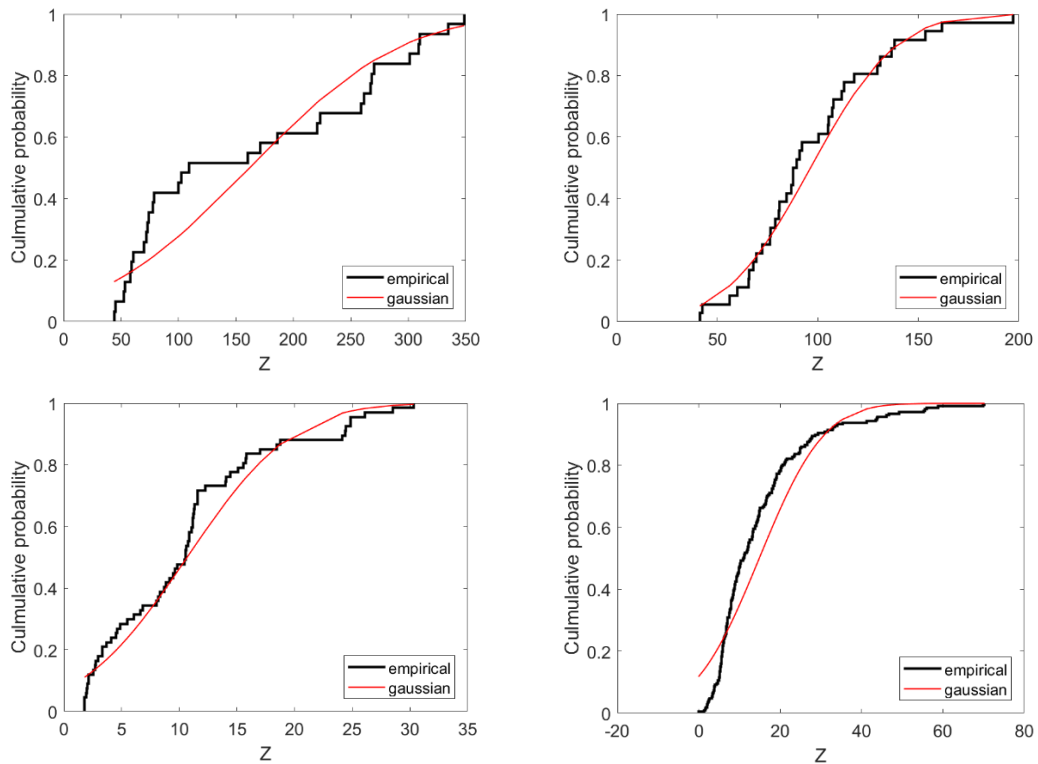
Figure 3.40: Cumulative Probability curve empirical and theoretical gaussian for clusters 1-2, 3-4
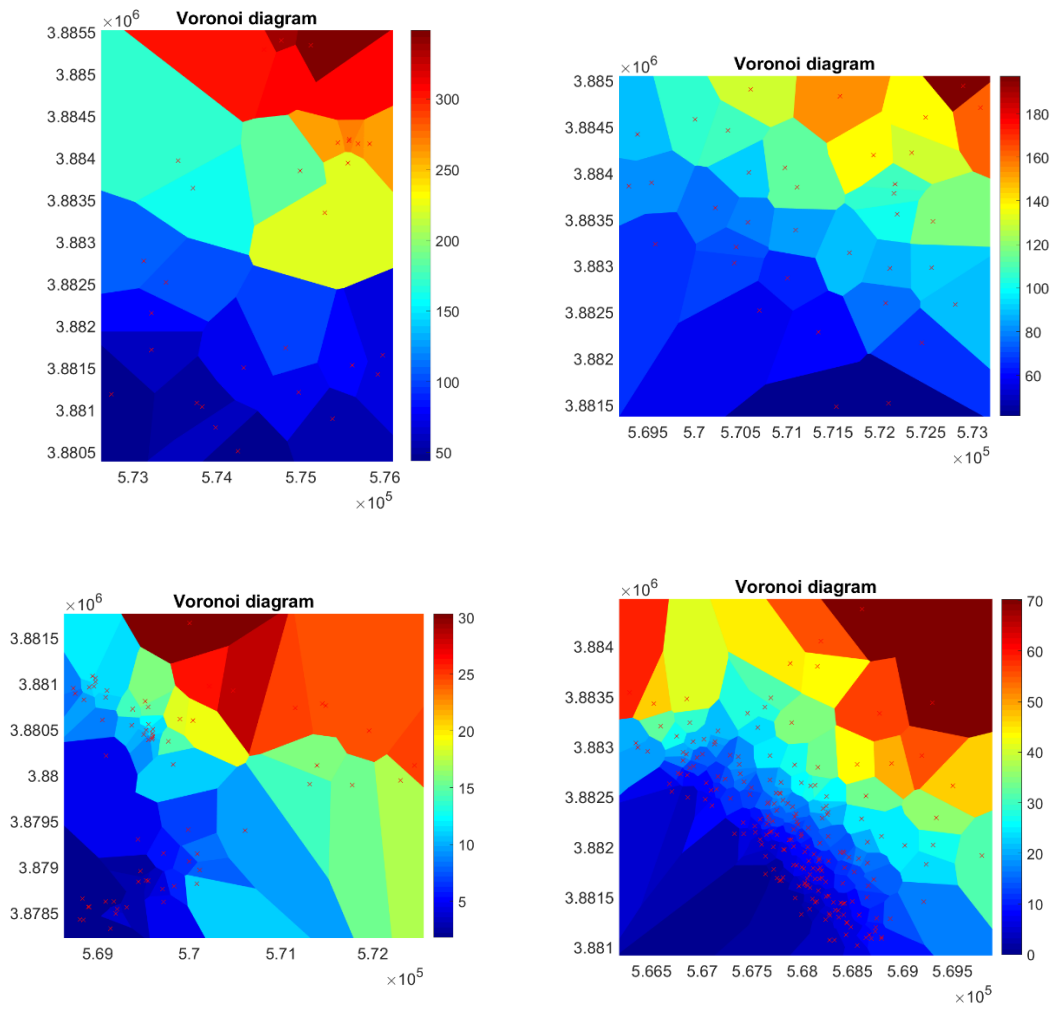
Figure 3.41: Voronoi polygons for hydraulic head observation points for clusters 1-2, 3-4
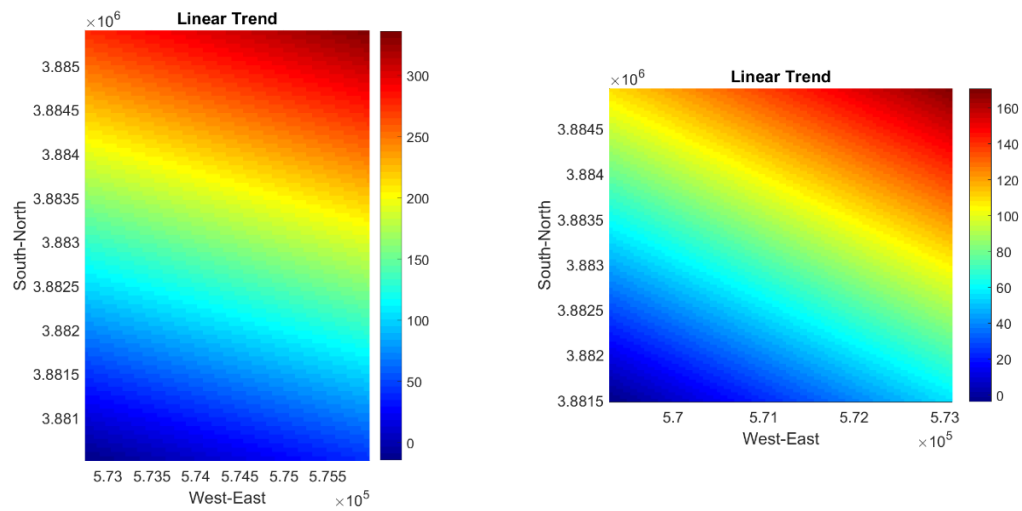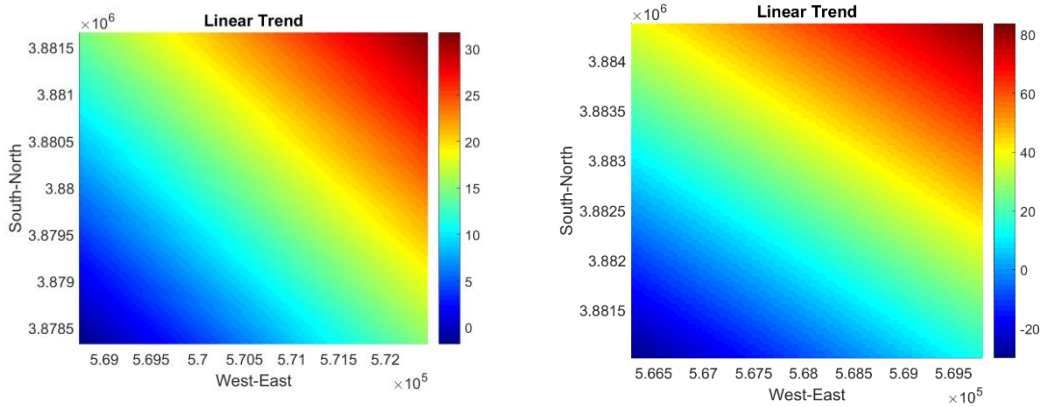
Figure 3.42: Linear trend for clusters 1-2, 3-4
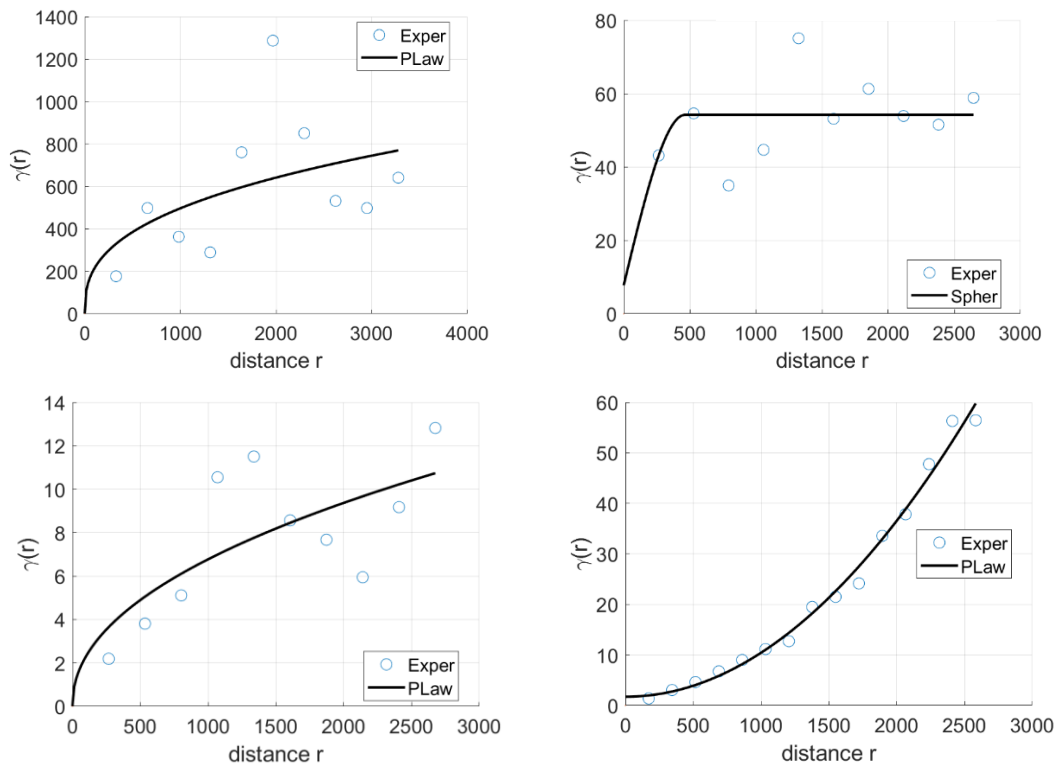
Figure 3.43: Variograms for clusters 1-2, 3-4
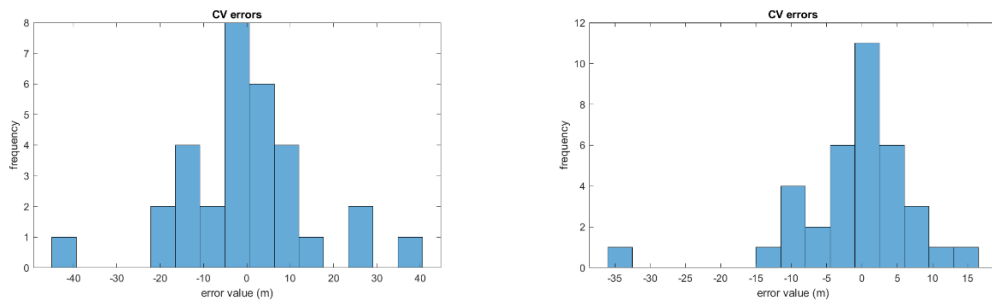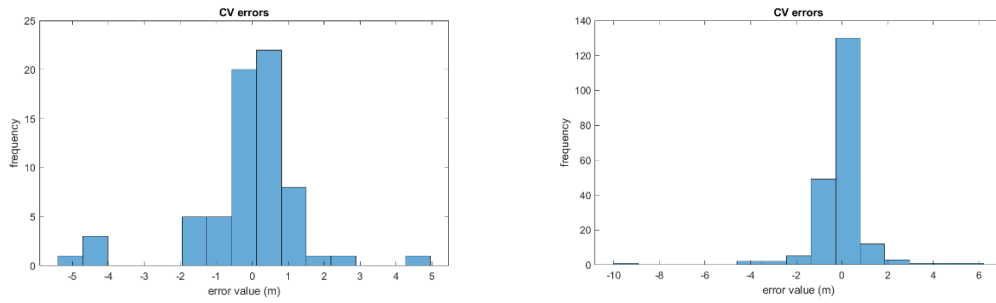
Figure 3.44: Cross Validation error for estimations of clusters 1-2, 3-4
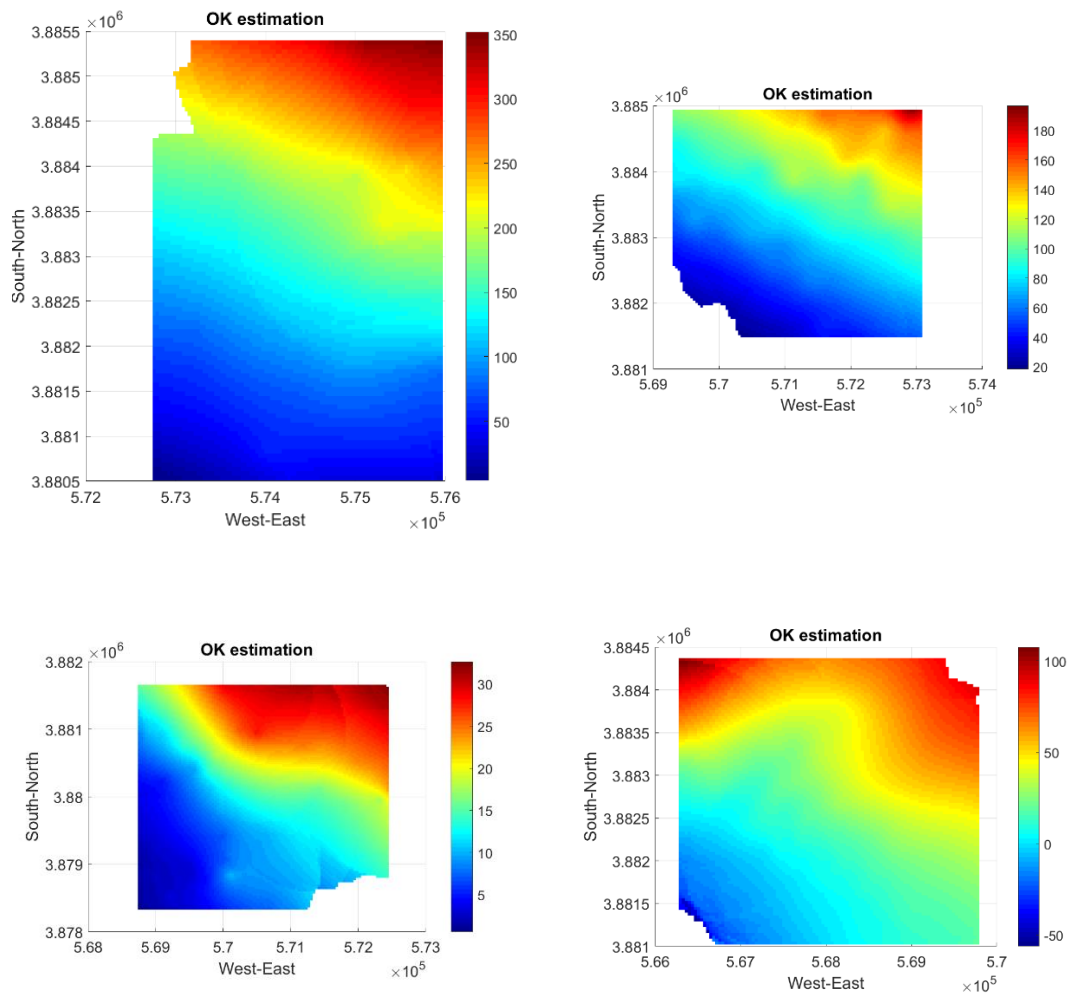
Figure 3.45: Ordinary Kriging estimation for clusters 1-2, 3-4
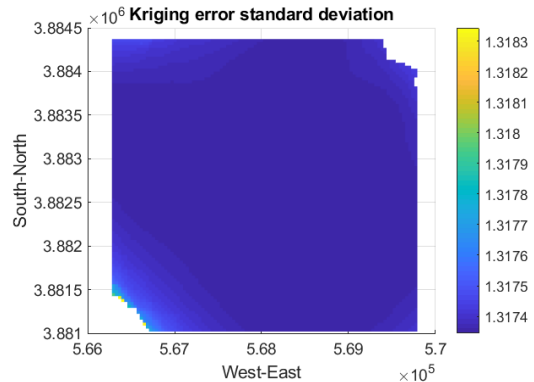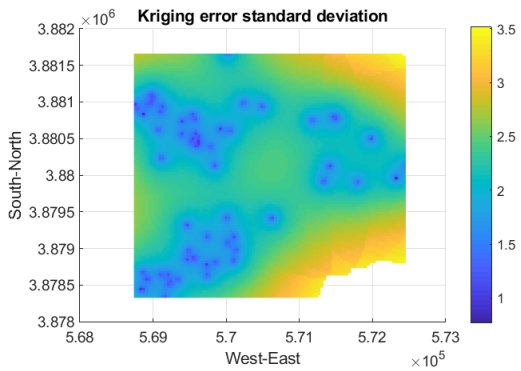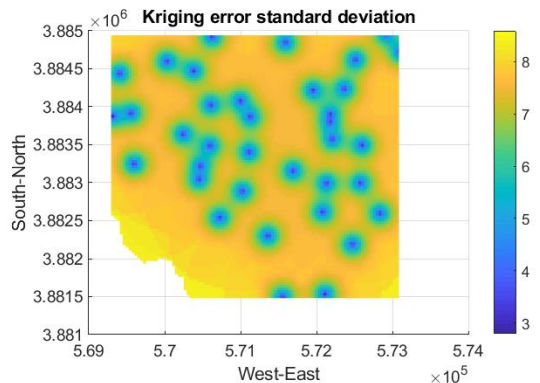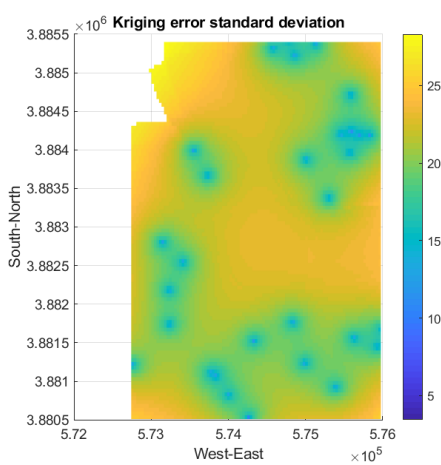
Figure 3.46: Kriging error standard deviation for clusters 1-2, 3-4

3.2.5 Topology 2x3
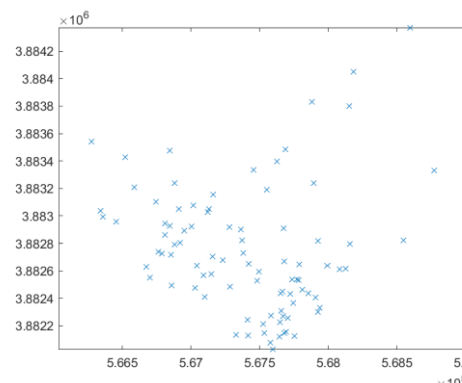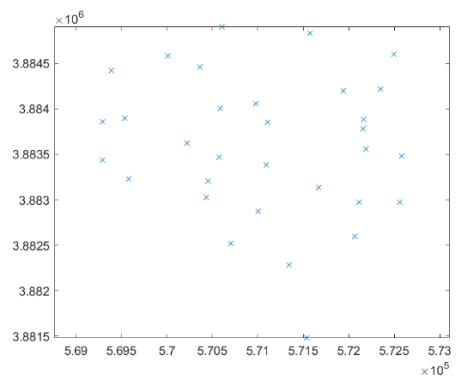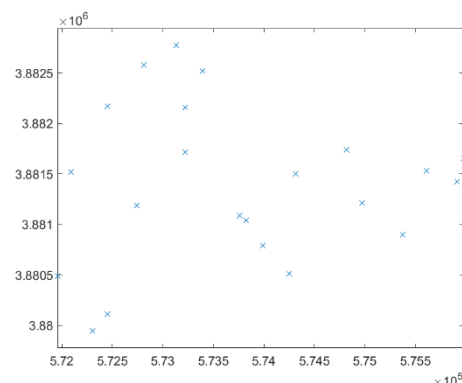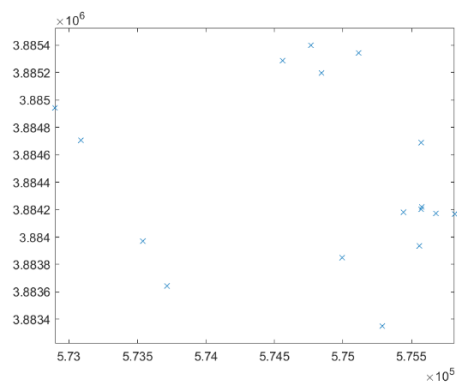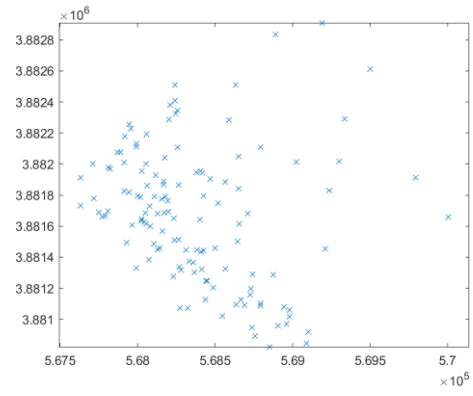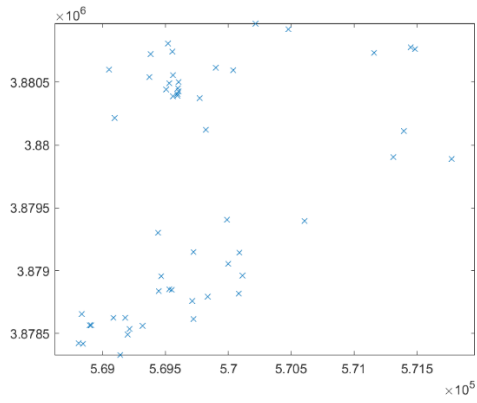
Figure 3.47: Spatial distribution of observation points for clusters 1-2, 3-4, 5-6
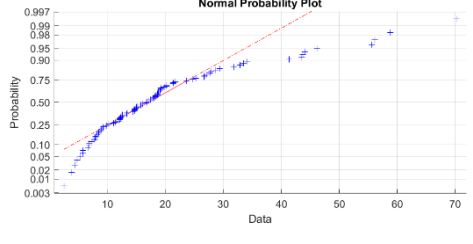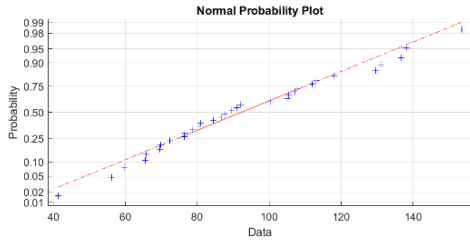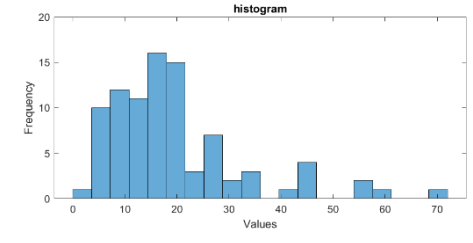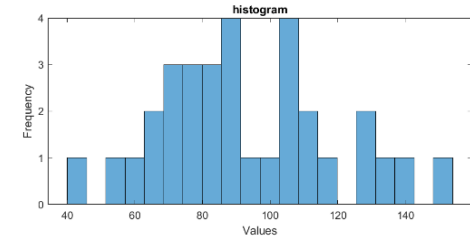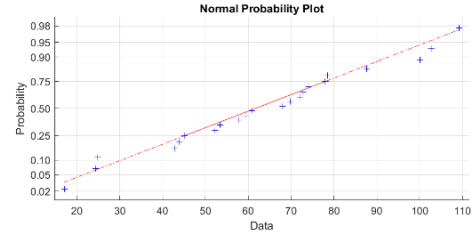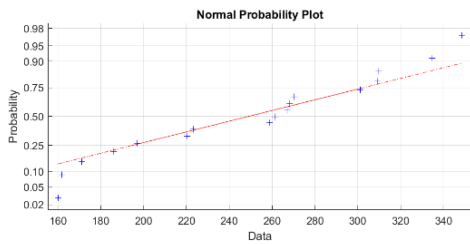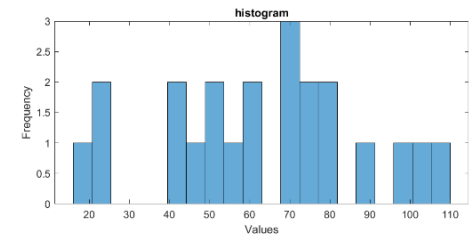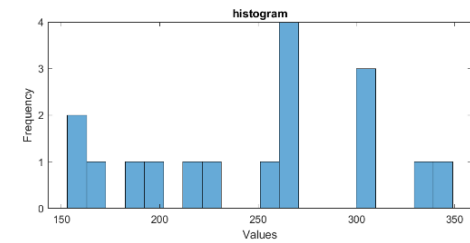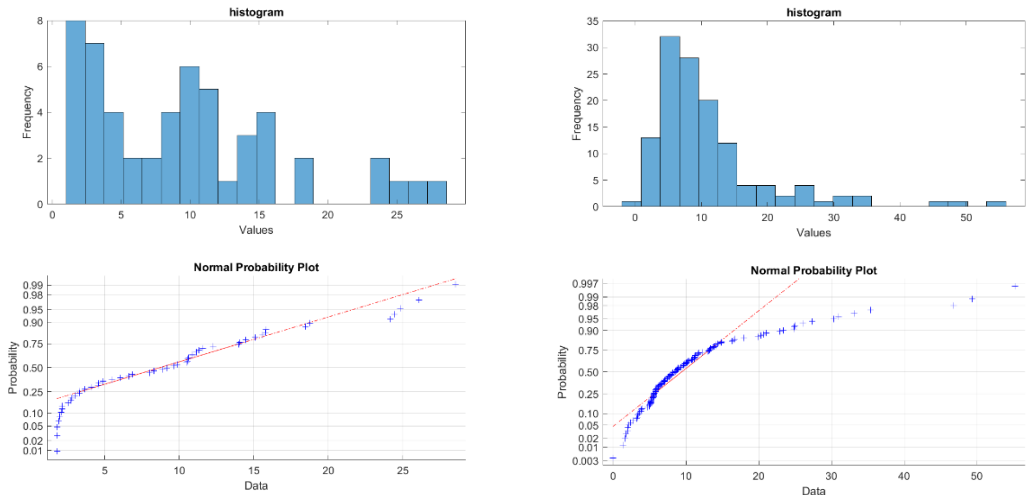
Figure 3.48: Cumulative Probability curve empirical and theoretical gaussian for clusters 1-2, 3-4, 5-6
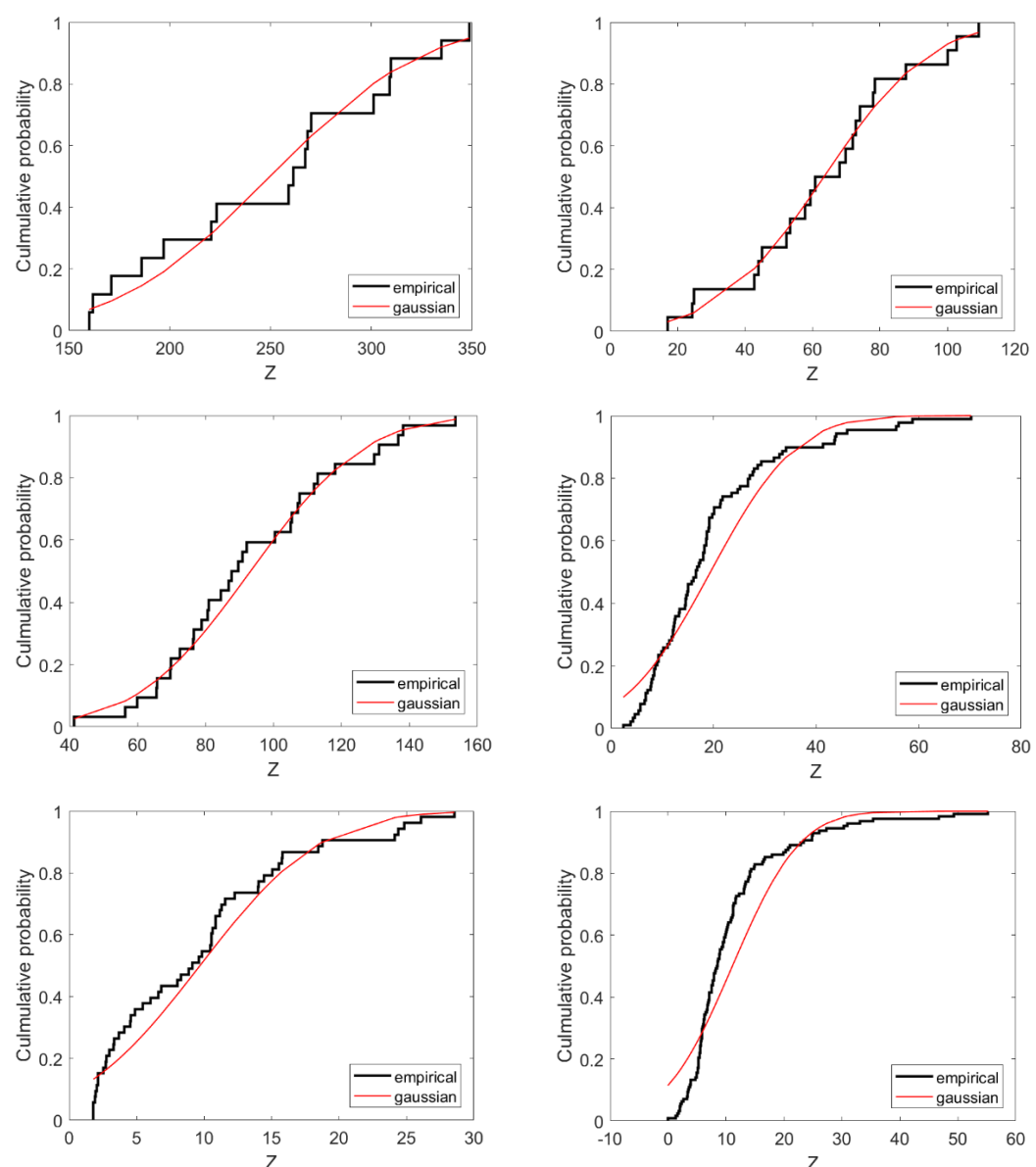

*Figure 3.49: Cumulative Probability curve empirical and theoretical gaussian for clusters 1-2, 3-4, 5-6*
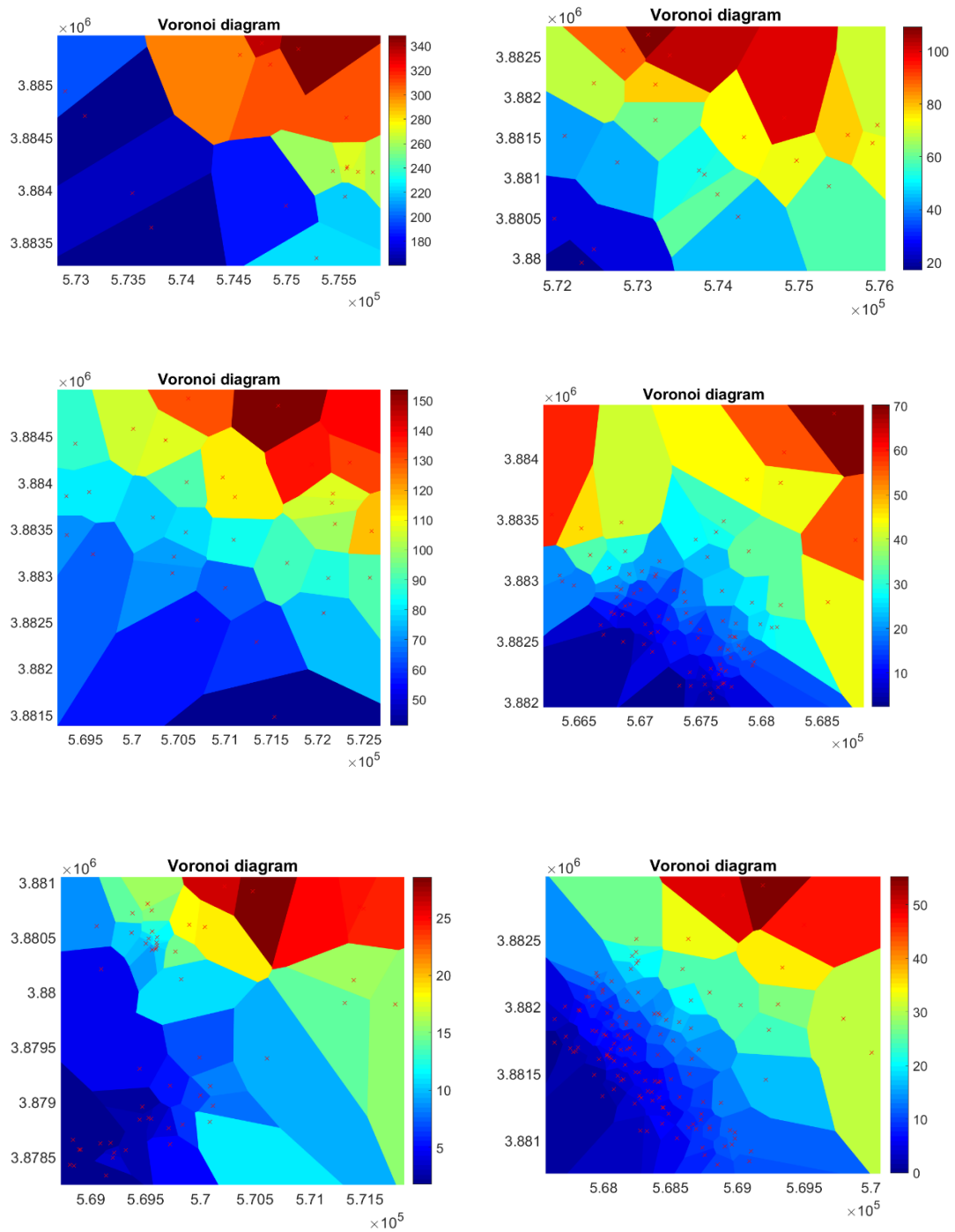
*Figure 3.50: Voronoi polygons for hydraulic head observation points for clusters 1-2, 3-4, 5-6*
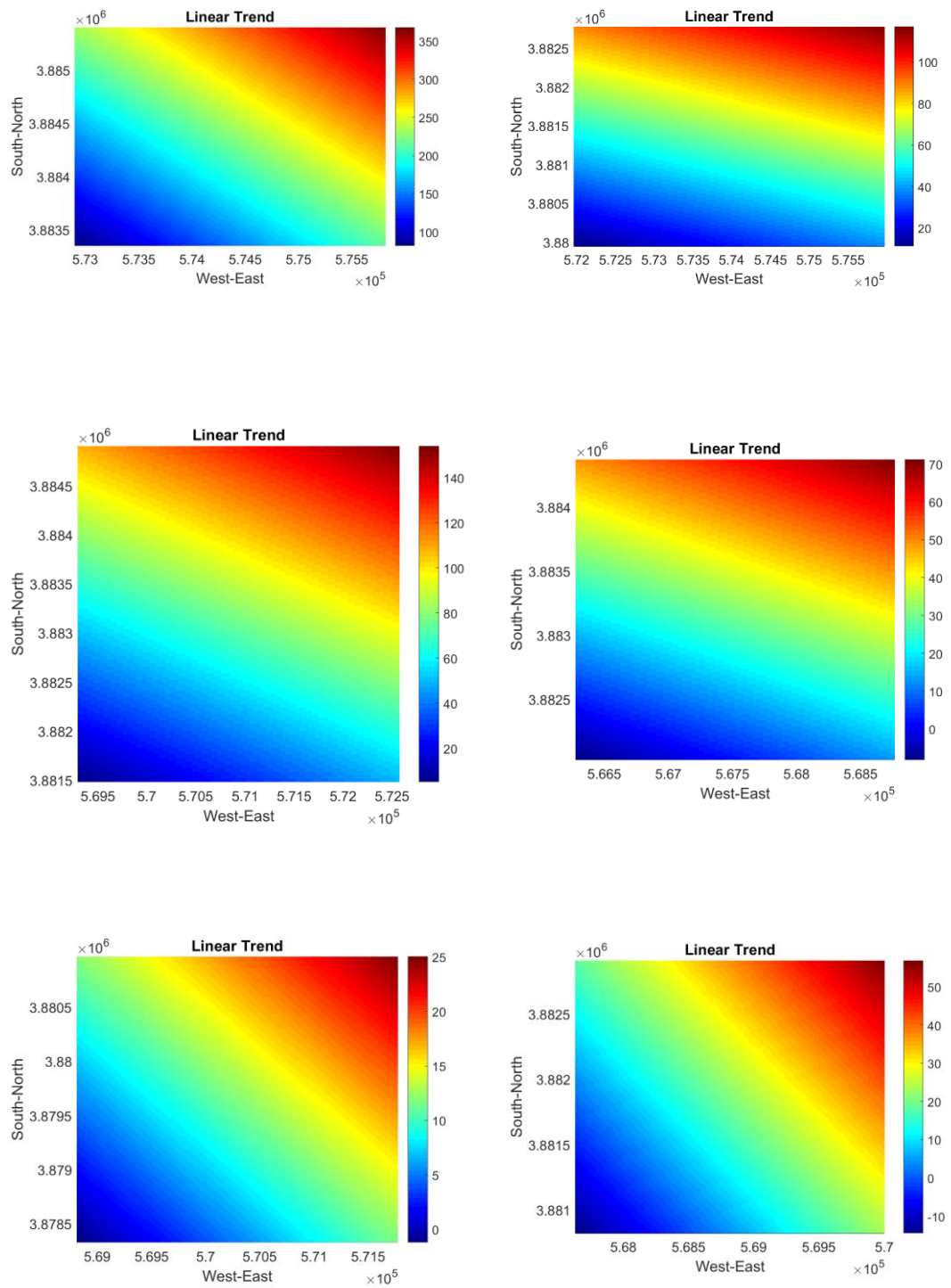
Figure 3.51: Linear trend for clusters 1-2, 3-4, 5-6
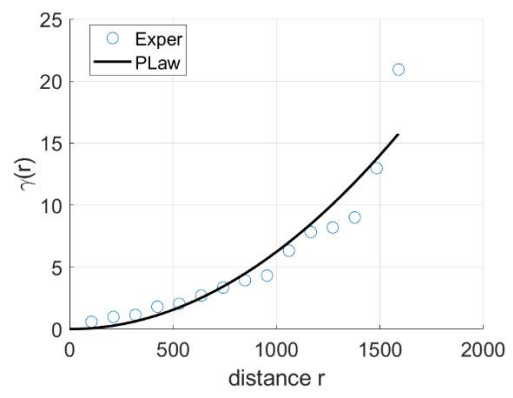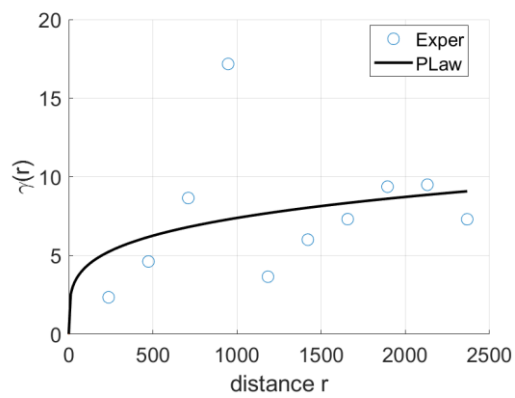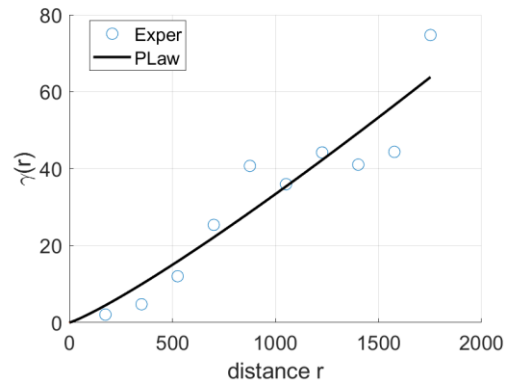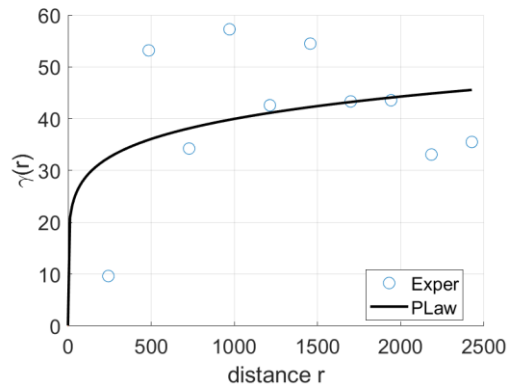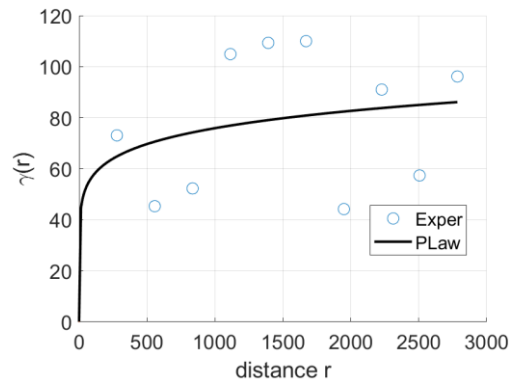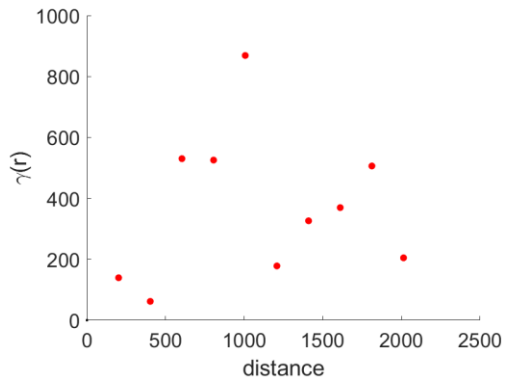
Figure 3.52: Variograms for clusters 1-2, 3-4, 5-6
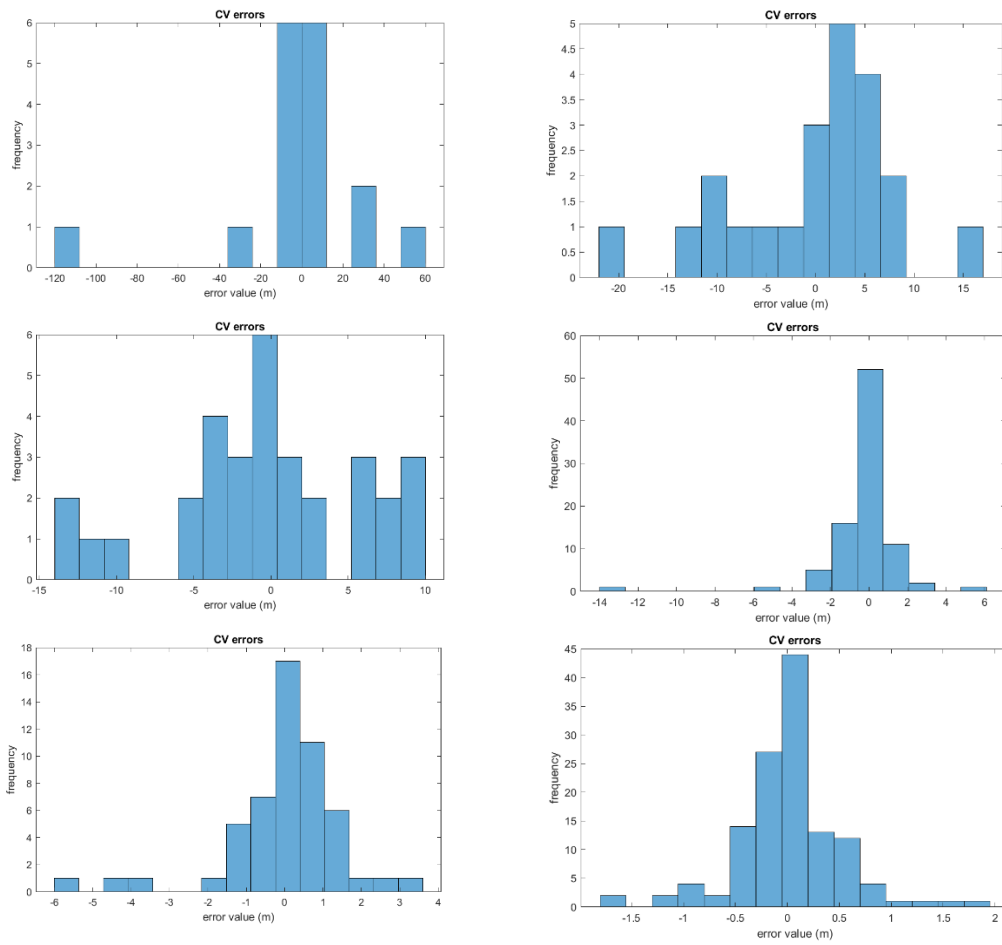
Figure 3.53:Cross Validation error for estimations of clusters 1-2, 3-4, 5-6
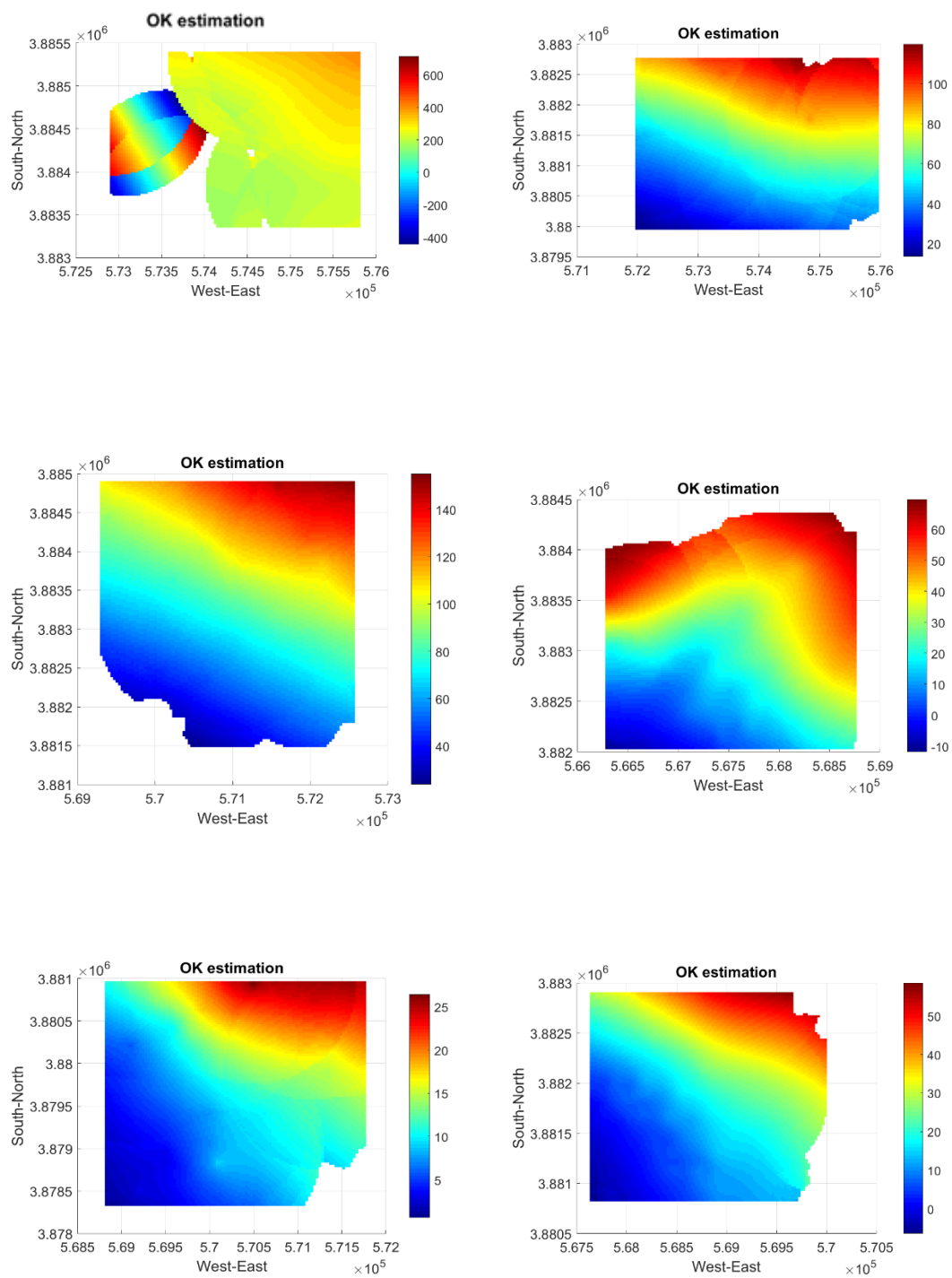
Figure 3.54: Ordinary Kriging estimation for clusters 1-2, 3-4, 5-6
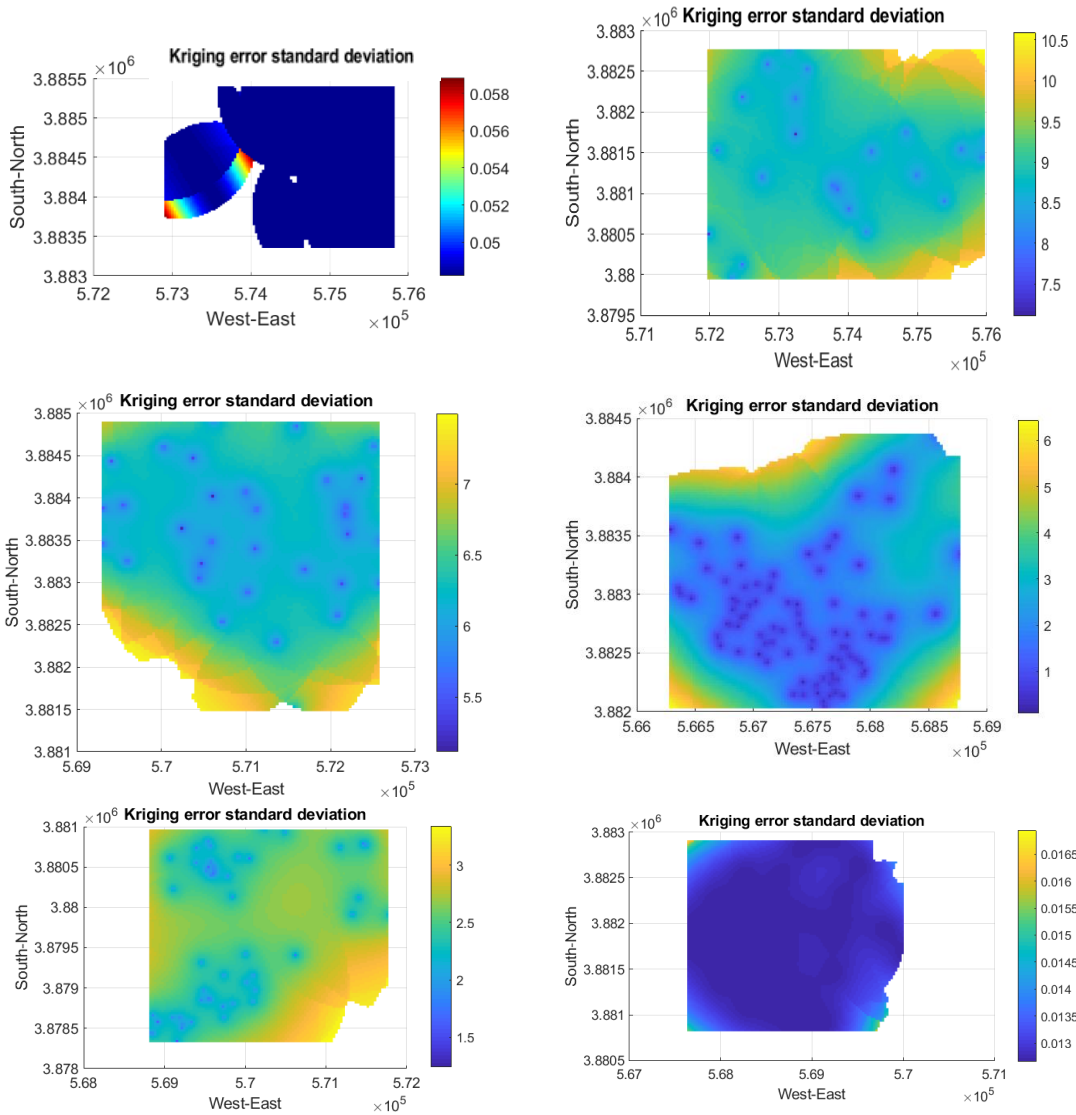
Figure 3.55: Kriging error standard deviation for clusters 1-2, 3-4, 5-6

3.2.6 Topology 3x2
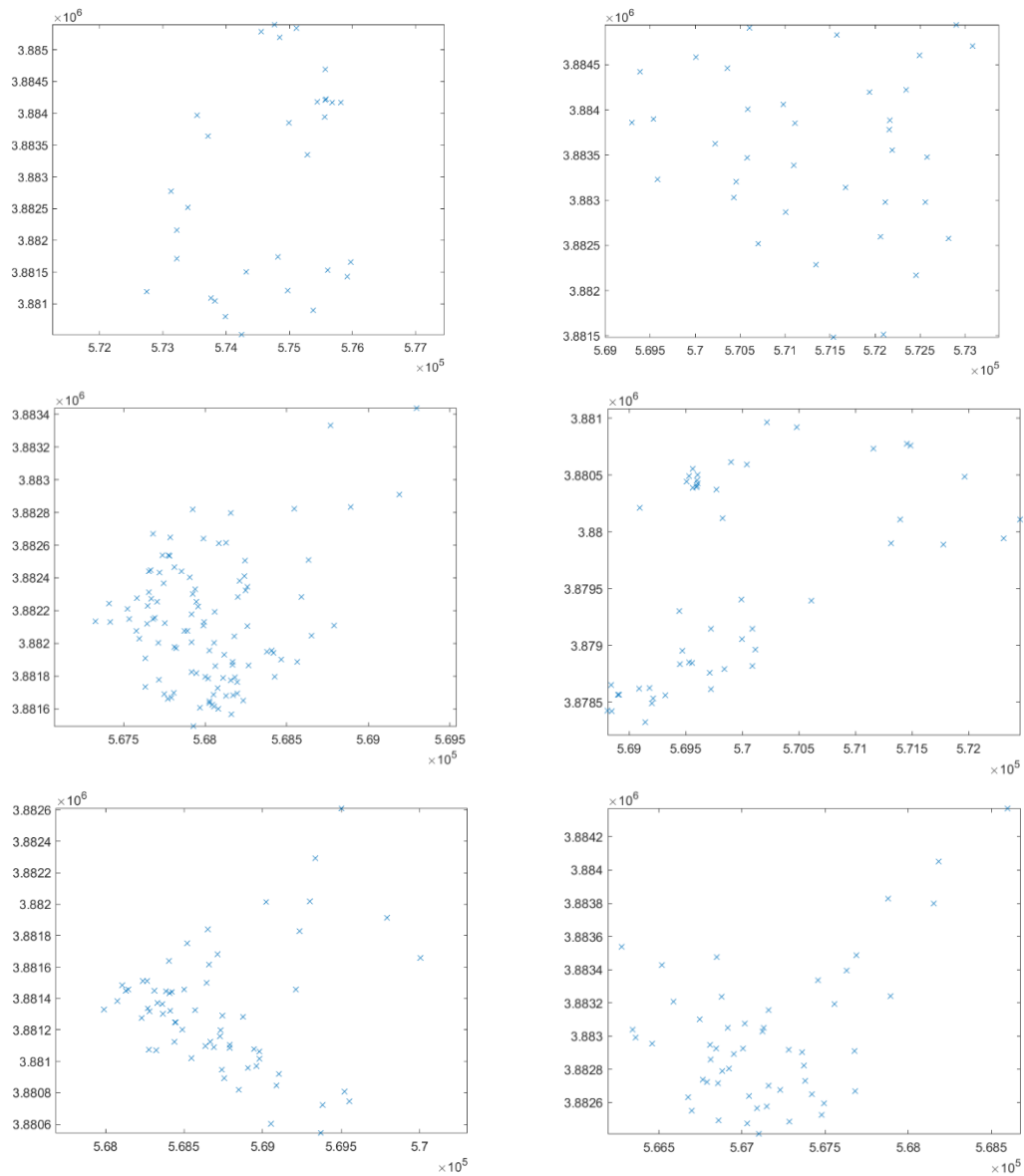
Figure 3.56: Spatial distribution of observation points for clusters 1-2, 3-4, 5-6
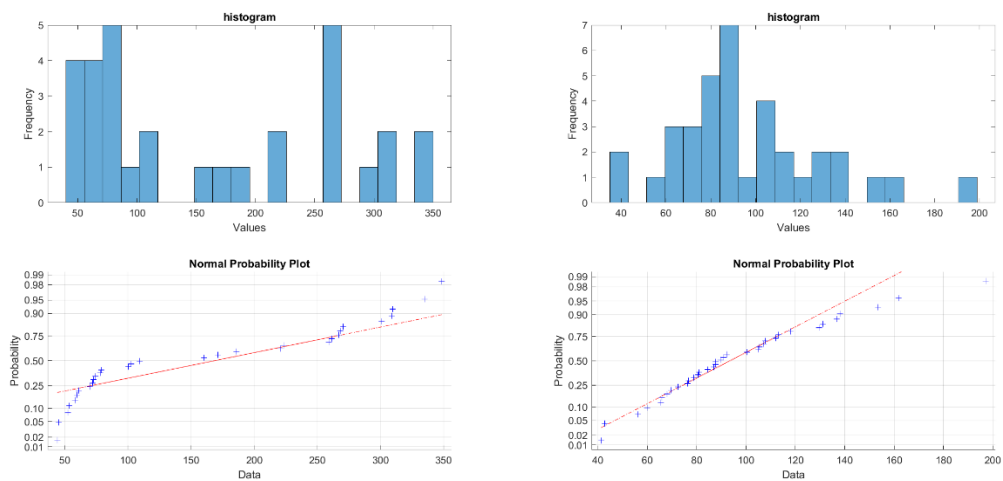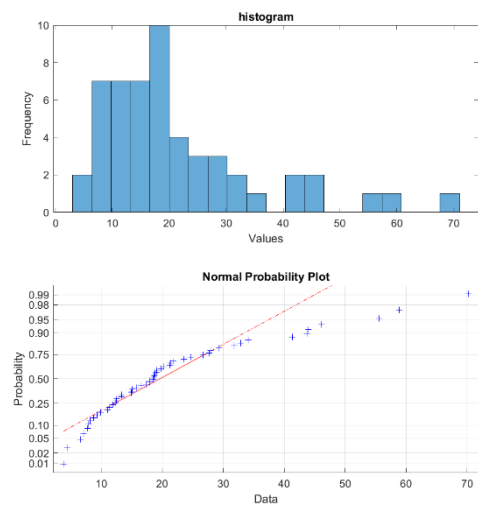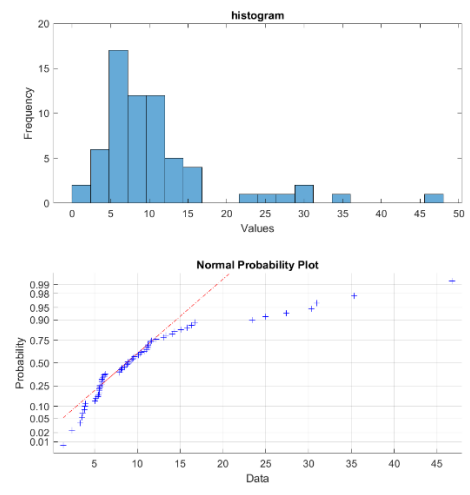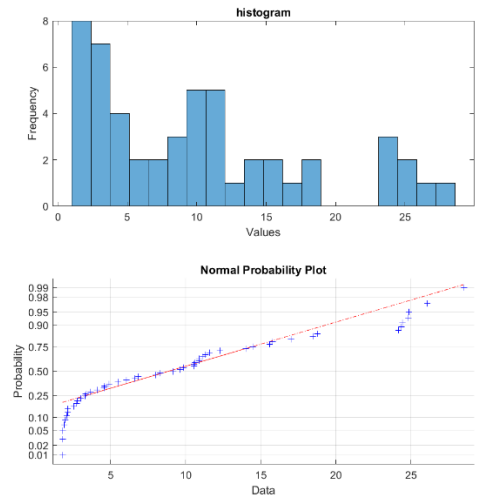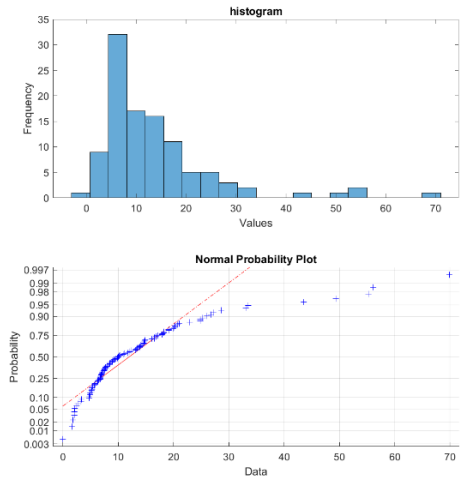
Figure 3.57: Cumulative Probability curve empirical and theoretical gaussian for clusters 1-2, 3-4, 5-6.
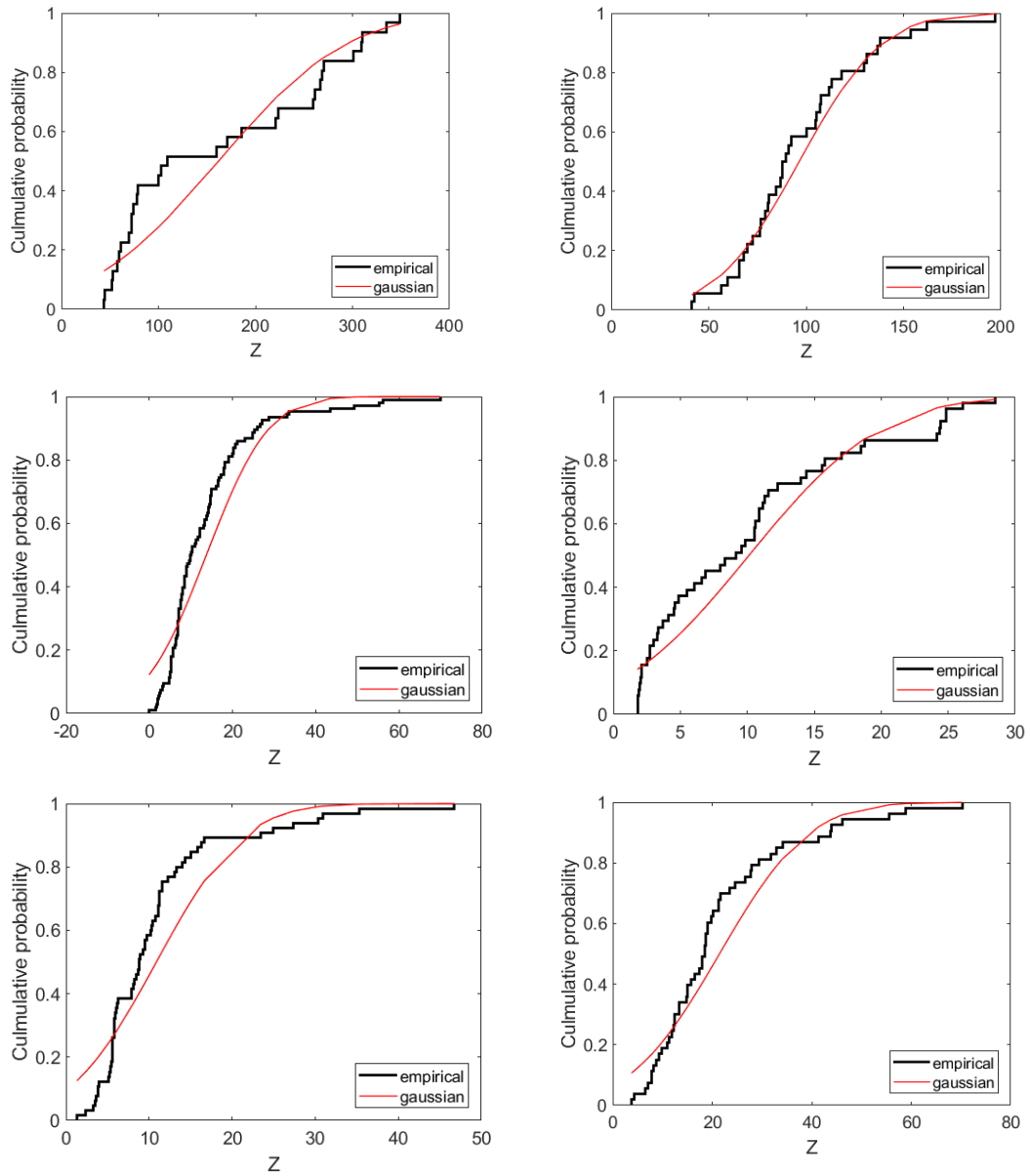
Figure 3.58: Cumulative Probability curve empirical and theoretical gaussian for clusters 1-2, 3-4, 5-6
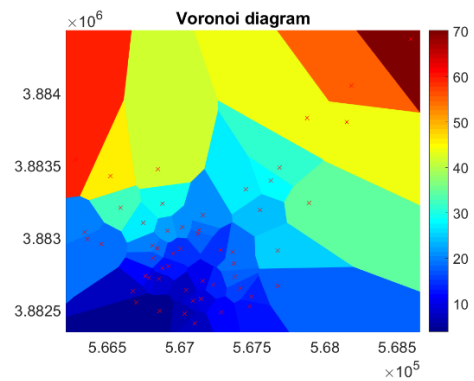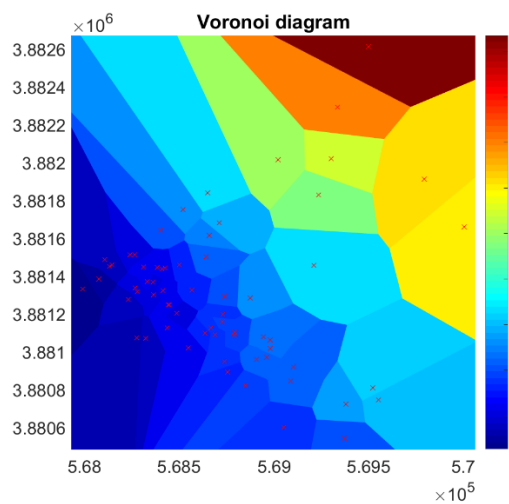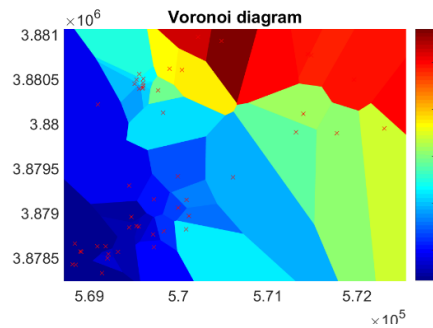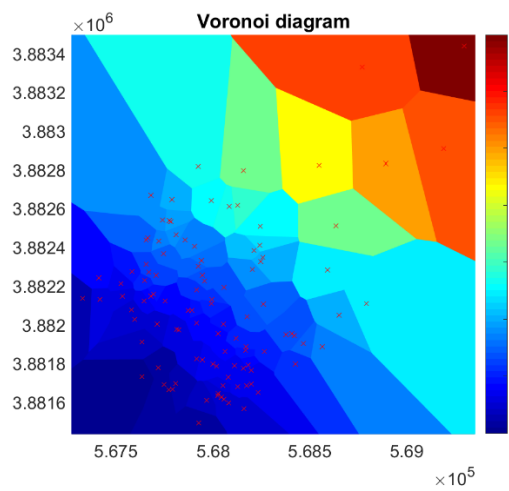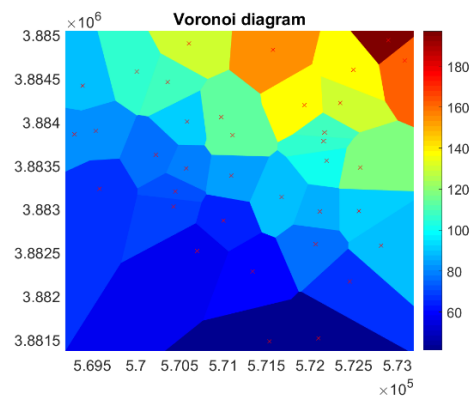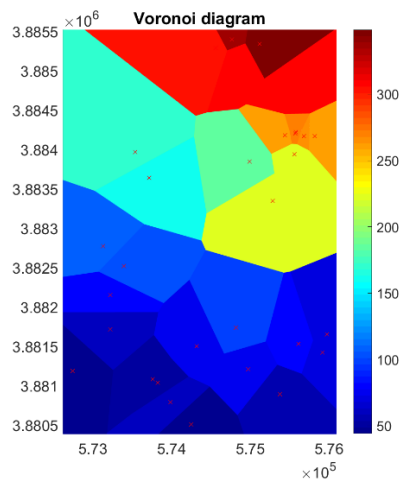
Figure 3.59: Voronoi polygons for hydraulic head observation for cluster 1-2,3-4,5-6
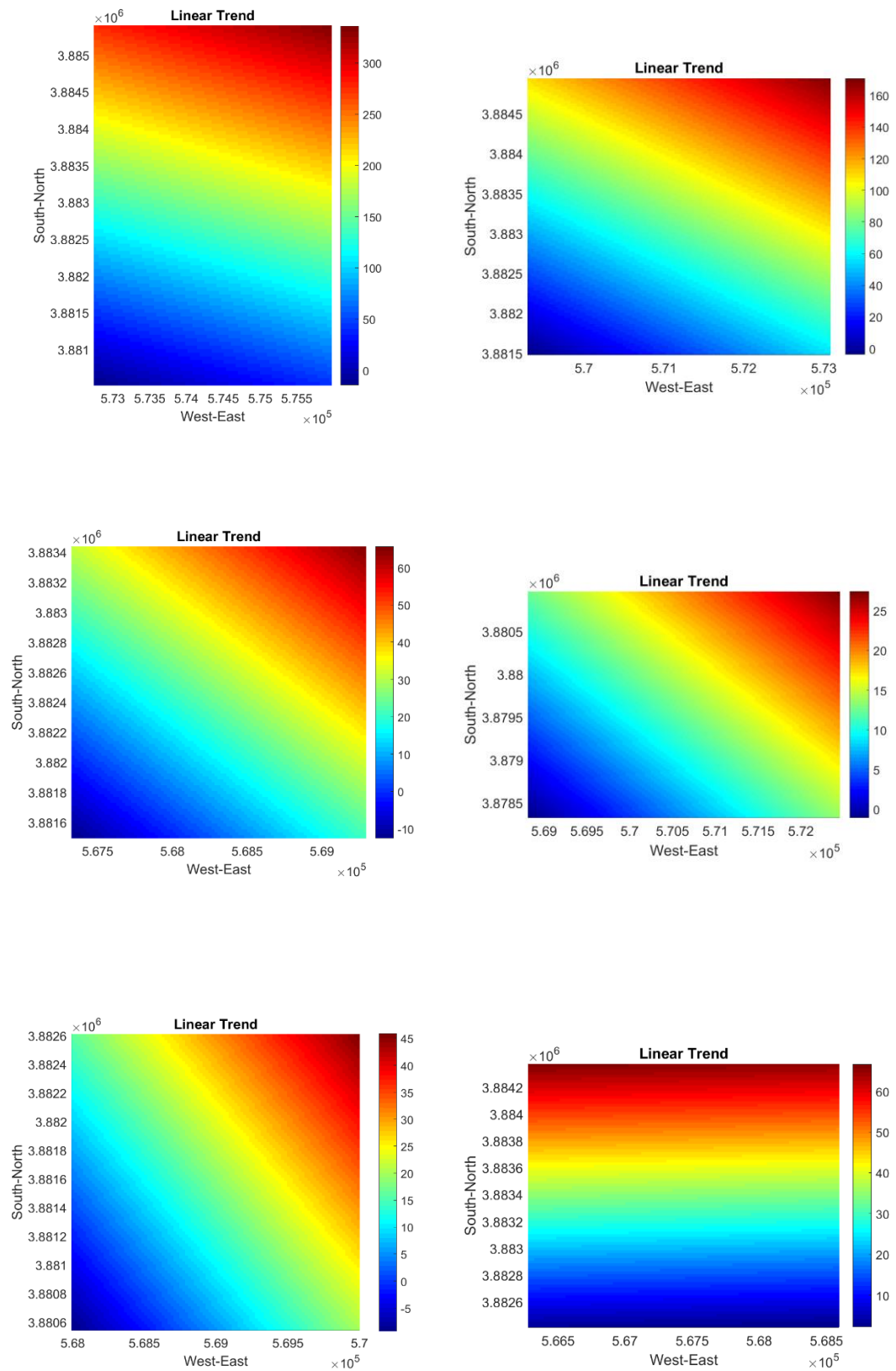
Figure 3.60: Linear trend for cluster 1-2,3-4,5-6
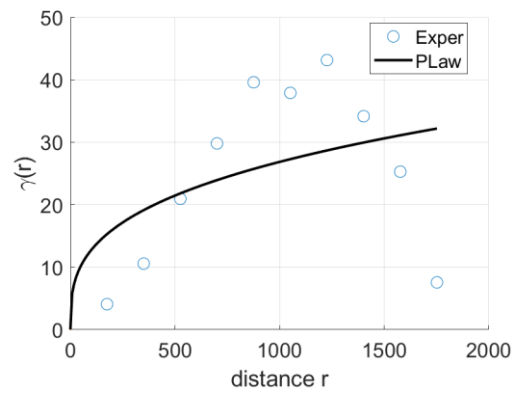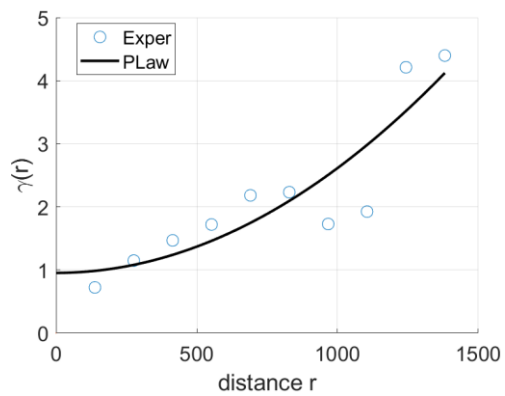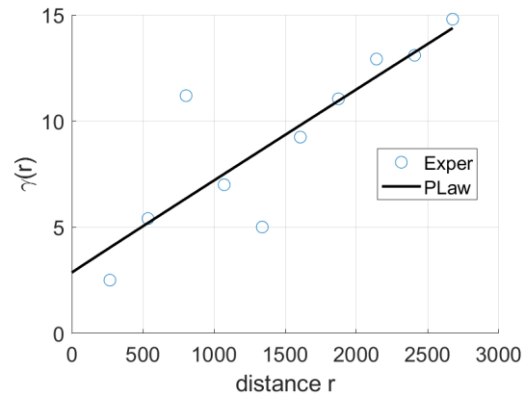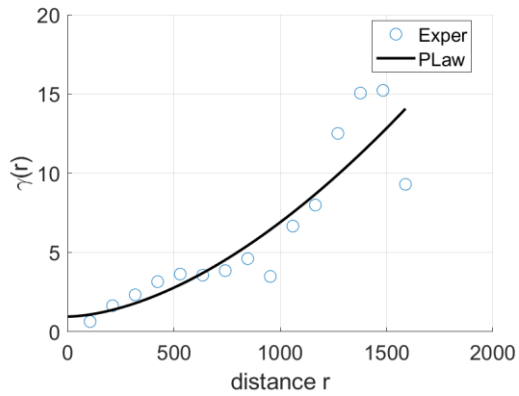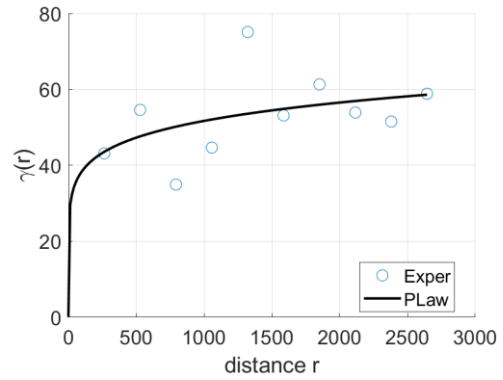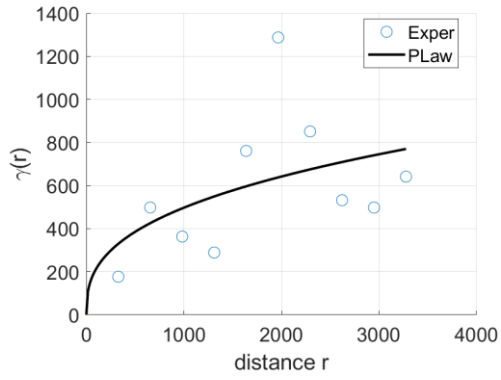
Figure 3.61: Variographs for cluster 1-2,3-4,5-6
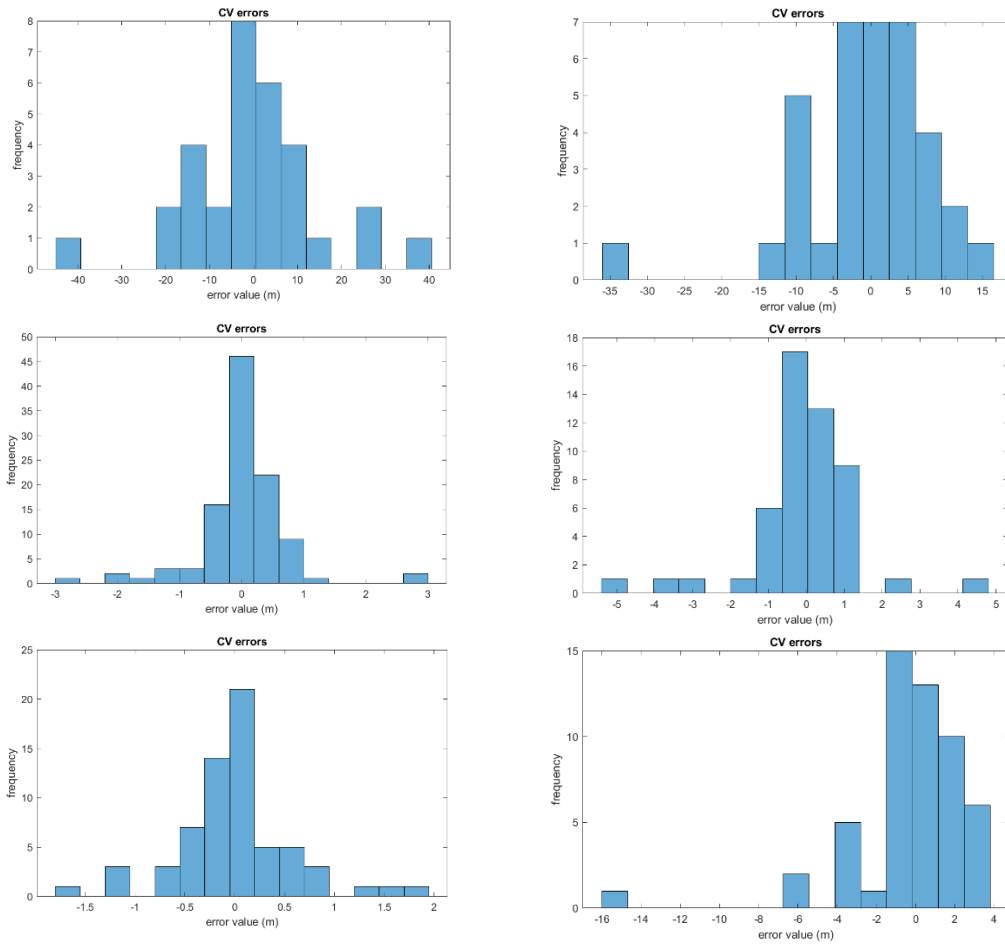
*Figure 3.62: Cross Validation error for estimations of clusters 1-2, 3-4, 5-6*
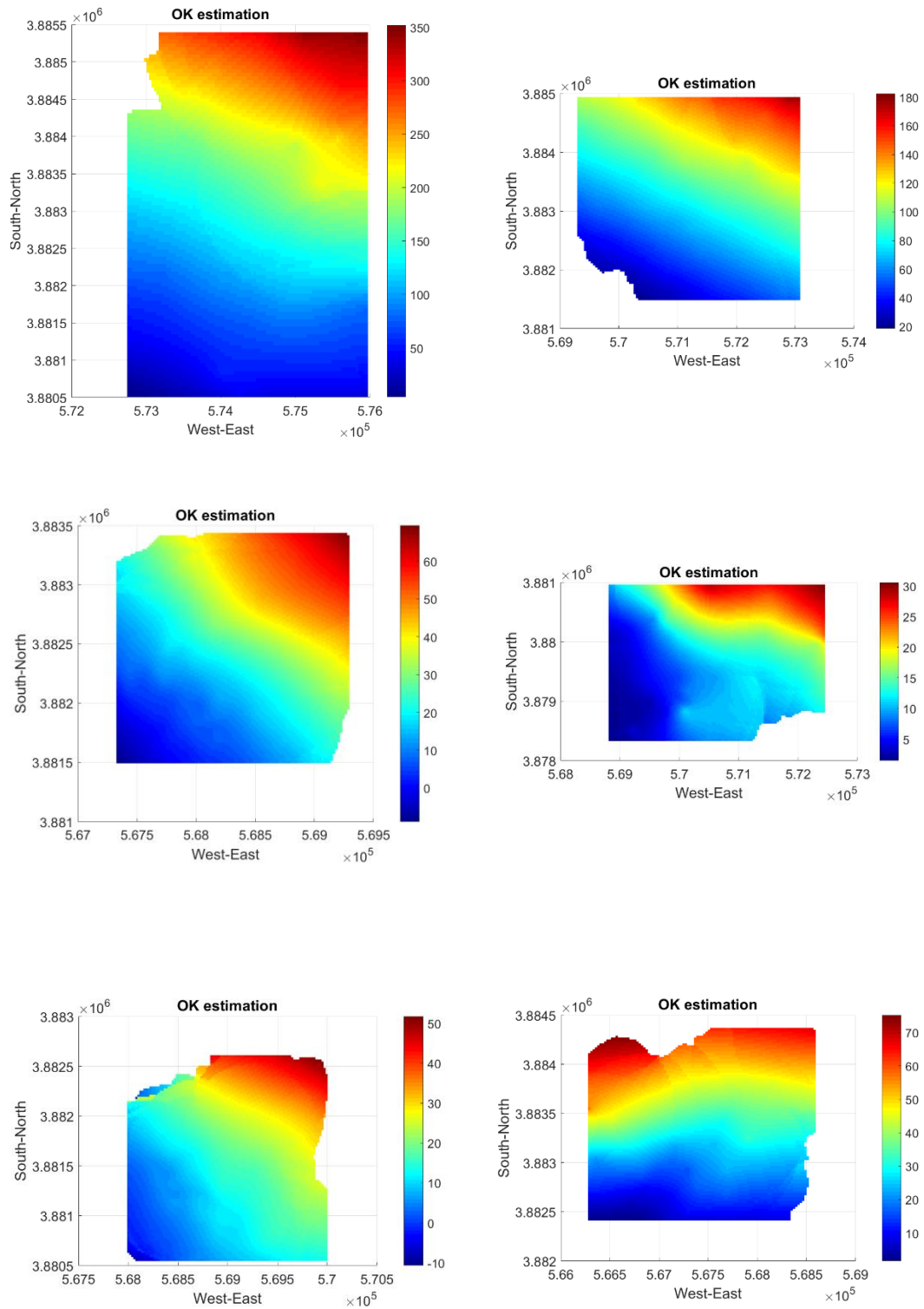
Figure 3.63: Ordinary Kriging estimation for clusters 1-2, 3-4, 5-6
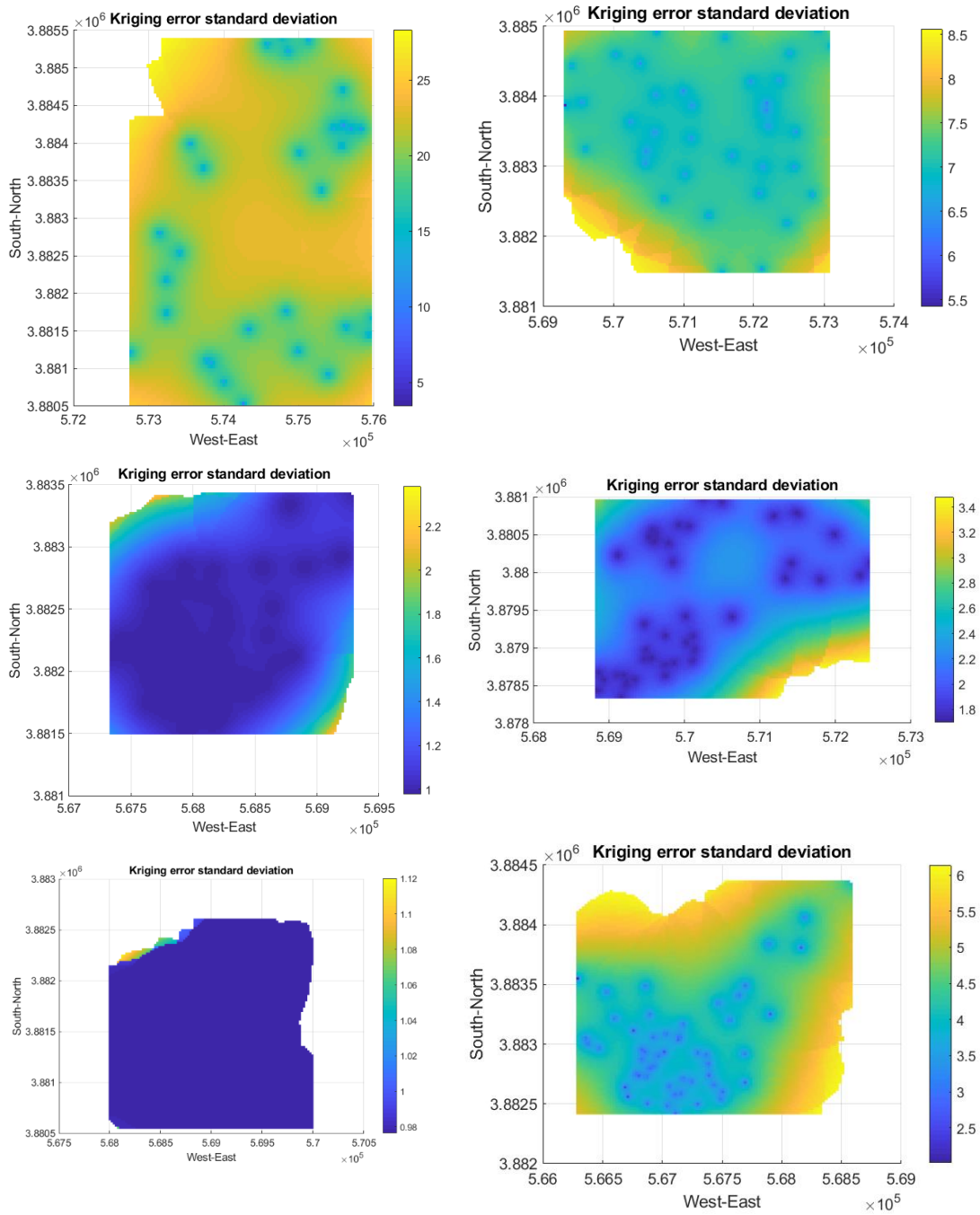
Figure 3.64: Kriging error standard deviation for clusters 1-2, 3-4, 5-6

3.3 Validation Criteria Results
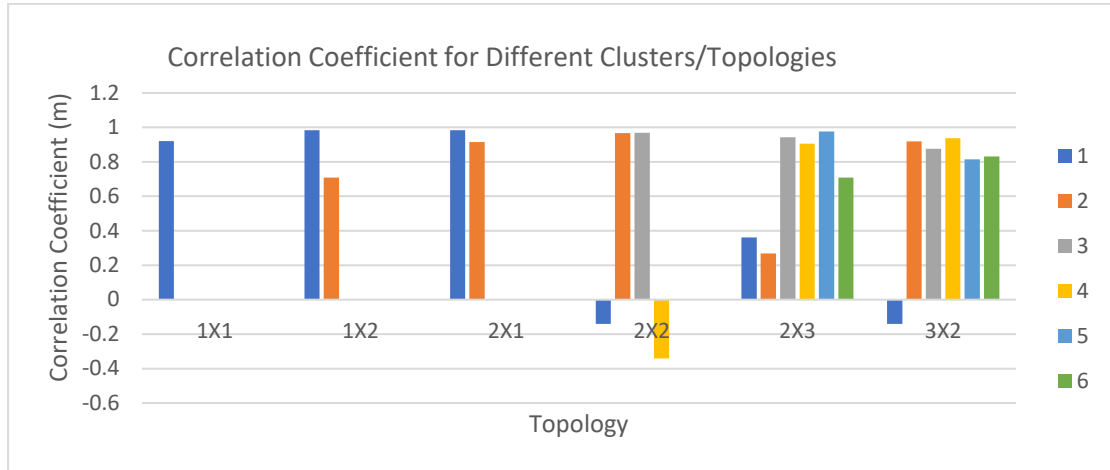
Figure 3.65: Correlation Coefficient for Different Clusters/Topologies
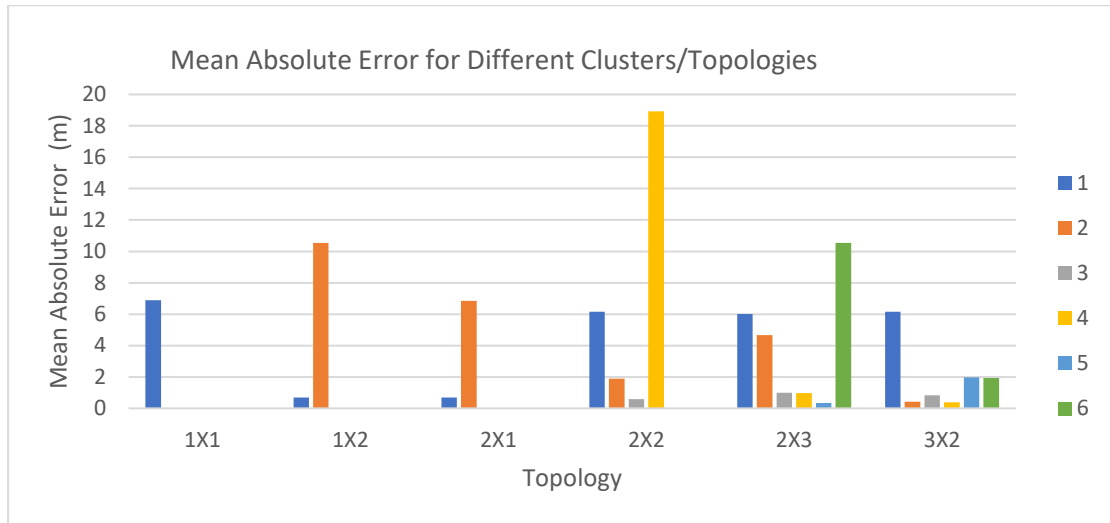
Figure 3.66: Mean Absolute Error for Different Clusters/Topologies
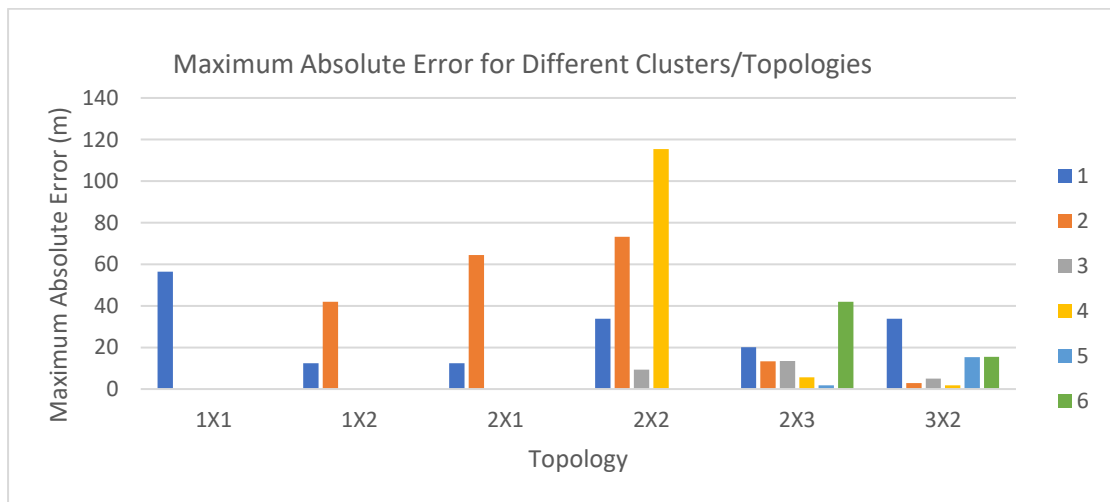
Figure 3.67: Maximum Absolute Error for Different Clusters/Topologies
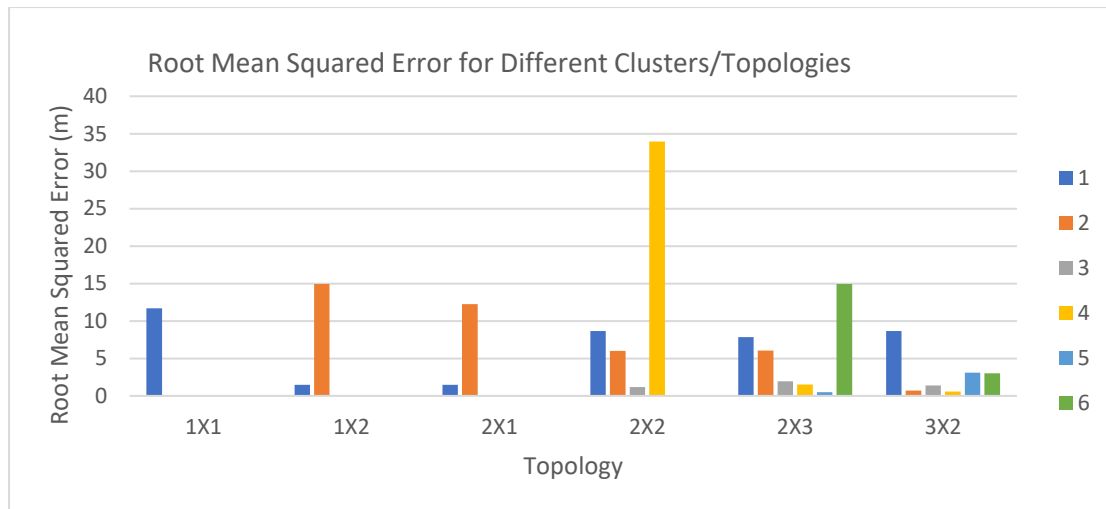
Figure 3.68: Root Mean Squared Error for Different Clusters/Topologies

4 Discussion

4.1 Topology 1x1

For the topology 1x1 the SOM algorithm was not used. In Figure 3.12 there can be seen that the sample of observations has a range of values from 0 to 350 m. The most common values for hydraulic head values are between 0 to 50 m. This range of values follows the normal probability curve. The remaining observations in the sample have a wider range of hydraulic head values, but the frequency of their occurrence is much lower. According to Figure 3.13, the cumulative probability curve of the gaussian variogram and the empirical variogram indicate that the observation sample as a whole does not follow the normal probability distribution to its totality. As can be seen in Figure 3.14, there is a clear distinction between the observations. They are separated by an axis from northwest to southeast. Most of the observation points with values (0 to 50 m) seem to be located near the coastal front, while the remaining points are scattered in the rest of the study area with different hydraulic head values. This is confirmed by Figure 3.15, where the linear trend is from the northeast to southwest so the differentiation shown above is valid. Examination of the variogram in Figure 3.16, shows that the power law is the best-fitting theoretical model. As mentioned earlier, the unbound variogram implies either a lack of sufficient observations or a strong correlation between the lags. Of the two possible interpretations, the second seems to be the more plausible. Since the case study is quite small and the hydrogeologic system studied, is generally a homogeneous porous aquifer system despite its discontinuities. The Kriging estimate, shown in Figure 3.18, is similar to the linear trend, with changes following the morphology of the study area. The error standard deviation maps (Figure 3.19) indicate a low error throughout the area, but this is also due to the high density of observations, particularly on the coastal front. Figure 3.17 provides additional insight: Aalthough, there is a high frequency of simple errors in the -10 to 10 m range, there are outliers that can reach as high as -60 m. The validation criteria indicate reasonable performance of the OK technique, i.e., Mean Absolute Error 6.90 m, Root Mean Square Error 11.7 m, Maximum Absolute Error 56.5 m and Correlation Coefficient 0.92% (Figures 3.65-68). The problem with this estimate is the high Maximum Absolute Error value which indicates either extended generalization of the prediction. This can be attributed to the fact that the areas with the highest density of observations have similar hydraulic head values, while the less dense areas have a wider range of values. In the following topology configurations, the creation of groups

(clusters) of observations aims to create subsections of the study area where the validation criteria may exceed to some extent those presented here.

4.2 Topology 1x2

The 1X2 topology resulted in 2 clusters, with the first cluster containing 69 observations and the second 279, as shown in Figure 3.1. As expected, the observations were partitioned in the same way as described in the previous section. This is a consequence of the structure of the input data. The X-Y coordinates correspond to weight 1 and weight 2 in Figure 3.2 and appear to strongly influence the classification for this topology. The hydraulic head value is the third weight and does not significantly affect the clusters. This is the result of the correlation between hydraulic head and altitude mentioned earlier. In general, the observation points were grouped into a coastal front group with low hydraulic head values, and small distance between them, all belonging to the same hydrogeological substructure. On the other hand, the other group had a large variation in hydraulic head values and the observation points were scattered in the rest of the area and belonged to all three hydrogeological substructures.

The two resulting clusters are shown in Figure 3.20. For the first cluster, the normal probability curve appears to approach the theoretical line, while for the second cluster there appear to be some extreme values (Figure 3.21). For both clusters the empirical cumulative probability curve approaches the gaussian curve similar to the previous topology (Figure 3.22, Figure 3.13). The Voronoi polygons (Figure 3.23) for both clusters show the same general trend as before. However, the linear trend plot (Figure 3.24) there appears to be a skewing of the trend near the costal front. Both variograms conform to the theoretical power law model and are unbound, further indicating a strong correlation between the lags (Figure 3.25). An improvement in the cross-validation error is shown in Figure 3.26, for both clusters. The Ok estimate is more detailed and in Figure 3.27 the gradient in hydraulic head is particularly evident in cluster 2. The Kriging error standard deviation map in Figure 3.28 shows high error values for extrapolation outside the range of observation points. The validation criteria of the OK procedure for cluster 1, i.e., Mean Absolute Error 0.69 m, Root Mean Square Error 1.46 m, Maximum Absolute Error 12.5 m and Correlation Coefficient 0.98%, represent an almost 10-fold improvement in the error criteria. This is in contrast to cluster 2 which did not appear to improve as all error metrics appeared to increase with the exception of maximum absolute error. Cluster 2 is formed by the coastal front observations which means that further subgrouping is required.

4.3 Topology 2x1

The difference between the 1x2 and 2x1 topology according to Figure 3.3 is the arrangement of the clusters and an observation is transferred from cluster 2 to cluster 1. In general, the spatial distribution of observations in each cluster follows the same pattern as in the 1x2 topology (Figure 3.4). This also confirms the statements made in the section on topology 1x2.

The clusters in this topology have the same behavior as the previous one as shown in Figure 3.29. The same as from Figure 3.30 to Figure 3.37. However, it should be noted that the change of an observation from one cluster to another gave some unexpected results. Looking at Figures 3.65 to 3.68, it can be seen that no change occurred in cluster 1, which had already improved compared to topology 1x1. Cluster 2 showed improvement in some validation criteria, i.e., Mean Absolute Error 6.84 m, Root Mean Square Error 12.2 m, Maximum Absolute Error 64.5 m and Correlation

Coefficient 0.91%. This difference between the two seemingly identical clusters (cluster 2 from topologies 1x2 and 2x1) first confirms the hypothesis that all possible topology configurations must be investigated to obtain an optimal result. In addition, it is partially confirmed that the inclusion of all observation points strangulates the Kriging estimation. This can be attributed to the high density of observation points in one area compared to other areas in the case study. So does as the granularity of the grid created for the Kriging estimation. In the dense observation areas, a grid square may contain more than one observation, while in the less dense areas, several grid squares maybe empty. Subdividing the study area increases the granularity of the grids without requiring additional computational power. Although the margin of error may increase, the validation criteria indicate an overall in the estimates.

4.4   Topology 2x2

The 2x2 topology yields 4 clusters, cluster 1 contains 31 observations, cluster 2 contains 36, cluster 3 contains 67 and cluster 4 contains 214 (Figure 3.5). Cluster 1 contains observations in the northeastern part of the study area (Figure 3.38). They are located over the area of the porous aquifer characterized by 25% infiltration of 25%. Cluster 2 contains observations in the northern part of the case study (Figure 3.38). They are located over the domain of all three aquifers, but the hydraulic heads are similar. Cluster 3 contains observations located in the southern part of the coastal front (Figure 3.38). Finally, cluster 4 contains the majority of observations located on the coastal front (Figure 3.38). According to Figure 3.6, the four subclusters are subdivided based on position and hydraulic head value. As mentioned earlier, cluster 1 and cluster 2 have different hydrologic characteristics despite their proximity to each other. Cluster 3 and cluster 4 have similar hydrogeologic characteristics, but the river that discharges in the southern part of the case study and the agricultural activity in the northern part of the coastal front, create different hydrogeologic conditions.

Figure 3.39 shows that the classification of observations in each cluster follows a normal distribution. This is also confirmed by Figure 3.40, in which all empirical cumulative probability curves approximate the theoretical gaussian cumulative probability curve. Figure 3.41 and Figure 3.42 continue to show the same decreasing trend of hydraulic head toward the northeast with to southwest, with the exception of cluster 1. The difference in the direction of the trend can be attributed to the different hydrogeologic characteristics of the formation. The empirical variograms were fitted to the theoretical power law mode, except for cluster 2. The variogram of cluster 2was fitted to the spherical variogram which has a clear and well-defined range. This can be attributed to the heterogeneity of hydraulic head values and hydrogeologic properties of the formations in this cluster, which distinguishes cluster 2 from the other clusters. Cross-validation errors appear to have greatly decreased as only cluster 1 has four outliers and cluster 2 has only one (Figure 3.44). These two clusters \ have different values of hydraulic head, as mentioned earlier, so this is an expected result. The Kriging estimates show even greater granularity compared to previous results (Figure 3.45) and the piezometric lines appear to follow the patterns of the study area morphology the (Figure 1.1). The Kriging error standard deviation maps show a decrease in the range of error standard deviation, especially in cluster 4 the error standard deviation is 1.3 m in the whole domain (Figure 3.46). The correlation coefficient shows an improvement in clusters 2 and 3, but a steep decrease in clusters 1 and 4 (Figure 3.65). A Correlation coefficient that approaches zero indicates that the deterministic part of the methodology prevails in the estimation, in this case the linear trend. The Mean Absolute Error and Root Mean Square Error have been decreased

significantly for clusters 2 and 3. For cluster 1 has MEA and RMSE are close to the values for the 1x1 topology, while for cluster 4 there is a sharp increase in both errors (Figures 3.66 and 3.68). For cluster 4, the linear part of the estimate is more dominant, implying that outliers in the observation strongly influence the estimate, which can be confirmed by Figure 3.67, which shows a twofold increase compared to topology 1x1. This could be improved by further clustering to isolate the observations that show a clear linear trend.

4.5   Topology 2x3

The 2x3 topology yielded 6 clusters, cluster 1 contained 19 observations, cluster 2 contained 32, cluster 3 contained 23, cluster 4 contained 92, cluster 5 contained 53 and cluster 129 (Figure 3.7). Cluster 1 contains the observations in the northwestern part of the study area (Figure 3.8, Figure 3.47), all of which are on the porous aquifer with 25% infiltration (Figure 1.1.). Cluster 2 contains the observations in the southwestern part of the study area (Figure 3.8, Figure 3.47) on the porous aquifer with 20% infiltration. Cluster 3 spans through the central portion of the study area and contains observations from all three aquifers similar to cluster 3 in the previous topology (Figure 3.8, Figure 3.47). Cluster 4 contains the northern portion of the dense coastal front observations (Figure 3.8, Figure 3.47). The division of this area can be attributed to the different values of hydraulic head due to the steep decrease in altitude. Cluster 5 includes the rest of the observations in the remaining part of the northern coastal front. Finally, cluster 6 contain observations in the southern part of the coastal front (Figure 3.8, Figure 3.47).

In terms of observations conforming to the normal distribution, all clusters meet the criteria adequately with only cluster 6 showing some outliers (Figure 3.48, Figure 49). Similarly, the downward trends show the same behavior as the previous topologies, i.e., southward to the northern part and southwestward to the rest of the study area (Figure 3.50, Figure 3.51). All variograms were fitted to the theoretical power law l model, except for the variogram of cluster 1 (Figure 3.52). As prescribed in the methodology the global variogram was used for Kriging estimation. Cross validation showed an improvement in all clusters except cluster 1 (Figure 3.53). This may be due to model truncation it this cluster, as seen in Figures 3.54 and 3.55, where the maps produced overfit the observations. It is possible that by reconfiguring the topology, the overfitted observations could be distributed to different clusters. In Figure 3.55, cluster 6 appears to contain the smallest error standard deviation. The correlation coefficient for clusters 3 through 5 appears to be comparable to 1x1 topology. For clusters 1 and 2, the correlation coefficient approach zero and for cluster 6 it decreases but is still acceptable (Figure 3.65). As before, the low correlation coefficient of cluster 2 indicates strong linearity, while the results of cluster 1 are considered overfitting and thus not worth evaluating them. Mean Absolute Error and Root Mean Square Error show similar patterns in all clusters, with cluster 6 having the higher values for both criteria (Figure 3.66, Figure 3.68). The high error values of cluster 6 must be attributed to an outlier, which is confirmed by the high value of the Maximum Absolute Error (Figure 3.67). Despite an overall improvement in most of the clusters the overfitting of cluster 1 indicates that the proposed methodology for this case study has reached its limits.

4.6   Topology 3x2

The clustering in this topology is quite different from the previous topology (Figure 3.9). Cluster 1 contains 17 observations, cluster 2 contains 23, cluster 3 contains 31, cluster 4 contains 53, cluster 5 contains130 and cluster 6 contains 94. All

clusters span the same sub-areas as described in the previous section, but because of the different topology configuration, the observations have been assigned to different clusters and the cluster numbering is different (Figure 3.56). As shown previously for the 1x2 and 2x1 topologies, assigning fewer observations between clusters can greatly improve the final results of the model. Cluster 1 is located in the northern part of the study area as described previously. Cluster 2 is located in the cross section of the 3 porous formations in the middle of the case study. Cluster 3 is the bulk of the observed dense portion of the coastal front. Cluster 4 extend over the southern portion of the coastal front affected by the river discharge and a small portion of the inland affected by the river discharge. Cluster 5 extends across the southeastern portion of the case study at the intersection of two formations at relatively high altitude. Cluster 6 is located in the northern portion of the coastal front. From Figures 3.57 and 3.58, all clusters appear to conform to the normal distribution, with some outliers in clusters 3,5 and 6. The Voronoi diagrams (Figure 3.59) for each cluster showed that the ranges of hydraulic head values are significantly restricted. The linear trends in all clusters are as previous described, except for cluster 6 (Figure 3.60). The area that makes up cluster 6 is associated with an aquifer with higher infiltration which increases water flux compared to the water flux in the rest of the coastal front. Higher values of hydraulic head are expected in this location especially when altitude change is considered change. All variograms were fitted to the theoretical power law model with moderate success (Figure 3.61). Cross-validation errors show the same outliers in clusters 1 and 2, but given the variability in hydraulic head values at these locations this is acceptable (Figure 3.62). Figure 3.63 shows that kriging estimates appear to be possible except for a small area in cluster 4, but this irregularity can also be attributed to water fluxes from the river. In Figure 3.64, the standard deviation shows variation in most maps. The standard error deviation of cluster1, despite its apparent affectedness, is a reasonable approximation considering that the said cluster has a range of values from 50 m to more than 300 m. On the other hand, clusters 3 and 5 seem to be overfitted but the validation criteria argue against. The correlation coefficient is above 80% for all clusters except for cluster 1 with a value of -14% suggesting a strong deterministic linearity. Mean Absolute Error and Root Mean Squared Error behave similarly with errors in clusters 2 to 6 not exceeding 2 m and 3 m respectively. Cluster 1 does not perform as well as the other clusters but shows improvement over the 1x1 topology in all cases, even in Maximum Absolute Error which is almost halved (Figure 3.67).

5   Conclusions

As general remarks, it could be stated that the assumption that the Ordinary Kriging technique is able to describe the conditions of groundwater is verified, since all mathematical assumptions have been satisfied. In all cases of differing topologies, the results were adequate, with varying success. In addition, both from the literature and the results of this work, it has been verified that subdividing the sample of observations to smaller groups greatly improves the OK estimations. Given the different configurations of clusters, it could be stated that subgrouping arbitrarily could yield some results but in more complex systems than the current case study, this practice will be detrimental to the results. SOM is a promising algorithm for performing clustering by utilizing additional information such as hydraulic head value to spatial coordinates. Clustering as a technique of reducing the error of prediction has its restrictions. An upper bound to this technique is the data driven nature of Kriging methodologies. There is no definable number of observations within a cluster because of the specific hydrogeological conditions of each domain. Elaborating further, a small cluster area with high heterogeneity might require more observation for the performance of Kriging compared to a large homogenous area. The mechanistic clustering, as proposed from the methodology, should be applied within the context of the physical problem, i.e., geological, hydrogeological background and water extraction. In this case study, six clusters were elected with a higher configuration not yielding any results due to lack of observations within the clusters. In conclusion, the coupling of OK with SOM yields more accurate results compared to simple use of OK but is a data intensive process that in this point requires semi-manual optimization due to multiple tests that are required to be performed.

Regarding the model results, Topology's 1x1 performance was considered adequate, although it had a high error rate. OK can describe the hydrogeologic conditions of the case study, but by classifying the observations, OK can provide more accurate results. The use of SOMs can greatly improve predictions even for simple topologies such as 1x2 and 2x1. Small differences can greatly affect the results of Kriging as can be seen when comparing the two topologies. This means that the configuration of the topology is important and related to the physical problem at hand. Topologies 1x2 and 2x1 divided the study area into two groups based on the location of the observations and the change in the linear trend of the hydraulic head. In topology 2x2 the subgroups were subdivided in even greater detail, taking into account the hydrogeologic characteristics of each group. In topologies 2x3 and 3x2 the groups were subdivided in more detail, and this subdivision led to different results. In topology 2x3 the model was strangulated and did not provide acceptable results for a cluster, while topology 3x2 provided the most accurate and best results compared to topology 1x1. Topology 3x2 was selected as the best fit for this case study based in all metrics. In cluster 1 of mentioned topology, the correlation coefficient approached zero, but this indicates that the cluster can only be described by the deterministic linear trend. However, the low correlation coefficient score though does not affect the robustness of the prediction since all other error values outperform the original topology. For the optimal description of the hydrogeological conditions of the case study, 6 groups were defined. The first group is located in the northwestern part of the study area, on the porous aquifer with 25% infiltration. The second group is located in the cross section of the 3 porous formations in the middle of the case study. The third group consists of the coastal front with the most intensive agricultural activity. The fourth group is located in the northern part of the case study influenced by the river discharge. The fifth group is located on the mainland in a cross-sectional area of high-altitude aquifers. The last

group is located on the coastal front but differs from the other coastal groups due to its different morphology. Clustering performed with SOM provided detailed granularity in grouping with what appeared to be reductive inputs. Coordinate inputs had the greatest influence on grouping in the 1x2 and 2x1 topologies. In other topologies where there was more room for diversification, the hydraulic head value strongly influenced the grouping results. There are two explanations for this: First as a numerical input, the SOM algorithm grouped observations that were in close proximity to each other and had similar hydraulic head values. Second, the hydraulic head value is strongly correlated with secondary parameters such as hydraulic conductivity or altitude. Altitude is easily extracted as information, but measurements of hydraulic conductivity are rare and subject to uncertainty. Thus, hydraulic head an input contains secondary information that the SOM algorithm can use for improved grouping. In conclusion, the pairing of SOM-enhanced OK can provide highly defined and accurate results compared to a simple OK technique. The proposed method is generic meaning that it can be applied to different case studies by simply changing the inputs as described above and testing different topology configurations. This work provides spatial predictions, future development of the proposed methodology aims to include the temporal aspect of hydrogeologic conditions in a case study.

6 References

Amiri, V., Nakagawa, K., 2021. Using a linear discriminant analysis (LDA)-based nomenclature system and self-organizing maps (SOM) for spatiotemporal assessment of groundwater quality in a coastal aquifer. J. Hydrol. 603, 127082. https://doi.org/10.1016/j.jhydrol.2021.127082

Aryafar, A., Khosravi, V., Karami, S., 2020. Groundwater quality assessment of Birjand plain aquifer using kriging estimation and sequential Gaussian simulation methods. Environ. Earth Sci. 79, 210. https://doi.org/10.1007/s12665-020-08905-8

Belkhiri, L., Mouni, L., Tiri, A., Narany, T.S., Nouibet, R., 2018. Spatial analysis of groundwater quality using self-organizing maps. Groundw. Sustain. Dev. 7, 121–132. https://doi.org/10.1016/j.gsd.2018.04.001

Belkhiri, L., Tiri, A., Mouni, L., 2020. Spatial distribution of the groundwater quality using kriging and Co-kriging interpolations. Groundw. Sustain. Dev. 11, 100473. https://doi.org/10.1016/j.gsd.2020.100473

Bouhout, S., Haboubi, K., Zian, A., Elyoubi, M.S., Elabdouni, A., 2022. Evaluation of two linear kriging methods for piezometric levels interpolation and a framework for upgrading groundwater level monitoring network in Ghiss-Nekor plain, north-eastern Morocco. Arab. J. Geosci. 15, 1016. https://doi.org/10.1007/s12517-022-10283-3

Canion, A., McCloud, L., Dobberfuhl, D., 2019. Predictive modeling of elevated groundwater nitrate in a karstic spring-contributing area using random forests and regression-kriging. Environ. Earth Sci. 78, 271. https://doi.org/10.1007/s12665-019-8277-1

Chang, F.-J., Chang, L.-C., Huang, C.-W., Kao, I.-F., 2016. Prediction of monthly regional groundwater levels through hybrid soft-computing techniques. J. Hydrol. 541, 965–976. https://doi.org/10.1016/j.jhydrol.2016.08.006

Chen, I.-T., Chang, L.-C., Chang, F.-J., 2018. Exploring the spatio-temporal interrelation between groundwater and surface water by using the self-organizing maps. J. Hydrol. 556, 131–142. https://doi.org/10.1016/j.jhydrol.2017.10.015

Chen, L.-H., Chen, C.-T., Lin, D.-W., 2011. Application of Integrated Back-Propagation Network and Self-Organizing Map for Groundwater Level Forecasting. J. Water Resour. Plan. Manag. 137, 352–365. https://doi.org/10.1061/(ASCE)WR.1943-5452.0000121

Chowdhury, M., Alouani, A., Hossain, F., 2010. Comparison of ordinary kriging and artificial neural network for spatial mapping of arsenic contamination of groundwater. Stoch. Environ. Res. Risk Assess. 24, 1–7. https://doi.org/10.1007/s00477-008-0296-5

Dokou, Z., Dettoraki, M., Karatzas, G.P., Varouchakis, E.A., Pappa, A., 2017. Utilizing Successive Linearization Optimization to Control the Saltwater Intrusion Phenomenon in Unconfined Coastal Aquifers in Crete, Greece. Environ. Model. Assess. 22, 115–128. https://doi.org/10.1007/s10666-016-9529-z

Filippi, A.M., Jensen, J.R., 2006. Fuzzy learning vector quantization for hyperspectral coastal vegetation classification. Remote Sens. Environ. 100, 512–530. https://doi.org/10.1016/j.rse.2005.11.007

Goovaerts, P., AvRuskin, G., Meliker, J., Slotnick, M., Jacquez, G., Nriagu, J., 2005. Geostatistical modeling of the spatial variability of arsenic in groundwater of southeast Michigan: GEOSTATISTICAL MODELING OF ARSENIC. Water Resour. Res. 41. https://doi.org/10.1029/2004WR003705

Hasan, K., Paul, S., Chy, T.J., Antipova, A., 2021. Analysis of groundwater table variability and trend using ordinary kriging: the case study of Sylhet,

Bangladesh. Appl. Water Sci. 11, 120. https://doi.org/10.1007/s13201-021-01454-w

Hengl, T., European commission, Joint research centre, Institute for environment and sustainability (Ispra, I., 2007. A practical guide to geostatistical mapping of environmental variables. Publications Office, Luxembourg.

Jiang, S., Liu, J., Xia, X., Wang, Z., Cheng, L., Li, X., 2021. Simultaneous identification of contaminant sources and hydraulic conductivity field by combining geostatistics method with self-organizing maps algorithm. J. Contam. Hydrol. 241, 103815. https://doi.org/10.1016/j.jconhyd.2021.103815

Kavusi, M., Khashei Siuki, A., Dastourani, M., 2020. Optimal Design of Groundwater Monitoring Network Using the Combined Election-Kriging Method. Water Resour. Manag. 34, 2503–2516. https://doi.org/10.1007/s11269-020-02568-7

Kechiched, R., Nezli, I.E., Foufou, A., Belksier, M.S., Benhamida, S.A., Djeghoubbi, R., Slamene, N., Ameur-zaimeche, O., 2020. Fluoride-bearing groundwater in the complex terminal aquifer (a case study in Hassi Messaoud area, southern Algeria): hydrochemical characterization and spatial distribution assessed by indicator kriging. Sustain. Water Resour. Manag. 6, 54. https://doi.org/10.1007/s40899-020-00415-6

Kohonen, T., 1990. The self-organizing map. Proc. IEEE 78, 1464–1480. https://doi.org/10.1109/5.58325

Kourgialas, N.N., Dokou, Z., Karatzas, G.P., Panagopoulos, G., Soupios, P., Vafidis, A., Manoutsoglou, E., Schafmeister, M., 2016. Saltwater intrusion in an irrigated agricultural area: combining density-dependent modeling and geophysical methods. Environ. Earth Sci. 75, 15. https://doi.org/10.1007/s12665-015-4856-y

Kwon, Y.-S., Li, F., Chung, N., Bae, M.-J., Hwang, S.-J., Byoen, M.-S., Park, S.-J., Park, Y.-S., 2012. Response of Fish Communities to Various Environmental Variables across Multiple Spatial Scales. Int. J. Environ. Res. Public. Health 9, 3629–3653. https://doi.org/10.3390/ijerph9103629

Lee, K.-J., Yun, S.-T., Yu, S., Kim, K.-H., Lee, J.-H., Lee, S.-H., 2019. The combined use of self-organizing map technique and fuzzy c-means clustering to evaluate urban groundwater quality in Seoul metropolitan city, South Korea. J. Hydrol. 569, 685–697. https://doi.org/10.1016/j.jhydrol.2018.12.031

Li, J., Shi, Z., Wang, G., Liu, F., 2020. Evaluating Spatiotemporal Variations of Groundwater Quality in Northeast Beijing by Self-Organizing Map. Water 12, 1382. https://doi.org/10.3390/w12051382

Liang, C.-P., Chen, J.-S., Chien, Y.-C., Chen, C.-F., 2018. Spatial analysis of the risk to human health from exposure to arsenic contaminated groundwater: A kriging approach. Sci. Total Environ. 627, 1048–1057. https://doi.org/10.1016/j.scitotenv.2018.01.294

Lollino, G., Arattano, M., Rinaldi, M., Giustolisi, O., Marechal, J.-C., Grant, G.E. (Eds.), 2015. Engineering Geology for Society and Territory - Volume 3. Springer International Publishing, Cham. https://doi.org/10.1007/978-3-319-09054-2

Nakagawa, K., Yu, Z.-Q., Berndtsson, R., Hosono, T., 2020. Temporal characteristics of groundwater chemistry affected by the 2016 Kumamoto earthquake using self-organizing maps. J. Hydrol. 582, 124519. https://doi.org/10.1016/j.jhydrol.2019.124519

Nourani, V., Alami, M.T., Vousoughi, F.D., 2016. Self-organizing map clustering technique for ANN-based spatiotemporal modeling of groundwater quality parameters. J. Hydroinformatics 18, 288–309. https://doi.org/10.2166/hydro.2015.143

Panagopoulos, G., Giannakakos, E., Manoutsoglou, E., Steiakakis, E., Soupios, P., Vafidis, A., 2017. Definition of inferred faults using 3D geological modeling

techniques: A case study in Tympaki Basin in Crete, Greece. Bull. Geol. Soc. Greece 47, 605. https://doi.org/10.12681/bgsg.11087

Paparrizos, S., Maris, F., Matzarakis, A., 2016. Integrated analysis of present and future responses of precipitation over selected Greek areas with different climate conditions. Atmospheric Res. 169, 199–208. https://doi.org/10.1016/j.atmosres.2015.10.004

Rezaei, F., Ahmadzadeh, M.R., Safavi, H.R., 2017. SOM-DRASTIC: using self-organizing map for evaluating groundwater potential to pollution. Stoch. Environ. Res. Risk Assess. 31, 1941–1956. https://doi.org/10.1007/s00477-016-1334-3

Rivas-Tabares, D., de Miguel, Á., Willaarts, B., Tarquis, A.M., 2020. Self-organizing map of soil properties in the context of hydrological modeling. Appl. Math. Model. 88, 175–189. https://doi.org/10.1016/j.apm.2020.06.044

Rostami, A.A., Karimi, V., Khatibi, R., Pradhan, B., 2020. An investigation into seasonal variations of groundwater nitrate by spatial modelling strategies at two levels by kriging and co-kriging models. J. Environ. Manage. 270, 110843. https://doi.org/10.1016/j.jenvman.2020.110843

Senoro, D.B., de Jesus, K.L.M., Mendoza, L.C., Apostol, E.M.D., Escalona, K.S., Chan, E.B., 2021. Groundwater Quality Monitoring Using In-Situ Measurements and Hybrid Machine Learning with Empirical Bayesian Kriging Interpolation Method. Appl. Sci. 12, 132. https://doi.org/10.3390/app12010132

Stathatou, P.-M.G., 2011. Water Footprint, a tool to achieve effective agricultural policy. Case study: Messara valley, Crete 175 bytes. https://doi.org/10.26240/HEAL.NTUA.6626

Vafidis, A., Andronikidis, N., Hamdan, H., Kritikakis, G., Economou, N., Panagopoulos, G., Soupios, P., Steiakakis, E., Manoutsoglou, E., 2016. The CLEARWATER project: preliminary results from the geophysical survey in Tympaki, Crete, Greece. Bull. Geol. Soc. Greece 47, 1338. https://doi.org/10.12681/bgsg.10916

Yu, Z.-Q., Amano, H., Nakagawa, K., Berndtsson, R., 2018. Hydrogeochemical evolution of groundwater in a Quaternary sediment and Cretaceous sandstone unconfined aquifer in Northwestern China. Environ. Earth Sci. 77, 629. https://doi.org/10.1007/s12665-018-7816-5

Zhu, Y.-G., Gillings, M., Penuelas, J., 2020. Integrating Biomedical, Ecological, and Sustainability Sciences to Manage Emerging Infectious Diseases. One Earth 3, 23–26. https://doi.org/10.1016/j.oneear.2020.06.004

Zimmerman, D., Stein, M., 2010. Classical Geostatistical Methods, in: Gelfand, A., Diggle, P., Fuentes, M., Guttorp, P. (Eds.), Handbook of Spatial Statistics, Chapman & Hall/CRC Handbooks of Modern Statistical Methods. CRC Press, pp. 29–44. https://doi.org/10.1201/9781420072884-c3

Κριτσωτάκης, M., 2009. Διαχείριση Υδατικών Πόρων Μεσαράς Κρήτης (Management of Water Resources in Messara Crete) (Thesis). Πολυτεχνείο Κρήτης, Χανιά.

Σπυρόπουλος, Φ., 2021. Modular calibration improving the boundary conditions of a 3D groundwater model (FEFLOW) for the aquifer of Tympaki, Crete, Greece. https://doi.org/10.26233/HEALLINK.TUC.90393

Στεργιου, Μ., 2021. Simulation of the underground flow at the region of Timpaki Crete, using the FEFLOW model. https://doi.org/10.26233/HEALLINK.TUC.89239

Appendix I (Validation Criteria)

Topology	Cluster	MAE	RMSE	Rho	MaxAE
1X1	1	6.8919	11.6996	0.9207	56.4664
1X2	1	0.6943	1.4599	0.9845	12.466
1X2	2	10.539	14.9232	0.7093	41.9752
2X1	1	0.6943	1.4599	0.9845	12.466
2X1	2	6.8428	12.2325	0.9148	64.5159
2X2	1	6.1563	8.6636	-0.1405	33.844
2X2	2	1.8896	5.9893	0.9665	73.2067
2X2	3	0.5932	1.1743	0.9698	9.3454
2X2	4	18.9308	33.9562	-0.3423	115.3863
2X3	1	6.0106	7.8618	0.3614	20.1747
2X3	2	4.6657	6.0692	0.269	13.4004
2X3	3	0.9879	1.966	0.9433	13.4916
2X3	4	0.977	1.5051	0.9059	5.681
2X3	5	0.341	0.5069	0.9758	1.7339
2X3	6	10.539	14.9232	0.7093	41.9752
3X2	1	6.1563	8.6636	-0.1405	33.844
3X2	2	0.4346	0.7138	0.9191	2.9375
3X2	3	0.8383	1.374	0.8751	5.0426
3X2	4	0.3874	0.5819	0.9381	1.7296
3X2	5	1.9819	3.0933	0.815	15.316
3X2	6	1.9263	3.0267	0.8312	15.5042